UNIVERSITÀ DEGLI STUDI DI TRIESTE

UNIVERSITÀ DEGLI STUDI DI TRIESTE

XXXV CICLO DEL DOTTORATO DI RICERCA IN

BIOMEDICINA MOLECOLARE

PO FRIULI VENEZIA GIULIA- FONDO SOCIALE EUROPEO 2014/2020

LOCAL TRANSPORT AND TRANSLATION OF BDNF FOLLOWING SYNAPTIC POTENTIATION

Settore scientifico-disciplinare: **BIO/06**

DOTTORANDO / A
GIORGIA BIMBI

COORDINATORE
PROF.GERMANA MERONI

SUPERVISORE DI TESI
PROF.ENRICO TONGIORGI

ANNO ACCADEMICO 2021/2022

INDEX

ABBREVIATION

Arc: Activity-regulated cytoskeleton-associated protein

BDNF: Brain derived neurotrophic factor

CamKII: Calcium/Calmodulin-dependent protein kinase II

CDS: coding sequence

cLTP: chemical LTP

DIV: days in vitro

eGFP: enhanced green fluorescent protein

EX: exon

FISH: Fluorescent in situ hybridization

Kb: kilo bases

LTP: Long-term potentiation

MAP2: Microtubule-associated protein

MCP: MS2-coat protein

MOI: multiplicity of infection

pb: pair bases

RBPs: RNA binding proteins

ROI: Region of interest

RNP: RNA

ABSTRACT

The neurotrophin brain-derived neurotrophic factor (BDNF) plays a key role in neuronal survival, neurite out-growth, synaptogenesis and synaptic plasticity. BDNF mRNA can be transported in neuronal dendrites in an activity-dependent manner, following seizures or even in response to antidepressants or physical activity. A clear demonstration that BDNF mRNA is locally transported and translated at activated synapses in response to the induction of long-term potentiation (LTP) is still lacking. Here, the dynamics of BDNF mRNA trafficking during neuronal plasticity induced by chemical-LTP has been addressed. Besides, this work explores the correlations between selective dendritic transport and translation of BDNF transcripts after synaptic potentiation by means of SynActive, a molecular tag able to identify activated synapses. Analysis on the type of movements, the velocity and the localization of the mRNA granules is performed, showing that the vast majority of BDNF mRNA granules are confined. After cLTP induction the BDNF mRNA granules become even more confined with a reduction of anterograde and retrograde movement. Furthermore, after cLTP induction the percentage of BDNF mRNA granules present inside and under a spine increases. In addition to the BDNF mRNA, analysis of the BDNF-cds-GFP protein is conducted. The evaluation of the type of movements and the localization of the protein spots suggests that the CDS of BDNF protein is mainly confined before and after the cLTP stimulation and that after 60’ from cLTP induction, the CDS of BDNF is mainly located inside spines.

1. INTRODUCTION

1.1 Neurotrophin

Neurotrophins are a family of dimeric ligands that includes NGF, BDNF, NT3 (neurotrophin-3), and NT4 (neurotrophin-4). Neurotrophins have similar structures and sequences and are likely derived from a common ancestral gene (Lazear and Boterf, 2007). Their role is to balance cell fate decisions between life and death (Casaccia-Bonnefil et al., 1999; Lu et al., 2005). Although one single exon encodes the neurotrophin proteins, there are a multitude of alternatively spliced exons, which provide information regarding spatio–temporal expression. Once secreted, NTs can bind with specific affinities to transmembrane-receptors belonging to a small family of tropomyosin-related tyrosine kinases (Trk): TrkA (NGF), TrkB (BDNF and NT-4), and TrkC (NT-3). In addition, NTs can also bind to the p75 neurotrophin receptor (p75NTR) which belongs to the tumor necrosis family. The preferred ligands for p75 receptor are the precursors of mature NTs rather than the mature NTs (Figure I).

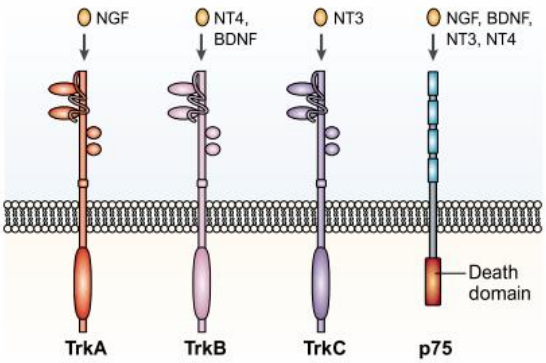

Figure I: Neurotrophins and their receptors. Each neurotrophin has a specific receptor affinity to which it can bind. Adapted from (Chao, 2003).

Once activated, receptors initiate several signal transduction cascades, including the mitogen activated protein kinase (MAP kinase) which promotes neuronal differentiation, the phosphatidylinositol 3-kinase (PI-3K) which promotes survival and growth of neurons and other cells, and the phospholipase C γ (PLC) pathway which promotes synaptic plasticity (Figure II).

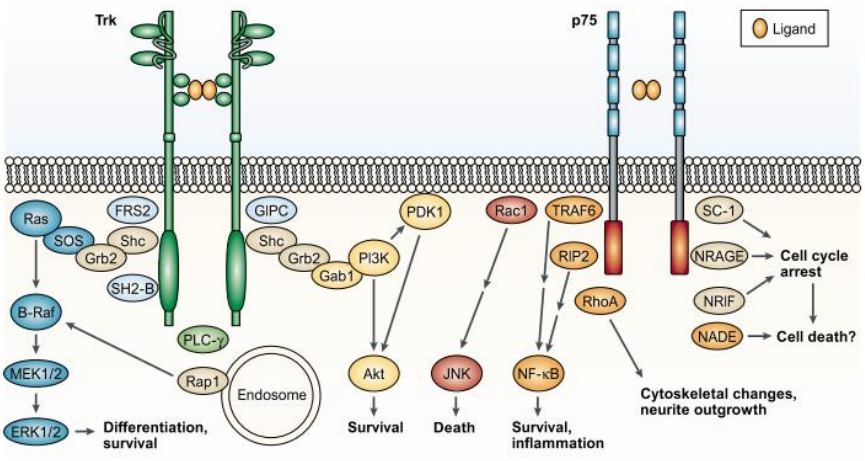

Figure II: Neurotrophin receptor signalling. Trk receptors mediate differentiation and survival signalling through extracellular signal-regulated kinase (ERK), phosphatidylinositol 3-kinase (PI3K) and phospholipase Cγ(PLC-γ) pathways. The p75 receptor predominantly signals to activate NF-κB and Jun N-terminal kinase (JNK), and modulates RhoA activity (Chao, 2003)

1.2 BDNF

1.2.1 Localization and maturation

BDNF protein is highly conserved among evolution, suggesting its fundamental role in regulating many different cellular functions (Berkemeier et al., 1991; Hofer et al., 1990). BDNF is widely expressed in the central nervous system, especially in cerebral cortex, hippocampus and amygdaloid complex (Ernfors et al., 1991; Hofer et al., 1990; Phillips et al., 1990; Wetmore et al., 1991) (Figure III), but it has been detected also in intestine, ovary, spleen, thymus, testis, pancreas and blood (Huang et al., 2003; Pruunsild et al., 2007; Rosenfeld et al., 1995).

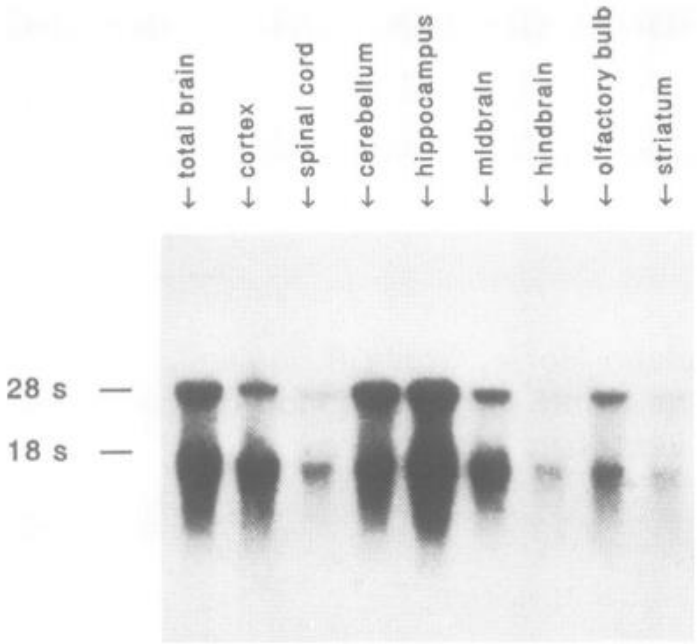

Figure III: Distribution of the BDNF mRNA in various brain regions of the adult mouse. Taken from (Hofer et al., 1990)

This widespread distribution of BDNF underlines its importance in a large number of different cellular processes, especially for what concerns neuronal function. However, some studies also reported that the basal (unstimulated) BDNF mRNA and protein have low expression in the rat hippocampus (Conner et al., 1997; Will et al., 2013). As many other secreted proteins, BDNF is initially generated as a pro-BDNF, that thought the N-terminal cleavage is transformed in the mature form (Mowla et al., 2001). At a cellular level, BNDF is first synthesized in the ER as a pro-BDNF, then it binds to the intracellular sortilin in the Golgi to facilitate proper folding of the mature domain. A motif located in the mature domain of BDNF binds to carboxypeptidase E (CPE), this interaction is responsible for the sorting of BDNF into large dense vesicles, that are components of the regulated secretory pathway. If the motif is not present, then BDNF is sorted into the constitutive pathway. After the sorting, BDNF is transported to the proper site and released. Intracellularly, pro-BDNF can be cleaved by furin into the mature 14kDa BDNF protein, or alternatively the pro-BDNF can be cleaved by metalloproteinases extracellularly (Figure IV). However, the neurotrophic factor can be as well released in its precursor form confirming that it can also act as signalling molecule (Lu et al., 2005). This tight regulation of BDNF signalling suggests the accurate establishment of different steady-state levels in different neuronal structure (Lu et al., 2005)

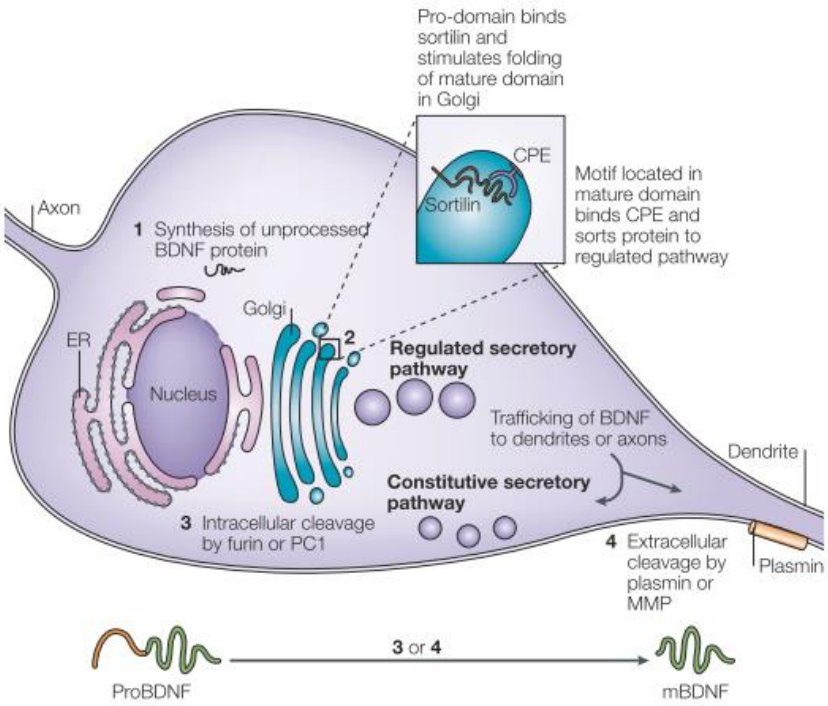

Figure IV: The synthesis and sorting of BDNF. A schematic showing the synthesis and sorting of brain-derived neurotrophic factor (BDNF) in a typical neuron. Description of the passages in the text (Lu et al., 2005)

Studies on hippocampal cultures have showed that BDNF is preferentially released from dendritic compartments in an activity-dependent way mediated by the activation of glutamatergic synapses that induces the entry of Ca2+ through NMDA receptors (Matsuda et al., 2009). There is also evidence that BDNF can be endocytosed at the postsynaptic level and further released after synaptic activity induced with 200µM glycine (Wong et al., 2015). After its secretion, mature BDNF binds specifically the tropomyosin-related kinase B (TrkB) which dimerizes and undergoes autophosphorylation activating several intracellular cascades: mitogen-activated protein kinase (MAPK) which promotes neuronal differentiation, phosphatidylinositol 3-kinase (PI3K) that mediate neuronal growth and survival, and phospholipase Cγ (PLCγ) pathway that promotes synaptic plasticity (Chao, 2003) (Figure V).

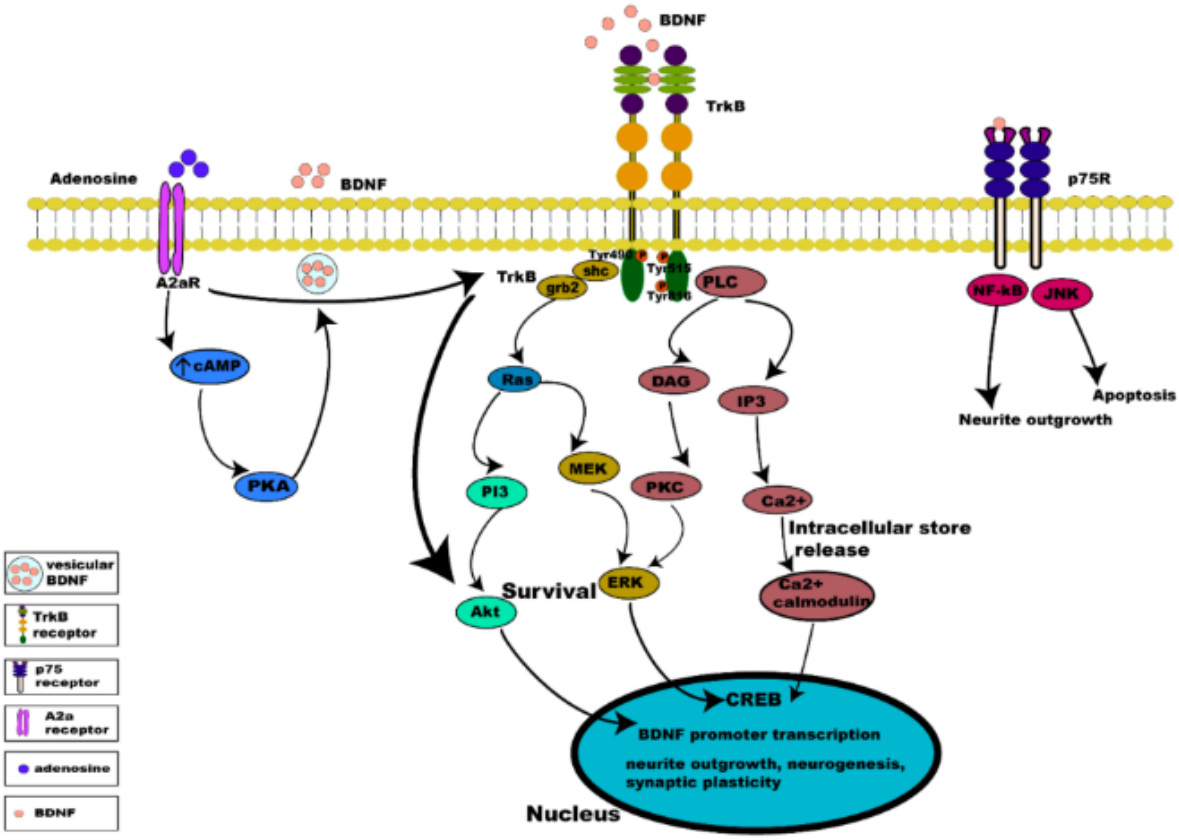

Figure V: intracellular signalling cascades of BDNF-TrkB. BDNF-TrkB activation predominantly initiates MAPK, PI3K, and PLC γ signalling pathways. Activation of the TrkB receptor at its Tyr490 and Tyr515 residue recruits Shc adaptor protein leading to binding of growth factor receptor bound protein 2 (grb2) which binds with GTPase Ras to form a complex and initiate extracellular signal regulated kinase (ERK) activation which in turn activates the mitogen activated protein kinase MAPK/ERK pathway, which results in the activation of CREB transcription factor. Both MAPK and PI3K signalling exert neurotrophic functions of survival, growth and differentiation, via activation transcription factors (CREB and C-myc). Phosphorylation of the TrkB receptor at its Tyr816 residue activates the phospholipase C γ (PLC γ) pathway, generating inositol-1, 4, 5-triphosphate (IP3) and diacylglycerol (DAG). The PLCγ/IP3 pathway results in calcium release from intracellular stores, in turn activating Ca2+/CaMKII. DAG activates PKC, leading to synaptic plasticity. pro-BDNF/p75 initiates JNK signalling and the NF-κB signalling cascade regulation of neuronal growth cone development and navigation, and neuronal survival. Taken from (Pradhan et al., 2019).

1.2.2 BDNF gene structure

Aid and Pruunsild (2007) have reported the structure of the BNDF rat gene. This gene contains multiple promoters that drive the expression of transcript bearing different non-coding exons spliced upstream of a common 3' exon. The detailed characterization of the BDNF gene has

revealed the existence of several promoters located upstream of the alternatively spliced exons, thus promoting a precise regulation in different cell types and in response to different stimula. In particular, the BDNF gene contains eight non-coding exons at the 5' and one common 3' protein coding exon. Since each exon has a unique promoter, it rises to eight different 5' untranslated BDNF exons each of which is spliced to the common 3' protein coding exon IX. However, they are much more than eight because exon II has three transcript variants (IIA, IIB, IIC) and because transcription can be initiated in the intron before the protein coding exon, which results in IXA transcripts containing 5' extended coding exon. The transcripts, following the nomenclature proposed by Aid in 2007, are named (1, 2A, 2B, 2C, 3, 4, 5, and 6A). This generates 11 transcripts in rodents (Figure VI). Each transcript has distinct tissue-specific expression profiles as showed in Figure VII.

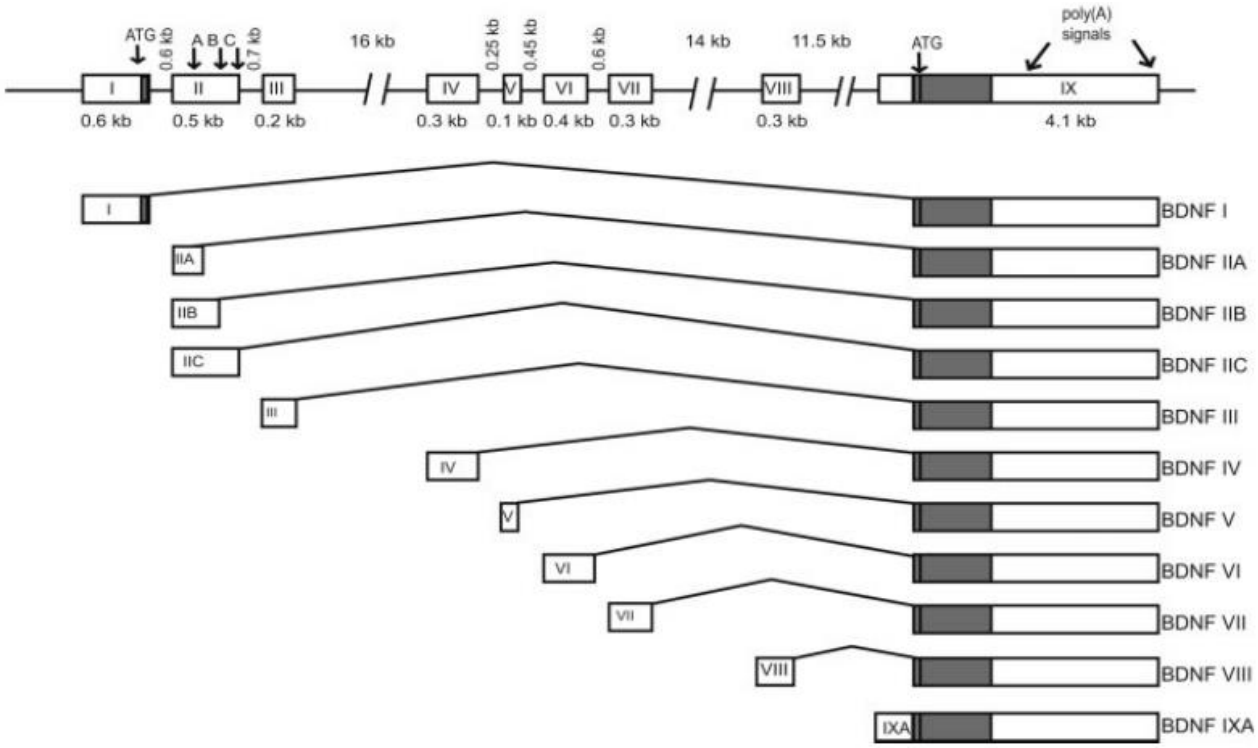

Figure VI: Representation of mouse and rat BDNF genes. Each of the eight 5' untranslated exons is spliced to the common 3' protein coding exon IX. In addition, transcription can be initiated in the intron before the protein coding exon, which results in IXA transcripts containing 5' extended coding exon. Each transcription unit may use one of the two alternative polyadenylation signals in the 3' exon (arrows). For exon II, three different transcript variants, IIA, IIB, and IIC, are generated as a result of using alternative splice-donor sites in exon II (arrows marked A, B, and C). From (Tamara Aid, Anna Kazantseva, Marko Piirsoo, Kaia Palm, 2007)

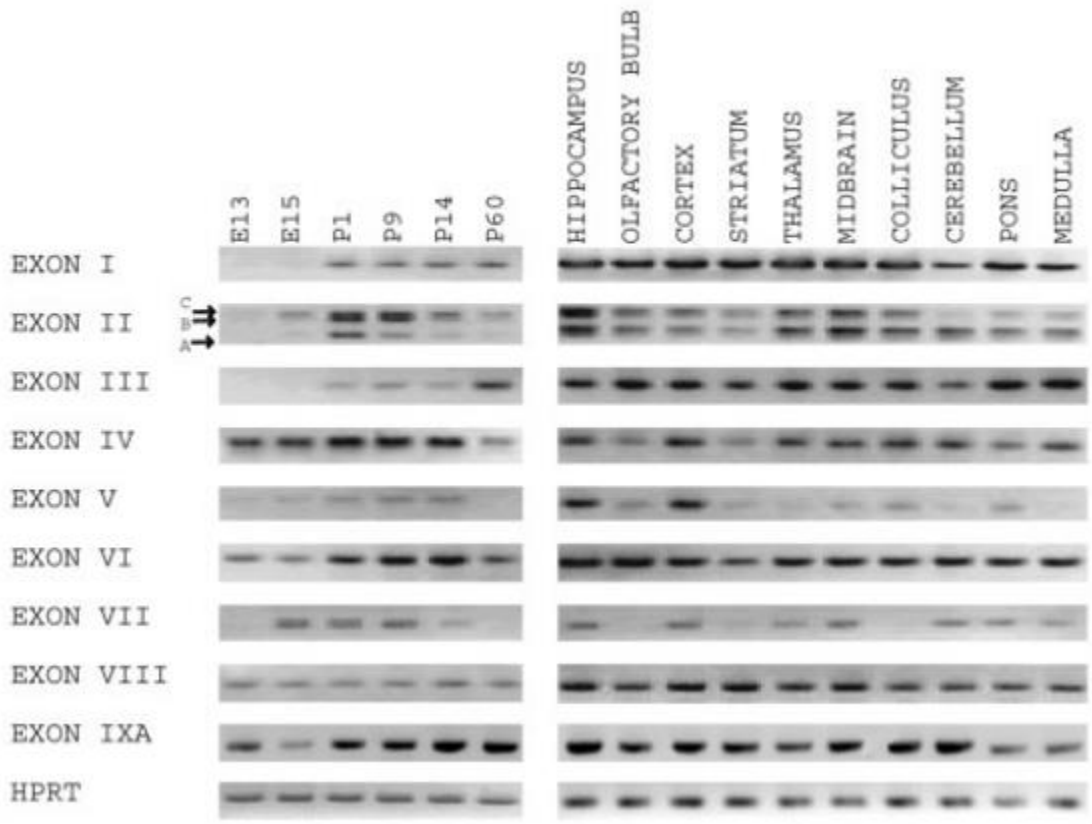

Figure VII: Expression analysis of mouse BDNF mRNAs. Semi-quantitative RT-PCR analysis of tissue-specific expression of mouse. In the hippocampus the two isoforms used in this thesis work are exon I and exon VI are expressed. Taken from (An et al., 2008a)*.*

In addition to that, different isoforms of BDNF are expressed in specific developmental stages: transcripts I and II (Aid et al., 2007) are only present in adults, whereas IV and V (Aid et al., 2007) can be found since early postnatal stages (Pattabiraman et al., 2005). These four isoforms are distributed in different subcellular compartments: while transcript I is only detected in cell bodies, transcript IV is located in soma and proximal dendrites and transcripts II and VI (Aid et al., 2007) are present in cell bodies and may reach the distal dendritic compartment. This organization can appear chaotic, but the generation of multiple transcripts from the same gene through alternative splicing is a general rule rather than an exception. It is relatively easy to appreciate the increase in functional diversity afforded by alternative splicing that produces mRNAs encoding different proteins. However, in many cases multiple transcripts encode exactly the same protein, as it is for BDNF.

1.2.2.1 5'UTR

In the last years, important experimental efforts have been devoted to the identification of the meaning of different spliced variants. Recently, it has been proposed that, owing to their different subcellular localization, BDNF splice variants represent a spatial and quantitative code for a selective local expression of BDNF(Chiaruttini et al., 2009a; Tongiorgi and Baj, 2008; Vaghi et al., 2014). This model is based on the finding that BDNF mRNA is one of the several hundreds of neuronal mRNAs that are transported to dendrites, where their local translation contributes to synaptic plasticity (Meignin and Davis, 2010; Tongiorgi and Baj, 2008). It has been observed that exons I and IV are mainly localized in soma or in proximal dendrites, while transcripts containing exon II or VI can be targeted to the distal dendritic compartment in response to neuronal activity induced by a medium containing high potassium concentration (Figure VIII) (Baj et al., 2011; Chiaruttini et al., 2009a). Recently, it has been reported that the isoform IIA, IIB and IIC encode a constitutively active dendritic targeting signal, possibly involving an HNRNPA1 and HNRNPA2/B1-mediated interaction between 5′ UTRs and CDS of BDNF to regulate BDNF mRNA dendritic trafficking (Colliva and Tongiorgi, 2021).

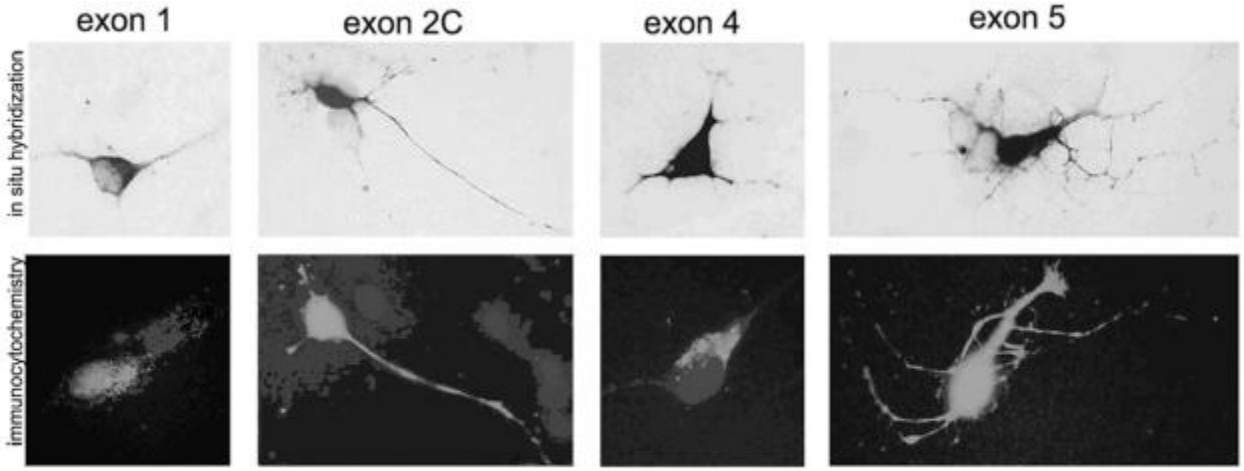

Figure VIII: mRNA and protein co-localization in hippocampal neurons. Hippocampal neurons were transfected with different BDNF–GFP chimeras encoding BDNF mRNA transcripts (BDNF 1, 2C, 4, 5) under physiological condition in the hippocampus. The mRNAs of the splice variants were localized through in situ experiments using a riboprobe against the region encoding GFP. Furthermore, the localization of the chimeric BDNF–GFP protein was detected through specific immunocytochemistry using a primary antibody against GFP and a fluorescent secondary antibody. Taken from (Tongiorgi and Baj, 2008)

1.2.2.2 3'UTR

A more puzzling finding is that BDNF mRNAs are polyadenylated at two alternative sites, leading to distinct populations of mRNAs: those with a short 3' untranslated region (UTR) and those with a long 3' UTR (Ghosh et al., 1994; Timmusk et al., 1993).Therefore, the total amount of the BDNF gene in rodents reaches 22 transcripts. Interestingly, it has been reported that neurons have longer 3'UTR mRNA variants for specific genes compared with other cell types (Tushev et al., 2018), suggesting the importance of this variant for mRNA spatial localization. Furthermore, it has been showed that through alternative poly-adenylation sites, a single gene can generate multiple mRNA transcripts harbouring 3'UTR of different lengths (Bae and Miura, 2020; Miura et al., 2014; Tushev et al., 2018), that is fundamental for mRNA dendritic localization (Tushev et al., 2018) stability (Pickard et al., 2008) and synapse function (Kuklin et al., 2017). The physiological significance of the two forms of mRNAs encoding the same protein has been studied in different studies. However, targeting a fraction of BDNF mRNAs to dendrites for local translation would facilitate differential regulation of BDNF functions in dendrites and somata. In the past years, it has been proven that the 3'UTR long can have a role in targeting BDNF mRNA to dendrites (Tang et al., 2008) (An et al., 2008a). By testing a mouse mutant that produces a truncated long BDNF 3' UTR, An et al. demonstrated that the 3' long controls the abundance of dendritic BDNF protein and regulates the pruning and enlargement of dendritic spines. They also reported a selective impairment in LTP at dendritic synapses, but not somatic synapses, in CA1 pyramidal neurons lacking dendritic BDNF mRNA (An et al., 2008). In addition, it has been reported that both long and short 3' UTR sequences promote dendritic targeting of a GFP reporter mRNA in response to stimuli such as KCl and selectively to NT-3 (short 3'UTR) or BDNF (long 3'UTR), suggesting that the localization is regulated by different sets of stimuli with strong implications on the local modulation of synaptic plasticity (Vicario et al., 2015). It has been showed that the majority of the hippocampal cytoplasmic BDNF mRNAs carry the short 3′UTR, which is actively translated and serves as the primary source of BDNF production at basal levels of neuronal activity. In contrast, the BDNF long 3′UTR has been reported to be a suppressor for BDNF translation at rest. However, the long 3′UTR, but not the short 3′UTR, is sufficient to elicit rapid and activity-dependent translation from a reporter mRNA in cultured hippocampal neurons. Furthermore, upon seizure-

induced neuronal activation, the endogenous long 3′UTR BDNF mRNA specifically undergoes robust translational activation in the hippocampus before transcriptional up-regulation of BDNF, which is temporally and spatially associated with a marked activation of TrkB. These results provide evidence for activity-dependent translational regulation of BDNF mediated by the distinct 3′UTRs, which offers a unique mechanism for controlling TrkB signalling to accommodate neuronal function (Lau et al., 2010). Considering the localization of the constructs containing the 3'UTR, An et al., (2008a) and Orefice et al., (2013) proposed that the short variant is restricted to the cell body promoting the neuronal survival and spine formation. However, this hypothesis is still discussed: the 3' UTR short sequence has been reported to have a role in the increment of dendritic branching over a wide range of distances from the soma; on the contrary, the 3'UTR long has been reported to act in a small region close to the soma (O'Neill et al., 2018). However, the results presented so far deal with an overexpression of BDNF constructs. Considering this aspect, the research group of Erin Shuman assessed the endogenous BDNF transcripts. They performed 3′ end sequencing on rat hippocampal slices, detecting two isoforms of BDNF containing either a short or a long 3′ untranslated region (3′UTR). They found that most of the BDNF transcripts contained the short 3′UTR and were present in low amounts relative to other neuronal transcripts. They did not clarify which could be the physiological significance of the short variant (Will et al., 2013). In addition, by means of a qPCR analysis, they found that the 3′UTR long isoform exhibits a shorter half-life than the short 3′UTR, observing that this may not be consistent with the hypothesis that 3'UTR long is transported to the dendrites (Will et al., 2013).

1.3 Function

BDNF, as a neurotrophin, supports cell proliferation, cell survival/death, differentiation, dendritogenesis and axonogenesis (McAllister et al., 1997), spine formation and maturation and synaptogenesis. It has been reported that it takes part in brain plasticity-related process, such as memory and learning (Tyler et al., 2002; Yamada et al., 2002). BDNF is essential for proper development of the cortex, maintaining neuronal size and the dendritic arborization (Gorski et al., 2003). Its activity is strictly connected to synaptic plasticity: it is released in activity dependent manner and it can act both on presynaptic TrkB receptors, improving exocytosis of glutamate vesicles, and on postsynaptic TrkB receptors, mediating phosphorylation of NMDAR

and AMPAR with the increment of synaptic efficacy (Leal et al., 2017). Accordingly, alterations in BDNF expression in specific neuronal subpopulations contribute to the onset of various pathologies, including depression, epilepsy, Alzheimer's, Huntington's and Parkinson's disease and Rett syndrome(Binder et al., 2014; Castrén and Rantamäki, 2010; Cheng and Yeh, 2003; Lu and Chow, 1999; Murer et al., 2001; Russo-Neustadt and Chen, 2005; Zuccato et al., 2005). For example, a human single nucleotide polymorphism (Val66Met) that reduces BDNF secretion and localization of the protein in dendrites is associated with reduced memory performance and bipolar disorder (Egan et al., 2003).

1.4 BDNF in LTP

The ability of synapses to change their transmission strength is termed synaptic plasticity. A model for the induction of long-term potentiation (LTP) was proposed in the mid-1980s, remaining substantially unaltered to this day. In brief, binding of glutamate to NMDARs coupled with depolarization of the postsynaptic membrane, which relieves the magnesium channel block, results in the entry of calcium through the NMDAR and a rise in spine calcium (Nicoll et al., 1988). Hippocampal LTP and LTD are arguably the most studied forms of synaptic plasticity. The induction of LTP in hippocampal neurons can be achieved mainly by two strategies: electrical stimulation and chemical stimulation. Through repetitive high-frequency (tetanic) presynaptic stimulation (HFS), in some cases coupled with a steady depolarisation of the postsynaptic neuron (Bekkers and Stevens, 1990),it is possible to induce LTP. Some chemical stimulations that allow molecular changes at potentiated synapses have been introduced, as for example glutamate (50 µM glutamate for 30s in Mg2+ free medium, (Malgaroli and Tsien, 1992)) or glycine (100–200 µM glycine, 5–10 min in Mg2+ free medium, (Shahi and Baudry, 1993)). BDNF is connected to synaptic plasticity and in particular to LTP and long-term depression (LTD). It has been demonstrated that BDNF expression (Castrén et al., 1992, 1993; Lu and Figurov, 1997; Patterson et al., 1992; Zafra et al., 1990) and release (Goodman et al., 1996) are intimately correlated to synaptic activity, showing that BDNF is a prominent factor for mediating the effects of neuronal activity. It is well-established that BDNF can exert its fast effects on synaptic transmission through post-translational modifications of synaptic proteins, modifying synaptic response through a protein synthesis-independent mechanism. A variety of genetic and pharmacological studies suggest that BDNF is necessary for L-LTP to occur. Direct

evidence of the role of BDNF in synaptic transmission came from studies using knockout mice (Korte et al., 1995; Pang and Lu, 2004), in which LTP was severely impaired and then rescued by application of exogenous BDNF or virus-mediated BDNF re-expression (Korte et al., 1996; Patterson et al., 1996), suggesting that an increase in BDNF may contribute to the maintenance of L-LTP. Remarkably, application of exogenous BDNF rescued the L-LTP deficit even when all new protein synthesis is blocked (Pang and Lu, 2004). Similarly, L-LTP is impaired in TrkB knockout mice (Minichiello et al., 1999). Curiously, the classic L-LTP induced by multiple tetani is normal in BDNF+/- mice, suggesting that BDNF is not involved in all forms of long-term synaptic plasticity (Chen et al., 1999; Kang et al., 1997; Patterson et al., 2001). Thus, BDNF may be the key protein synthesis product responsible for the long-term maintenance of L-LTP. Taken together, these results support a model in which LTP-inducing stimuli increase endogenous BDNF and this increase may support the expression of L-LTP. Despite its critical role in L-LTP, BDNF by itself is not able of inducing synaptic potentiation. Earlier reports show that a brief bath application of BDNF for several minutes can trigger a sustained potentiation of synaptic efficacy at CA1 synapses in hippocampal slices (Kang and Schuman, 1995), but this result was hard to be replicated (Malenka and Nicoll, 1999).

1.5 Memory and BDNF

Long term synaptic modification, such as long-term potentiation/ depression (LTP/LTD) and structural plasticity are correlated with memory formation, strengthening and recall suggesting shared mechanisms between synaptic and memory consolidation (Basu and Siegelbaum, 2020). The neurotrophin hypothesis suggests that neuronal activity enhances the expression, secretion and/or actions of NTs at the synapse to modify synaptic transmission and connectivity (Schinder and Poo, 2000), leading to a connection between neuronal activity and synaptic plasticity. It was reported that BDNF mRNA can be transported into neuronal dendrites in an activity- dependent manner in vitro (Tongiorgi et al., 1997) but also in vivo (Capsoni et al., 1999a). Moreover a pharmacological induction of *status epilepticus* also induced to the localization of BDNF in hippocampal laminae containing the apical dendrites of pyramidal neurons and granule cells (Tongiorgi et al., 2004). All the previous findings are in accordance with the above-mentioned hypothesis. Moreover local translation of dendritic BDNF mRNA has

been postulated as a crucial molecular underpinning of the transition between early-long term potentiation (E-LTP) and late-LTP (L-LTP) and, more in general, a crucial step for synaptic tagging (Tanaka et al., 2008). Following the clustered plasticity model (Govindarajan et al., 2011a), a spine receiving a stimulus able to induce long term structural plasticity gets tagged, and this induce protein synthesis. The newly synthetized proteins will be captured and tagged to a spine inducing structural changes. However, a subthreshold stimulus, insufficient to induce protein synthesis itself, is able to capture the proteins from a late-LTP-induced spine when it was clustered within a distance of 50 µm from the LTP spine (Govindarajan et al., 2011a). Cues indicate that the protein synthesis should be local, however the exact location where proteins are synthesized in dendrites is still unknow. Tools able to detect simultaneously mRNA and its translation should enable a better understanding of the issue (Rangaraju et al., 2017).

1.6 Engram and memory

One of the greatest challenges in neuroscience is to understand the structure and the properties of the memory traces in the brain. The term *engram* was introduced by Richard Semon in 1904, roughly corresponding to a “memory trace”. It refers to the lasting physical changes in brain state and structure that occur in response to an event or an experience (Josselyn et al., 2017). In addition to a cellular engram, a synaptic engram can be defined as a combination/ population of tagged synapses that would be necessary and sufficient for the establishment and recall of a given memory. Memory resides in engram cells distributed across the brain. However, the site-specific substrate within these engram cells remains theoretical, even though it is generally accepted that synaptic plasticity encodes memories. Memory storage and retrieval require specific populations of neurons that show increased neuronal activity during memory formation. Several studies have identified these engram cells throughout various brain regions and demonstrated that activated engram cells can induce artificial retrieval of stored memories. Different techniques can be used in order to tag engram cells, such as the GRASP technique (Choi et al., 2018). In the last decade, this technique has been improved in order to have a subpopulation of neurons that express different compounds typical of the pre-synaptic and the post-synaptic environments. It has been showed (Choi et al., 2018) that injecting in two different regions (CA1 and CA3) two viruses expressing the pre-synaptic and the post-synaptic compound respectively, it is possible to map engram and non-engram neurons in brain slices

of a mouse after a contextual fear conditioning test (Figure IX). The advantage of the GRASP technique is that a realistic map of brain regions through single neurons and synapses activated during memory tasks is achievable. Consequently, with the same aim, the tool SYNACTIVE (Gobbo et al., 2017), used in this thesis work, was created in order to map potentiated synapses in the hippocampus.

.

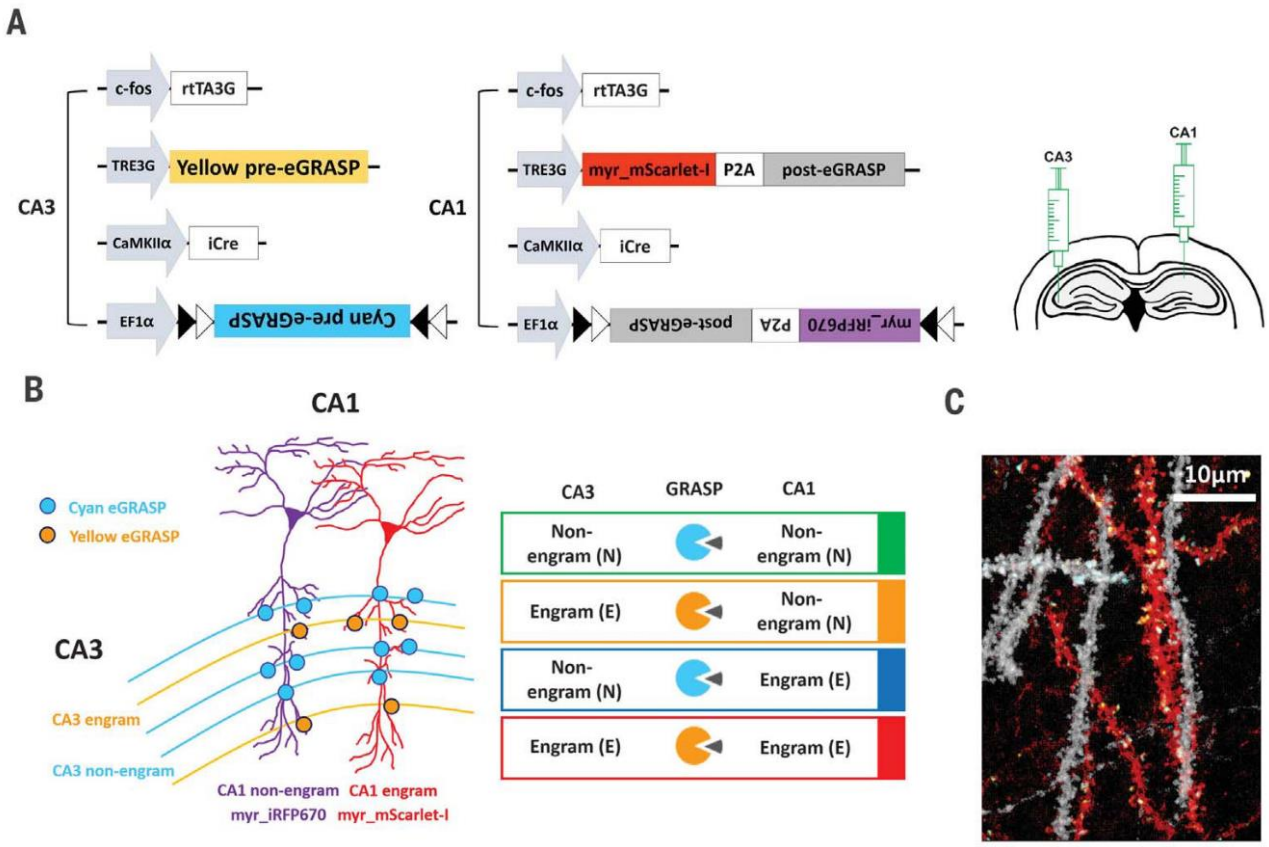

Figure IX: (A) Schematic illustration of injected AAVs. Injection in each site was performed with a complete cocktail of all the virus infected in each site. (B) Schematic diagram of the four possible synapse populations among engram and non-engram cells. (Right) On the right representation of neurons infected with the constructs. Adapted from (Choi et al., 2018)

1.6.1 SYNACTIVE

Recently, a PRIN project called **"**Synaptic engrams in memory formation and recall**"** has been approved by the Italian Ministry of Research in 2017 with the aim to better understand the memory process through the engram paradigm. A group of top scientists with complementary skills and expertise has been working with an innovative tool: a hybrid RNA/protein called SYNACTIVE has been developed to enable selective tagging of potentiated spines following the encoding of a memory. The overarching aim of the project is to use SYNACTIVE to corroborate the concept of synaptic engrams, by mapping potentiated synapses in the hippocampus and ablating or re-activating previously activated synapses. Our group is focused on studying the role of synapse specific BDNF isoforms and the BDNF "spatial code" in the formation of synaptic engrams. SYNACTIVE is constituted by two different constructs: one construct that works as a filler and has the rTTA transactivator responsible for the expression of the second construct, that has a fluorescent synaptic tag followed by Arc RNA sequences. SYNACTIVE expression is controlled by a Tet-responsive TRE promoter, and by the application of Doxycycline, the Tet-off blocking is removed and the expression of the construct is allowed (Figure X).

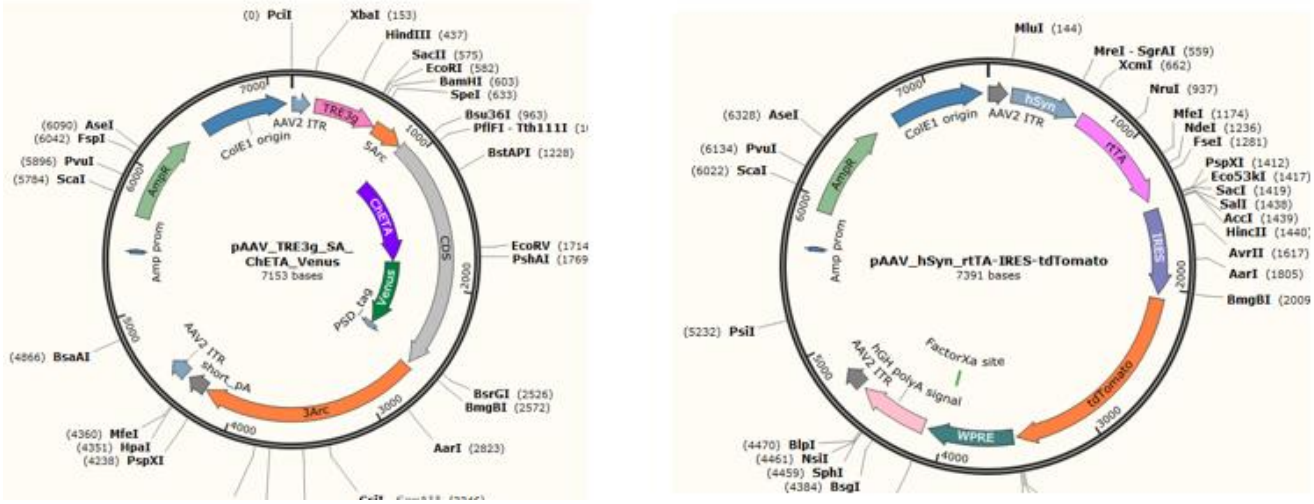

Figure X: Two constructs of the SYNACTIVE tool. On the right the construct that should allow the visualization of potentiate synapses through the Arc gene and the PSD tag with the mVenus fluorophore. On the left the filler construct that allows the filling in tdTomato of neurons. Maps created with SnapGene

Arc is transcribed in an activity-dependent manner and its messenger RNA localizes near synapses that experienced recent activity. In resting conditions, it is believed to be translationally repressed within ribonucleoparticle (RNP) granules (Steward et al., 2015), whereas after a plasticity event, such as the cLTP, the Arc mRNA and protein localize near active synapses (Steward et al., 2015). Consequently, the 5' and the 3' sequence of Arc present in SYNACTIVE, together with the post-synaptic density tag, enable the localization to the activated synapses after cLTP induction (Figure XI). From collaborators of the PRIN project, it has been showed that the SA-Channelrhodopsin variant is locally translated at synapses in *vitro* and in *vivo*, and the exploration of a novel context increases the number of hippocampal synapses expressing the opsin, revealing a non-random distribution of the activated synapses along dendrites.

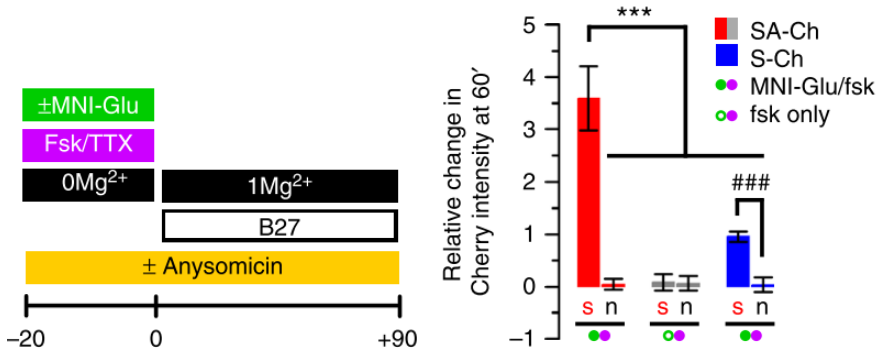

Figure XI: Synactive intensity changed after glutamate uncaging compared with s (activated spines) from the n (not activated one). Adapted from (Gobbo et al., 2017).

1.7 mRNA, LTP and local protein synthesis

The transport of mRNA to the activated synapses and the LTP induction are two faces of the same coin. Considering the molecular level of the LTP induction, there are at least two known phases: an early phase over the first few hours (1-3h), which is protein-synthesis independent, and a late phase (up to 24h), which depends on new protein synthesis (Bailey and Chen, 1983; Bailey et al., 2015; Frey et al., 1988; Stanton and Sarvey, 1984; Sutton and Schuman, 2006). A key mechanism in the field is the synaptic tagging hypothesis, a prominent model that accounts for synapse-specificity of L-LTP (Frey and Morris, 1997). In this hypothesis, a strong

tetanic stimulus induces protein synthesis of these “plasticity-related proteins” (PRPs). These newly synthesized PRPs are subsequently “captured” at the tagged spine leading to spine-specific structural changes. However, it was not clear if these PRPs were synthesized locally in the dendrites or in the soma. In order to address this, another spine was “tagged” by a subthreshold stimulus—insufficient to induce PRP synthesis by itself (S2, S3, Figure XII). It was observed that the subthreshold-tagged spine (S2) was able to show spine-specific structural plasticity by capturing PRPs, only when it was clustered within a distance of ~50 μm from the late-LTP-induced spine (S1). Spines distributed beyond this spatial distance (S3) did not show acquired plasticity, suggesting that PRP synthesis cannot be somatic but has to be local (Govindarajan et al., 2006, 2011b). This effective distance of the cluster is dependent on the number of neighbouring tagged synapses that compete for the limited pool of PRPs. The more neighbouring tagged synapses, the more promptly the PRPs are captured, thereby shortening the spatial spread of the nascent proteins and the size of the effector compartment. However, the specific sets and the spatial spread of mRNAs recruited, and the subsequent proteins newly made are still question of debate in the scientific community. Additional studies were made following single-spine PSD-95 photoactivation, where the photoactivated proteins redistribute and stay “captured” in spines within a defined spatial range of 10–15 μm of a dendritic shaft (Gray et al., 2006). However, these experiments argue that the site of action of nascent proteins (effector compartment) is defined but not limited to the site of synthesis (source compartment) or structural boundaries. It is likely that the intensity of the stimulation, the amount of nascent protein made, the nature of the nascent protein (transmembrane, cytoskeletal, or cytosolic), its diffusional property, and the number of competing slots for trapping the nascent protein influence its spatial spread and functional outcome. An open issue in the field is to define the temporal details of the following processes: redistribution of translational machinery, protein translation, the ensuing spatial spread of the nascent proteins, and their functional outcome. Moreover, more detailed studies should be carried out in order to define how the stimulus strength influences the size of the different translation compartments such as the source compartment, the spatial spread of the nascent protein, the effector compartment, and functional outcome.

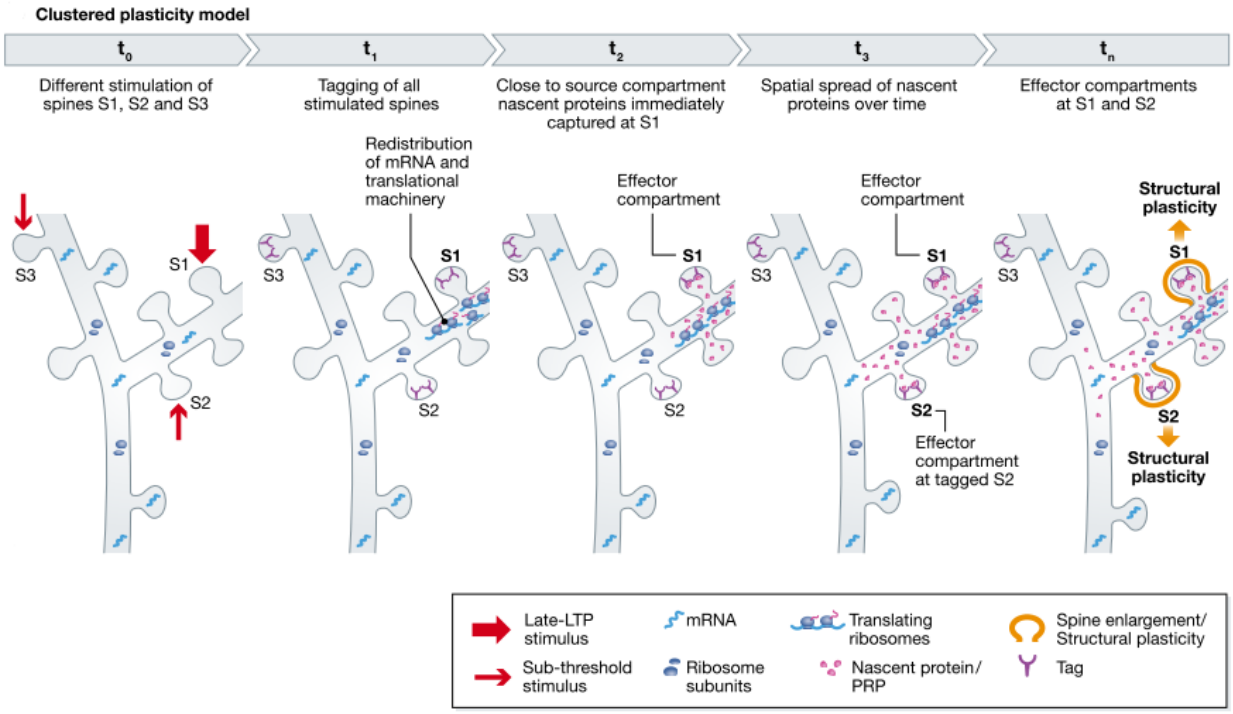

Figure XII: According to the clustered plasticity model, a spine receiving a stimulus that leads to long-term structural plasticity (late-LTP stimulus) (S1) gets "tagged" in a protein synthesis-independent manner and also leads to the synthesis of PRPs. Spines S2 and S3 receive a subthreshold stimulus (t0). All three spines get tagged but mRNA and translational machinery redistribute only close to spine S1 that received the late-LTP stimulus (t1). The newly translated proteins—source compartment—are instantly captured at spine S1 (t2) and with time, the spatial spread of the nascent proteins increases allowing for its additional capture at adjacent tagged spine S2 (t3). Both the tagged spines S1 and S2 that capture nascent proteins—effector compartment—undergo spine-specific structural plasticity—functional outcome (tn). However, only tagged spines clustered within a nascent protein spatial spread of ~50 µm show this functional outcome—tagged spine (S3) present beyond this spatial spread does not. Modified from (Rangaraju et al., 2017)

Several lines of evidence suggest that BDNF could serve as a PRP. First, substantial experimental data support the fact that strong tetani enhance the expression of BDNF as a PRP in the soma of CA1 pyramidal neurons (Castrén et al., 1993; Dragunow et al., 1993; Patterson et al., 1992). This is possibly mediated by BDNF transcription through promoter III (Lee et al., 2005). Microarray experiments demonstrate that strong, L-LTP inducing stimulation results in an increase in the expression of 100 genes, but only three genes qualify statistically as L-LTP specific genes. Among the three, BDNF fits the best as a PRP (Barco et al., 2005). Direct proof of the trafficking of newly synthesized BDNF and its capture at the tetanized synapse has yet to be reported. If BDNF is a PRP, a natural question is whether TrkB, the receptor for BDNF,

can serve as a synaptic tag. A synaptic tag has to satisfy several criteria (Kelleher et al., 2004): 1) the tag can be activated by a weak tetanus that induces only E-LTP; 2) the lifetime of the tag is about 1–2 hours; 3) the activation of the tag does not require protein synthesis; 4) the tag is induced in an input-specific and physically immobile manner; and 5) the tag interacts with PRP for L-LTP. A twist of the “tagging” model here is that the PRP (BDNF) needs to be secreted before it can be captured by the tag (TrkB). Demonstrating that TrkB is a “synaptic tag” represents the ultimate challenge in the hypothesis that BDNF-TrkB is a PRP-tag pair in synaptic tagging.

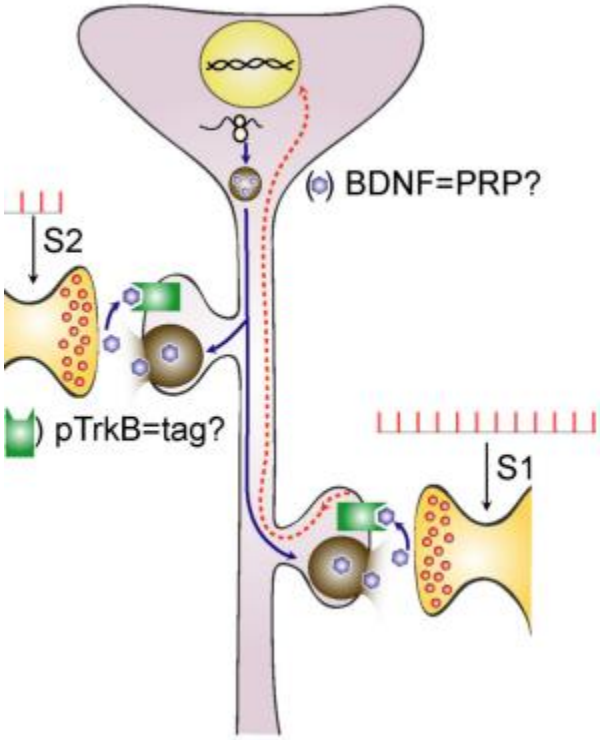

Figure XIII: Short-lived synaptic tag can be generated by strong tetanus and weak tetanus, while the PRPs can only be induced by strong tetanus. When one afferent pathway (S1) is activated by strong tetanus, a weak tetanus applied to a second independent pathway (S2) usually induces L-LTP because it creates a tag that captures the PRP induced by the strong tetanus in S1.(Lu et al., 2008)

Therefore, the synthesis of new protein is essential for the development of long-term memory. That is why the demonstration that new protein synthesis can occur locally at active synapses (Kang and Schuman, 1996; Wu et al., 2016) is a key finding for the issue. Thanks to the translation of locally available mRNAs through ribosomes, the synthesis of the encoded protein and its integration into the synapse is possible, this allows the rearrangement of the synaptic proteome, and it affects synaptic plasticity (Doyle and Kiebler, 2011). Recently, the dendritic protein synthesis sites have been observed, thanks to sophisticated and cutting-edge technologies (DNA U-PAINT, and BONCAT assay) and by labelling and measuring both

assembled ribosomes and nascent proteins in mature, cultured rat hippocampal neurons. A cohort of newly synthesized proteins has been monitored, correlating their spatial distribution with that of assembled ribosomes over time, following locally and globally induced plasticity. A widespread protein synthesis near synapses under both basal and stimulated conditions was reported (Sun et al., 2021) (Figure XIV).

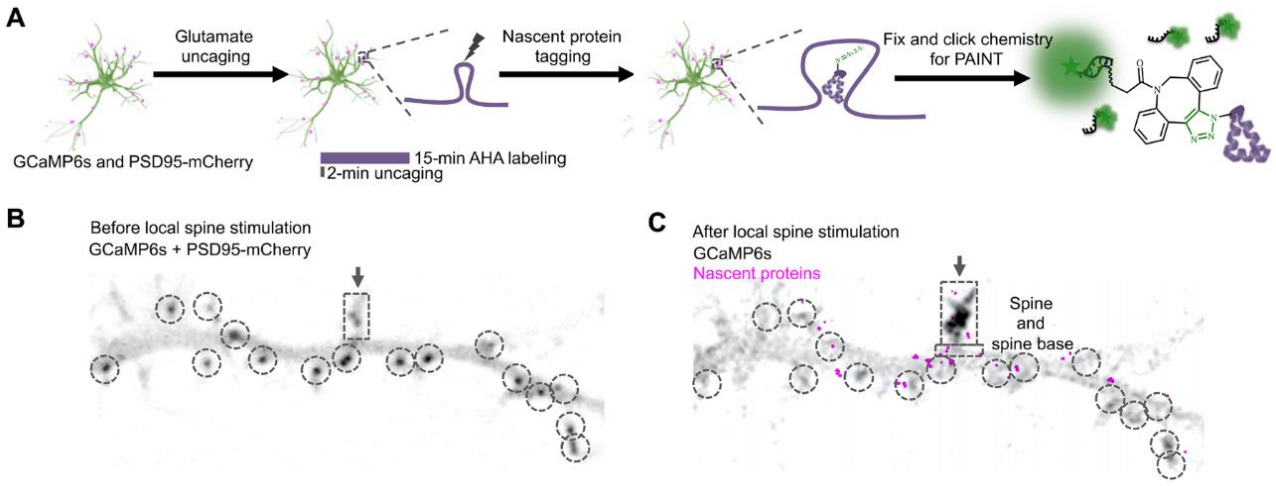

Figure XIV: Single-spine stimulation induced a local increase in nascent protein among nearby synapses. (A) Cultured rat hippocampal neurons were transfected with GCaMP6s and PSD95-mCherry before single-spine stimulation (two-photon glutamate uncaging in AHA-containing buffer). (B) Spinning disk micrograph with overlay of GCaMP6s and PSD95-mCherry showing the spine of interest before local stimulation (dashed box) and its neighbouring synapses (encircled dark puncta). Scale bar, 2 µm. (C) After spine stimulation in magenta are showed locally translated nascent proteins. Taken from (Sun et al., 2021).

Recently, it has also been showed that by chemical silencing of neuronal activity the mRNA trafficking to the synapses was impaired (Bauer et al., 2019). In addition, Schuman et al. have reported that after two distinct stimula (cLTP and mGluR-LTD) the mRNA dynamic of three different transcripts is attenuated in comparison with control conditions (Donlin-asp et al., 2021). Furthermore, by means of a Puro-PLA method that permits to couple a general labelling of nascent protein with a specific label for a protein of interest, they observed a locally protein synthesis after the plasticity events. The mechanism by which an mRNAs associated with activated synapses become translational activated likely depends on signaling cascades underlying various forms of synaptic plasticity. In fact, specific signaling cascades are turned on by distinct forms of plasticity (Malenka and Bear, 2004). These cascades likely influence

changes in posttranslational modifications of RBPs on particular transcripts, regulating their "translatability."

1.8 RNA

1.8.1 mRNA in dendrites

Neurons are highly polarized cells with a soma, an axon and multiple dendrites. Along with this structure a particular efficient mechanism of intracellular trafficking driving maintenance and functionality of neurons is necessary. The subcellular compartmentalization of messenger RNAs is a common feature of highly polarized cells and represents an efficient way to concentrate particular proteins in a specific subcellular district because of the possible local regulation of their translation into protein. There is evidence that in dendrites are present all the components of translational machinery including endoplasmatic reticulum and Golgi apparatus (Pierce et al., 2000). At the same time, hundreds of mRNAs from the dendrites have been isolated and studied through *in situ* hybridization analysis such for example: BDNF and TrkB (Tongiorgi et al., 1997), Arc mRNA (Guzowski et al., 2000), CamkIIa (Donlin-asp et al., 2021), MAP2 (Garner et al., 1988). Some mRNAs have been studied also in living neurons: CamkII (Rook et al., 2000), Psd95 (Donlin-asp et al., 2021), β-Actin (Turner-Bridger et al., 2018). Early microarray approaches identified ∼285 mRNAs (Poon et al., 2006; Zhong et al., 2006) in dendrites and the high-throughput in situ hybridization screen performed by the Allen Brain Project identified only 68 mRNAs in the synaptic neuropil (Lein et al., 2007). However, the number of mRNA present in the dendrites have been increased recently by the huge progress of RNAseq. In fact, deep sequencing has revealed over 2,500 mRNAs present in the hippocampal neuropil (Cajigas et al., 2012). Surprisingly this number is largely caused by previously undetected neuropil mRNAs, suggesting that mRNA localization may be more of a rule, than the exception (Cajigas et al., 2012). These data sets suggest an enormous potential for protein translation that is independent of the principal cell somata and resident locally within the neuropil. Moreover, the presence of specific transcripts and the local translational machinery in spines suggests that the local translation is regulated in an activity dependent manner. The mechanism that allows these mRNA to be targeted in dendrites can be explained

as follow: once the mRNA is transcribed and spliced in the nucleus, it is exported from the nucleus to the cytoplasm. There, it is packed into translationally repressed ribonuclear particles (RNPs) containing many proteins, including RNPs (Doyle and Kiebler, 2011). In particular the presence of cis-acting localization elements (LEs) or zip-codes generally located in the 3' untranslated region (3' UTR) of localized transcripts, and the recognition of these signals by trans-acting RNA-binding proteins, (RBPs) allows the assembly of RBPs with their cargo RNAs into transport ribonucleoprotein particles (RNPs). For example, sorting signals, usually within the 3´untranslated region (3´UTR) of the mRNA, play a crucial role in mRNA localization(Holt and Bullock, 2009; Martin and Ephrussi, 2009; Mayr, 2017). Such signals are able to interact with specific RNA binding proteins (RBPs), such as ZBP1, FMRP or Staufen2 (Stau2), to form neuronal RNA granules (Dictenberg et al., 2008; Fernandez-Moya et al., 2014; Kiebler and Bassell, 2006). Analysis of the RNA granule composition has led to the "RNA operon theory" (Keene and Tenenbaum, 2002), according to which several mRNAs with similar functions, such for example the ones involved in synaptic plasticity, share common signals and RBPs. The presence of a limited number of cis-acting signals and the trans-acting factors, present in each transcript, can determine a unique scenario for finely regulate mRNA localization and expression. The transport is ranging from active transport by motor proteins along the cytoskeleton to diffusion and trapping by a localized anchor as well as local protection from degradation (Palacios and St Johnston, 2001; St Johnston, 2005). However, the most studied way of transport is the active transport by motor proteins by which the particles are transported along microtubules and microfilaments, the “railway” of the neuron. One example of these proteins is the Kinesin 17, present in the dendrites (Kanai et al., 2004). The observed velocities of RNPs in various publications are all consistent with motor-driven transport (Köhrmann et al., 1999; Park et al., 2014) (Köhrmann et al., 6.4 µm/min; Park et al., 1.3 µm/s). If dependent on motor proteins, then the directed displacement of RNPs along microtubules is an ATP dependent process and must be regulated at a cellular level. However, the mechanism by which the mRNA is transported along dendrites is still a matter of debate in the scientific community. One of the major hypotheses is that the mRNA, together with RNPs patrol a group of synapses in dendrites as a “sushi belt” transport (Doyle and Kiebler, 2011). Following the comparison to the transport of sushi on a circulating conveyor belt to the customers in a restaurant: the RNPs patrol dendrites in multiple directions and they are not irreversibly anchored at one destination (the synapse) but, a specific cue, such as synaptic activity, would result in the local capture of

an RNP, where the mRNA (in a repression state) can be released, and the translation can occur. If a particular synapse becomes activated, it may recruit dynamic microtubules that extend into dendritic spines allowing specific delivery of RNPs (Figure XV).

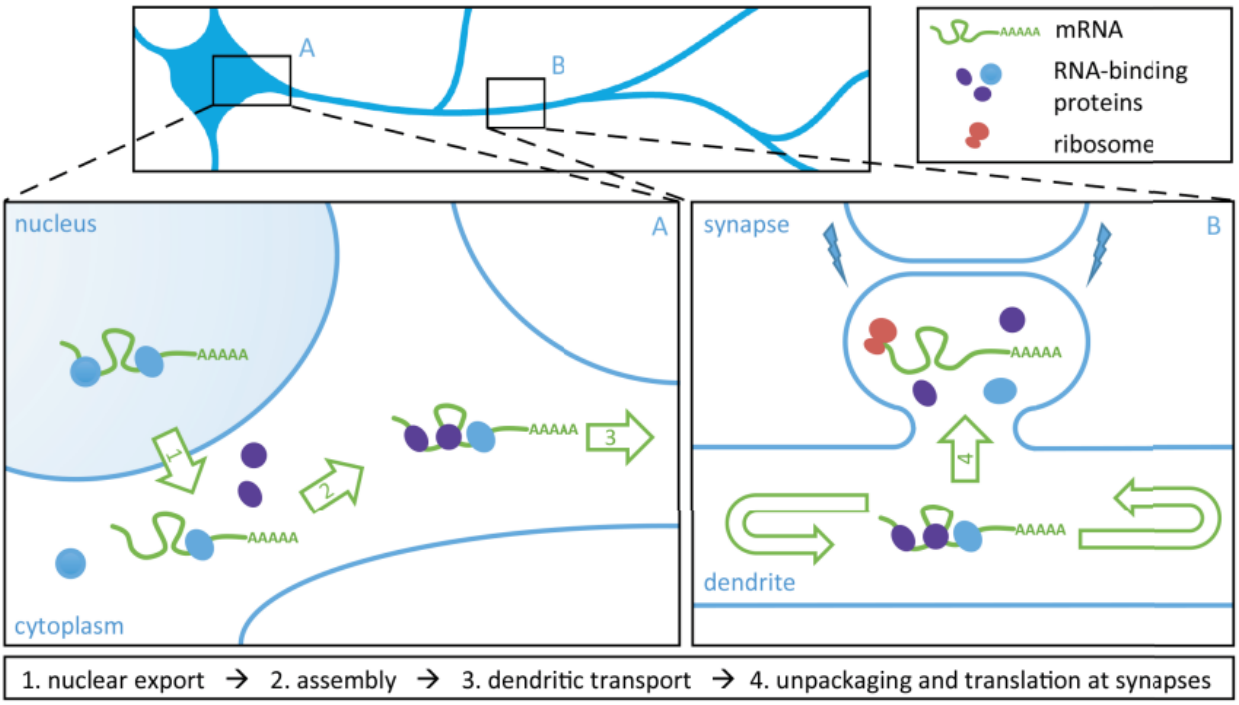

Figure XV: Model of neuronal mRNA transport and local translation at synapses. Insets A and B represent the soma (A) and dendritic compartment (B) of a schematic neuron. Neuronal mRNA transport, processing and translation is illustrated step by step by numbered green arrows. This model is based on Doyle and Kiebler, EMBO Journal, 2011.

This allows a specific and strictly correlation with the localization of mRNA and the localization of newly protein. During mRNA translation, multiple ribosomes can occupy an individual mRNA (a complex known as a polysome), resulting in the generation of multiple copies of the encoded protein. Polysomes have been detected in neuronal dendrites (Ostroff et al., 2002). Interestingly, it has been recently reported that also monosomes can actively translate proteins. In addition to that, monosomes are reported to be the preferred mode of protein synthesis in neuronal processes with the presumable role to satisfy the local proteins demands under basal conditions (Biever et al., 2020). Recently, as it has been reported (Donlin-asp et al., 2021) that the mRNA sequestration alone does not lead always to translation, which is what happens after a plasticity event (cLTP and mGLUR-LTD)(Donlin-asp et al., 2021). However, following

the model of the sushi belt, a fraction of mRNAs is constantly in flux, moving in dendrites and waiting to be tagged to a synapse. This mechanism is somehow energy demanding for the cell because of the motor protein which are ATP dependent. Considering this last observation, it is plausible that pools of static mRNA are present in some specific regions and that they move at the occurrence. Several groups (Chiaruttini et al., 2009a; Huang et al., 2003; Schuman et al., 2006; Tiruchinapalli et al., 2003; Vicario et al., 2015) have studied the dynamics of the transport of RNA granules reporting that in most of the cases the granules are stationary, while a minor fraction displays oscillatory movements as well as anterograde and retrograde movements. The mechanism described above for the RBPs formation and aggregation, can be impaired or impeded by some mutations. It was reported that Fragile-X syndrome is connected to alteration of RBPs and dysregulated local protein synthesis (Bassell and Warren, 2008) and unpublished data from the laboratory are going in the same direction shedding light to similar mechanism for the Rett syndrome. In fact, proteins involved in the formation of transporting granules (TG) stress granules (SG) and processing body granules (PB) were analysed *in vitro* cultures of primary hippocampal neurons confirming a dysregulation of them in Rett syndrome neurons. Additional proof on the dynamics of these granules in live condition are necessary to confirm the hypotheses.

1.8.2 BDNF mRNA in dendrites

The first evidence that BDNF mRNA was present in mature dendrites was reported in 1997 (Tongiorgi et al., 1997) thanks to the study of hippocampal rat neuronal cultures (Figure XVI).

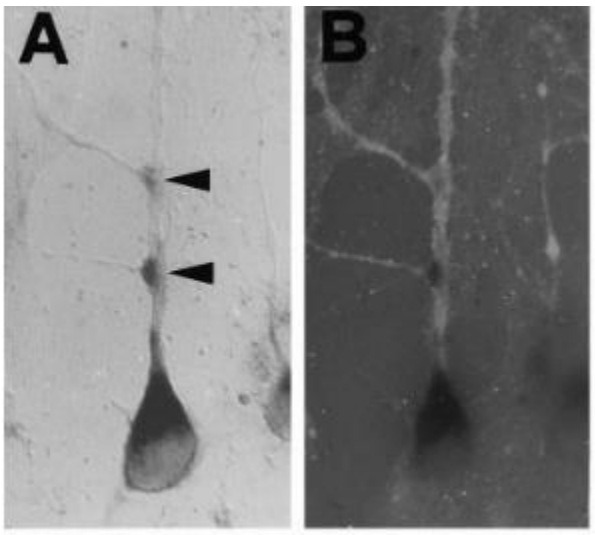

Figure XVI: Subcellular distribution of BDNF mRNAs in cultured hippocampal neurons. Staining by nonradioactive in situ hybridization with digoxigenin-labelled riboprobes and oligonucleotides. A) The BDNF riboprobe labels the cell soma and a dendrite B) Double-labelling with an anti-MAP2 monoclonal antibody. Modified from (Tongiorgi et al., 1997)

In hippocampal neurons under basal conditions, BDNF mRNAs was found at an average distance of 31.5 μm from the cell soma considering all types of dendrites, and within a range of 30–100 μm from the cell soma, when considering apical dendrites only. However, in response to tetanic electrical activity induced by elevated concentrations of KCl (10 or 20 mM), these mRNAs extended to the distal dendrites (at distance > 100 μm). Some years before, the L. Maffei's laboratory contributed to the investigation of the role of BDNF in activity-dependent plasticity, by investigating the expression of BDNF mRNA and protein in the rat visual cortex (Bozzi et al., 1995). The main results of this work were that cortical BDNF expression is up-regulated by pharmacologically increasing cortical activity and down-regulated by decreasing electrical activity afferent to the visual cortex. Similar results have been reported also in vivo, showing an accumulation of BDNF mRNA into distal dendrites in response to visual activity (Capsoni et al., 1999b) or seizures (Simonato et al., 2002; Tongiorgi et al., 2004). Subsequent studies proved that neuronal activity enhances the dendritic trafficking of BDNF mRNA both in cultured hippocampal neurons and in CA1 neurons in vivo (Simonato et al., 2002). The first step in the cascade of events leading to this phenomenon appears to be the activation of NMDA receptors. In *vitro* and *in vivo* evidence supports this idea: (1) in culture, electrical activity-dependent dendritic targeting of both BDNF mRNA can be completely abolished by blockers of glutamate receptors (Tongiorgi et al., 1997); (2) in vivo, the NMDA receptor antagonist (MK801) blocks seizure-induced dendritic targeting of BDNF mRNA (Tongiorgi et al., 2004). Dendritic targeting of BDNF mRNA does not appear to depend on an increase in gene transcription, because NMDA receptor agonists do not induce BDNF mRNA expression (Zafra et al., 1990), and because activity dependent BDNF mRNA targeting in vitro occurs without new mRNA transcription (Tongiorgi et al., 1997). Accumulation of BDNF mRNA in distal dendrites requires the presence of Ca2+ in the external culture medium and Ca2+ influx into the cell through glutamate receptors (NMDA-type) and voltage-gated L-type Ca2+ channels (Righi et al., 2000; Tongiorgi et al., 1997, 2004). This first study, however, did not address the important question of whether the mRNA for BDNF is present in distal dendrites constitutively. Through high resolution in situ hybridization on rat brain sections at the electron microscopy level, BDNF mRNA has been found to be localized in apical dendrites of CA1 neurons of untreated animals, at distances greater than 70 μm from the soma (Tongiorgi et al., 2004). More recent findings

by the group of Erin Schuman addressed the constitutive localization of BDNF. Using a next-generation sequencing and high-resolution in situ hybridization approach in the rat hippocampus, the question of the localization of BDNF was examined again, shedding light on the prevalence of BDNF mRNA in the somatic compartment of rat hippocampal slices or the somata of cultured rat hippocampal neurons. While it was rarely detected in the dendritic processes, pharmacological stimulation of hippocampal neurons induced BDNF expression but did not change the ratio of BDNF isoform abundance. The findings indicate that endogenous BDNF mRNA, although weakly abundant, is primarily localized to the somatic compartment of hippocampal neurons(Will et al., 2013). Other past experiments on binocular visual experience deprivation (Capsoni et al., 1999a) or local treatment of the visual cortex with tetrodoxin (Pattabiraman et al., 2005) demonstrated that translocation of BDNF mRNAs to dendrites, especially those encoding exon VI, is dependent on electrical activity. Concomitantly, different BDNF splice variants were found to have specific intracellular localizations in rat hippocampal neurons after an epileptogenic-inducing stimulus (Chiaruttini et al., 2009a). Under basal conditions, no BDNF mRNA splice variants were detected in distal dendrites; however, in response to pilocarpine administration, exons II and VI were found in the dendrites, whereas I and IV continued to be confined to cell soma. Curiously, after kainate administration, only exon VI was found in dendrites. Since the pilocarpine model induces a more dramatic status epilepticus than kainate, the different pattern of distribution of BDNF mRNA is thought to be involved with its main targeting to the most active synapses. Overall, these results suggest that activity dependent expression of different splice variants may act as a spatial code, supporting the accurate delivery of BDNF to specific targets in the cell soma or along the dendrites, where it can have diversified functions (Tongiorgi and Baj, 2008). Different regions were important in the dendritic signal localization and in the translation regulatory systems. Regions at the 5' UTR and on the 3' UTR were already discussed in a previous Section. In addition, it has been reported that a target site in which translin can bind is present in the CDS (Chiaruttini et al., 2009a).

1.9 BDNF protein in dendrites

BDNF mRNA studies and BDNF protein studies are strictly correlated in the panorama of synaptic tagging and LTP maintenance. Although, it has been reported that the unstimulated

basal abundance of both BDNF mRNA (Herzog et al., 1994) and protein (Dieni et al., 2012) are low in the brain (Conner et al., 1997) and also during development (Webster et al., 2006), it has to be mentioned that the transcription of BDNF is regulated by many processes, including diverse promoters (Pruunsild et al., 2007), DNA methylation (Cheng and Yeh, 2003), and alternative splicing (Pruunsild et al., 2007), suggesting that there is high possibility for increased BDNF expression. The half-life of BDNF has been measured to be 6.8 hours for the CDS and 3.2 hours for the 3′UTR long (Will et al., 2013) as expected for an activity-induced gene for which the half-life is generally shorter compared to the half-lives of not activity-induced neuronal mRNAs, which range from 16 to 24 hours (Schwanhäusser et al., 2011; Yang et al., 2003). The research group of Erin Schuman has reported an extensive next sequencing analysis that under basal conditions, BDNF protein translation is most likely to take place in the somatic compartment where the mRNA is located. When BDNF is overexpressed, it is possible to detect it in other compartments (Orefice et al., 2013), and it is also possible that some forms of physiological stimulation result in high transcript abundance and, consequently, the presence of the mRNA and/or protein in dendrites. However, it has also been reported that a brief depolarization by KCl is able to increase the endogenous protein levels of both BDNF and TrkB in distal dendrites. Since this increase occurred within 10 minutes, up to distances greater than 100 µm from the cell soma and BDNF protein trafficking is 0.1 µm/s (equivalent to 6 µm/min), it is unlikely that the protein level increase is due to transport of BDNF or TrkB from the cell soma. In addition, protein up-regulation occurred even under conditions in which microtubule-mediated transport was disrupted by application of nocodazole. This study strongly suggested that BDNF and TrkB mRNAs localized to the distal dendrites can be locally translated into protein (Tongiorgi et al., 1997). Using electron microscopy, BDNF has been reported together with polyribosomes (Tongiorgi et al., 2004) suggesting active translation**.** Others studies reported the translation of BDNF protein in hippocampal neurons (Baj et al., 2013; Verpelli et al., 2010). However, as already mentioned, different splice variants encode the same BDNF protein (Pruunsild et al., 2007), allowing to a redundancy necessary for the proper distribution of BDNF mRNA in order to respond to different conditions and to fulfil region-specific requests. It has been studied that different variants have different translatability and produce different quantity of BDNF in response to different neurotransmitters: in the order, from the most to the least translatable, 2a, 5, 3, 7, 8, 4, 1, 2b, 2c, 6, thus constituting a quantitative code (Vaghi et al., 2014). Segregated BDNF transcripts support local translation of BDNF protein with spatially

restricted effects on dendrites branching complexity (Baj et al., 2011).Taking into consideration that local BDNF synthesis plays a critical role in L-LTP, then the dendritic localization of BDNF mRNA is necessary. A conceptually more challenging issue is how locally synthesized secretory or transmembrane proteins get processed. There are number of post-translational modifications for BDNF, including glycosylation, proper folding, cleavage and sorting to constitutive or regulated secretion pathway. Folding and N-glycosylation are processed in ER whereas cleavage and sorting occur in Golgi apparatus. In the past years, Ehlers and colleagues demonstrated that at least in cultured hippocampal neurons, Golgi apparatus are absent in majority of dendrites (Cui-Wang et al., 2012; Horton and Ehlers, 2003). However, it has been showed that small Golgi-like organelles (so-called Golgi outposts) are selectively localized to dendritic branch points (Figure XVII). This study poses a number of important conceptual challenges to local synthesis of BDNF. First, most dendritically synthesized BDNF has to be transported back to the neuronal soma to be processed in Golgi apparatus. Second, even in the long (apical) dendrite, BDNF synthesized in distal dendrites still needs to be transported to the branch point to be sorted in the Golgi outposts. In both cases, a round-trip trafficking of BDNF is implicated, and synapse specificity is lost. Third, assuming that locally translated BDNF could be secreted after glycosylation and correctly folded in ERs in the distal dendrites without Golgi, it would only be secreted in a constitutive manner in the form of proBDNF, because sorting to the regulated secretion pathway and intracellular cleavage can only happen in Golgi. The requirement of round-trip transport for BDNF processing makes it difficult to ensure a selective modulation of the stimulated synapse (A in Figure XVII) without affecting other synapses (B and C in Figure XVII). Additional studies on the trafficking of BDNF protein in dendrites in basal and after stimulation are therefore required.

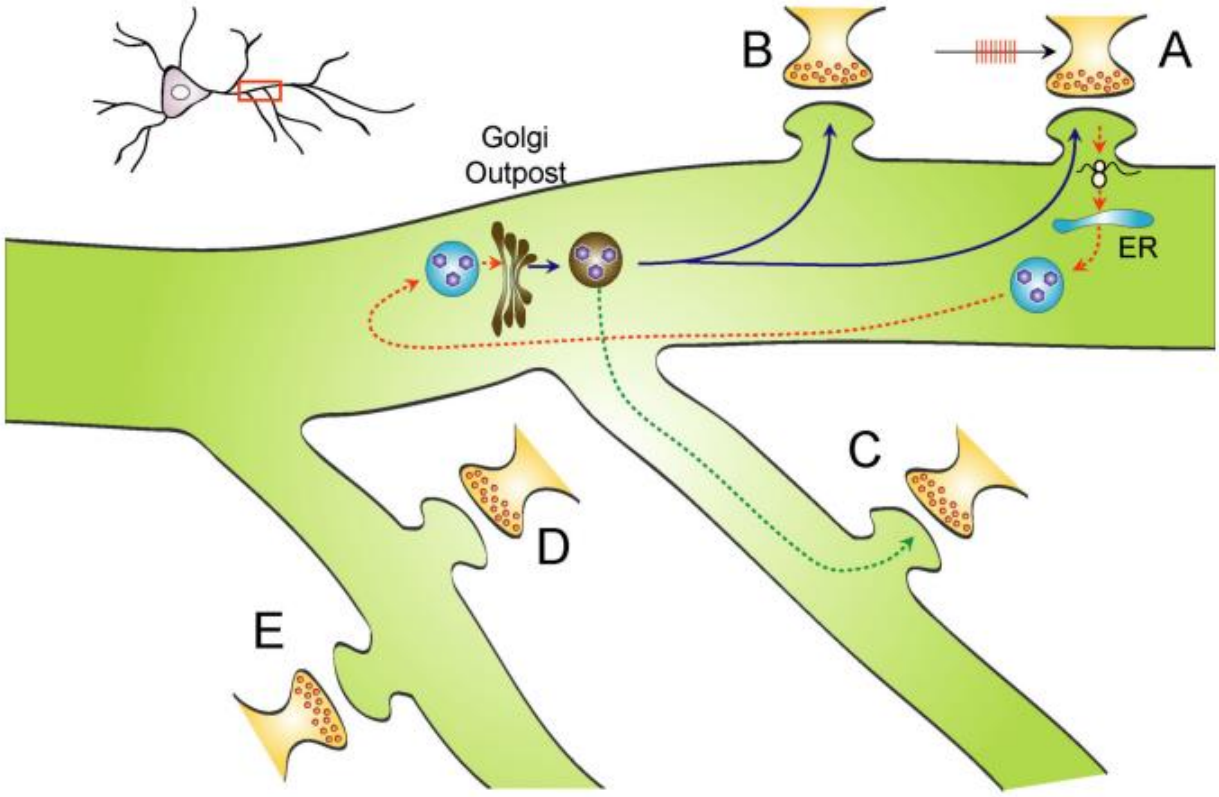

Figure XVII: Synaptic specificity is lost after locally synthesized proteins at stimulated synapses. When synapse A is stimulated with L-LTP inducing protocol, local protein synthesis is initiated. Since no Golgi apparatus is present at synapses, these proteins have to be delivered to Golgi in other places for processing, such as Golgi outpost at dendritic branch point. The newly processed proteins could be shipped back from Golgi to synapse A as well as synapse B on the same dendrite or synapse C on a different dendrite that share the same Golgi outpost. Synapses D and E are less likely to be affected (Pang and Lu, 2004)

Considering all these data it seems feasible that local translation of BDNF in dendrites can occur, but still a clear demonstration with exhaustive and cutting-edge technology is required. Using for example the proximity ligation assay (PLA), a strategy that detects the spatial coincidence of two antibodies: one that identifies a newly synthesized protein tagged with either FUNCAT or puromycylation and another that identifies a specific epitope in a protein of interest (POI) (Dieck et al., 2015) could be possible to see locally endogenous BDNF protein translation (Figure XVIII).

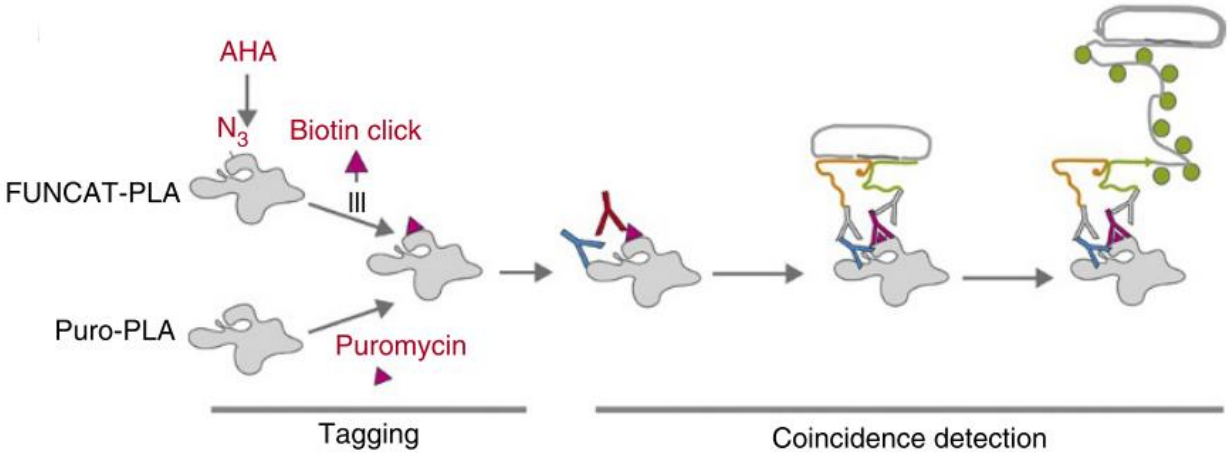

Figure XVIII: Specific labelling of newly synthesized proteins with FUNCAT-PLA and Puro-PLA. Newly synthesized proteins incorporate either with a non-canonical methionine surrogate, azidohomoalanine (AHA) or puromycin. AHA is biotinylated by click chemistry. Antibody (magenta Y) recognition of the 'newly synthesized' tag (biotin or puromycin, magenta triangle) and recognition of a POI (protein of interest) by a protein-specific antibody (blue Y) detects close proximity when PLA minus and PLA plus oligonucleotides (yellow and green squiggles) coupled to secondary antibodies (gray Y) are close enough to serve as a template arranging linker oligonucleotides such that subsequent formation of a circular product by a ligase and rolling-circle amplification is possible. Signal is obtained by binding of fluorescently coupled detection probes (green circles). Modified from (Dieck et al., 2015)

1.10 How to visualize RNA in living cells

There are different known methods to track mRNA in vitro. Some of them such, as the FISH or the RNA scope, requires a fixed sample. The hybridization *in situ* is a quite old, but still commonly used technique that through the hybridization between an RNA and its complementary sequence, permits to localize the RNA of interest (Gall and Pardue, 1969). Some other techniques can be used in living samples because they do not destroy, damage, or affect the sample in a way that would influence the biological read-out, but at the same time they introduce a detectable reporter into the cell, which specifically labels an RNA. Multiple methods have been developed and they can be divided in two main groups: one group that relies on a protein that binds to an RNA element and another group that relies on small molecules. The RNA element can be genetically encoded or can be endogenous RNA. For detecting endogenous RNA, molecular beacons have been used successfully in recent years (Donlin-asp et al., 2021; Turner-Bridger et al., 2018). Molecular beacons are oligonucleotide-based probes with a stem loop where the sequence in the loop is designed to hybridize with endogenous RNA of interest, and the termini are modified with a fluorophore and a quencher

(Mao et al., 2020). These probes are dark in the unbound state because the quencher is held in proximity to the fluorophore, while when they hybridize with the target RNA sequence, the beacon unzips and the fluorescence is visible (Figure XIX).

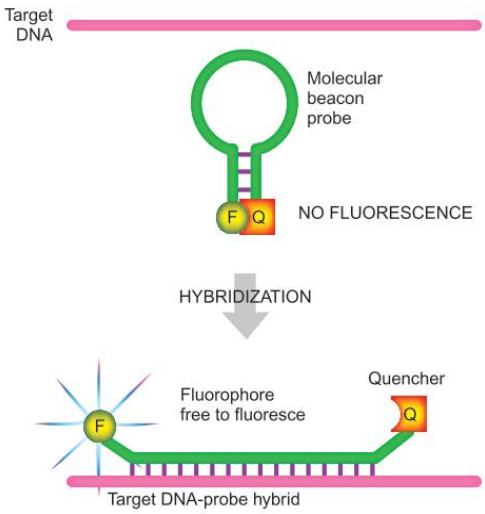

Figure XIX: A molecular beacon is a probe that has two engineered regions at the ends of the probe sequence. On the 5' side, a fluorescent tag is added (F), and on the 3' side, a quenching group is added (Q). Just inside the two tags are six base pairs that can form a stem-loop structure. In this state the probe cannot fluoresce. When the probe binds to the target sequence, the stem-loop structure is lost. Since the quenching group is no longer next to the fluorescent tag, the probe can now fluoresce. Taken from (David P. Clark, 2013)

However, their success depends on the sample and on the method by which they are introduced in the cell. It has been reported that fluorescently labelled probes enter in the endosomal/lysosomal pathway with the concomitant nuclease-mediated degradation. For this reason, a delivery method in which molecular beacons could enter the cell cytoplasm evading the endosomal pathway is highly desirable, such for instance microinjection or electroporation. In the table below, we report a schematic representation of the methods available for tracking RNA in live (Figure XX). The method employed in this thesis work is the MS2 system.

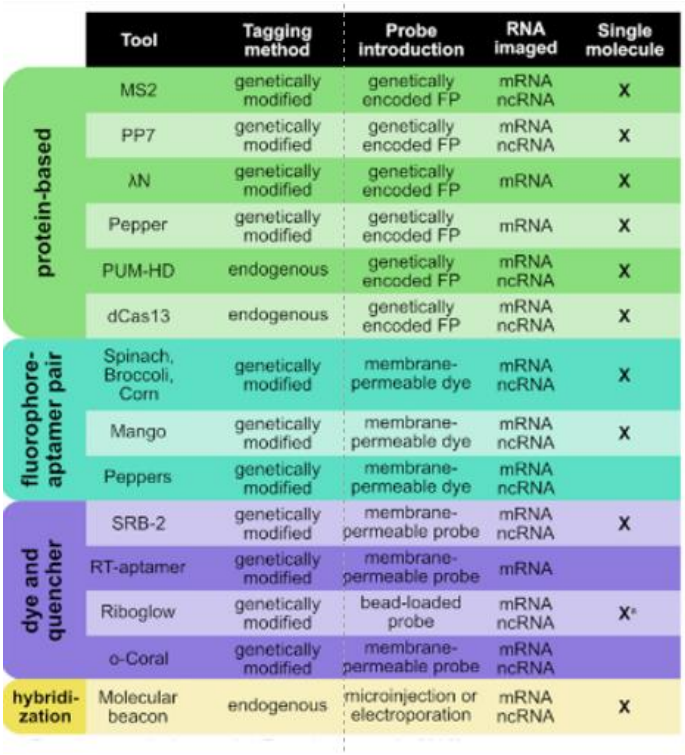

	Tool	Tagging method	Probe introduction	RNA imaged	Single molecule
protein-based	MS2	genetically modified	genetically encoded FP	mRNA ncRNA	x
	PP7	genetically modified	genetically encoded FP	mRNA ncRNA	x
	λN	genetically modified	genetically encoded FP	mRNA	x
	Pepper	genetically modified	genetically encoded FP	mRNA	x
	PUM-HD	endogenous	genetically encoded FP	mRNA ncRNA	x
	dCas13	endogenous	genetically encoded FP	mRNA ncRNA	x
fluorophore-aptamer pair	Spinach, Broccoli, Corn	genetically modified	membrane-permeable dye	mRNA ncRNA	x
	Mango	genetically modified	membrane-permeable dye	mRNA ncRNA	x
	Peppers	genetically modified	membrane-permeable dye	mRNA ncRNA	
dye and quencher	SRB-2	genetically modified	membrane-permeable probe	mRNA ncRNA	x
	RT-aptamer	genetically modified	membrane-permeable probe	mRNA	
	Riboglow	genetically modified	bead-loaded probe	mRNA ncRNA	x*
	o-Coral	genetically modified	membrane-permeable probe	mRNA ncRNA	
hybridi-zation	Molecular beacon	endogenous	microinjection or electroporation	mRNA ncRNA	x

Figure XX: Summary of tools for visualize RNA in living cells. Taken from (Braselmann et al., 2020).

1.11 MS2 system

The MS2 system was pioneered by the Singer Lab in the1990s. The MS2 system has been well established and greatly improved upon in the last decades (Bauer et al., 2017; Bertrand et al., 1998).To date, the system has been modified to address multiple biological questions and remains the most widely used RNA imaging system today. It was developed from MS2 bacteriophage coat protein dimers that bind to the RNA genome (Peabody, 1993). MS2 coat proteins (MCPs) are 129-amino acid proteins that form homodimers (Golmohammadi et al., 1993), they are fused to a fluorescent protein (mcherry for example). MS2 binding sites are 21-

nt RNA stem loops (abbreviated MS2) with a conserved loop region and bulge (Figure XXI) (Johansson et al., 1997).

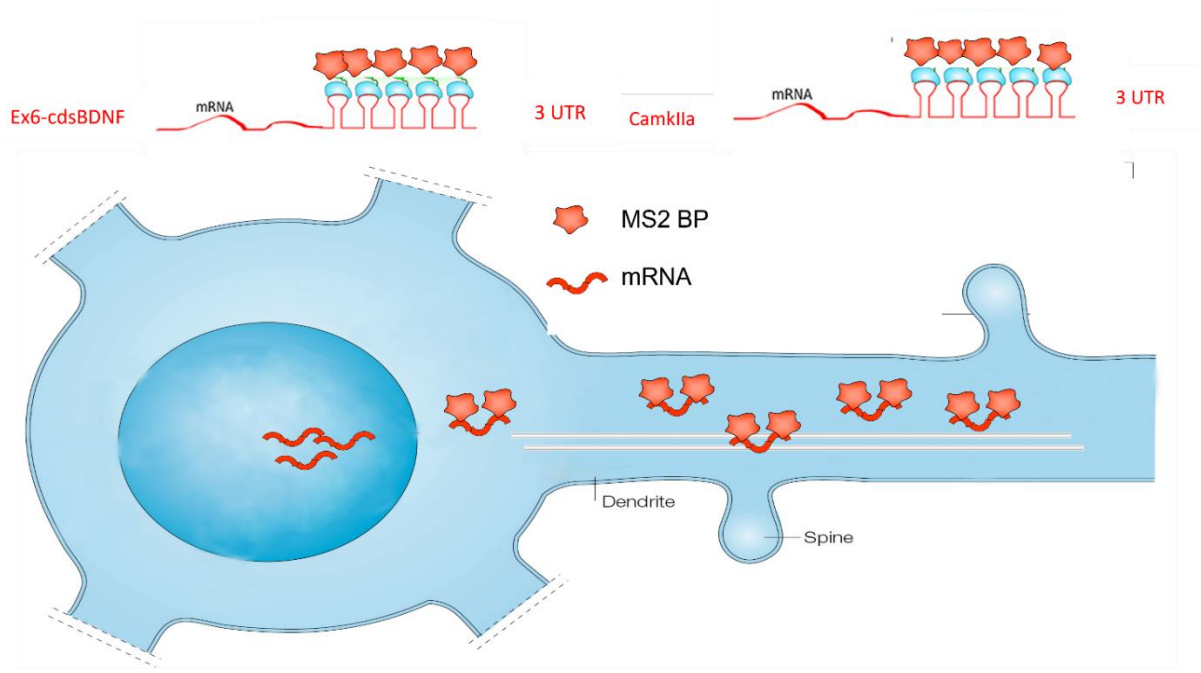

Figure XXI: Representation of MS2 stem loops system that consists on the coat protein of the MS2 bacteriophage, which contains an RNA-binding site with high affinity for RNA stem-loop structures. Tools used in this thesis work are showed: Ex6-cdsBDNF-12L-3UTR long and Ex1-cdsBDNF-12L-3UTR long together with a positive control plasmid: CamkIIa-12L-3UTR

The array of repetitive RNA stem-loops is used to recruit multiple fluo-molecules to the reporter mRNA via the mcherry-tagged MCP. To enhance the mcherry signal bound to the mRNA the number of stem-loops can simply be increased, thereby providing additional binding sites for MCP-mcherry. An advantage of this technique is the presence of loops at 3' UTR that does not interrupt cellular processing of the mRNA during experimentation (George et al., 2018). Importantly, the MCP has a high specificity in recognizing the RNA stem-loop and a high affinity for binding to it (Horn et al., 2004; Schneider et al., 1992; Stockley et al., 1995). As both the stem-loop and the MCP originate from the MS2 phage, the MCP should not bind to other nucleotide sequences in e.g. mammalian cells. In general, the MS2 loops are appended to the mRNA of interest. The number of stem loops can vary from 128-132 (Bauer et al., 2019) to 6 stem loops (Bertrand et al., 1998). This can vary the signal to noise ratio, increasing the visibility of the mRNA granules. Interestingly, it has been reported that a full coverage of all stem-loops

cannot be expected. For instance, when 24 stem-loops are used, on average only 13 were found to be bound by MCP in the cell (Wu et al., 2012). Another aspect to be considered is that the repetitive sequences of the stem loops array are prone to recombination, causing a possible loss of loops, so that the cloning of the loops can be challenging. In addition to that also the read-out of the experiment can be affected. In respect to the MCP, it is important to consider that unbound, diffusing MCP-mcherry in the cell will significantly increase background fluorescence, making the detection of individual MS2 RNA granules challenging. To address this issue, nuclear localization signals (NLS) have been added to the protein sequence to shuttle unbound MCP-mcherry to the nucleus, thereby reducing fluorescent background in the cytoplasm.

2. AIMS

The neurotrophin brain-derived neurotrophic factor (BDNF) plays a key role in neuronal survival and neurite out-growth, synaptogenesis and synaptic plasticity. BDNF mRNA can be transported in neuronal dendrites in an activity-dependent manner in particular, following seizures but also in response to antidepressants or physical activity.

At present, a clear demonstration that BDNF mRNA is locally transported and translated at activated synapses in response to the induction of long-term potentiation (LTP) is still lacking. Here, I study the dynamics of BDNF mRNA trafficking during neuronal plasticity induced by chemical-LTP. The main tasks for the project were to evaluate if: BDNF mRNA granules display directional trafficking following LTP and stop in proximity to the activated synapses and secondly if local translation of BDNF was occurring in response to LTP at individual synapses.

This thesis work consisted of methodological constraints of different and diverse protocols tried and optimized for the visualization of BDNF mRNA using the MS2 system in living neurons upon stimulation.

The project is part of the PRIN network “Synaptic engram in memory formation and recall”.

3. MATERIALS AND METHODS

3.1 DNA constructs

The plasmids already available in the laboratory **EX6-BDNFcds-gfp-3L** and **Ex1-BDNFcfds-gfp-3L** (Baj et al., 2011) were used for further cloning strategies. The plasmid with **pSL-12xMS2** containing the loops was a gift from Marco Mainardi, Scuola Normale Superiore and it was used in order to clone the 24xMS2. Another DNA construct used was the **HA-TRIM32,** a gift from prof. Germana Meroni, University of Trieste. Our collaborators from Pisa provided us the Synactive tool formed by a filler: **pAAV-hSyn-rTTA-p2A-mturquoise2** or **pAAV-hSyn-rTTA-p2A-Tdtomato** and **pAAV-hSyn-TRE-SA-Venus.** Two constructs cloned by Genscript were used for further experiments: **EX1-BDNFcds-12xMS2-3L** and **Ex6-BDNFcfds-12xMS2-3L.** DNA amplification and preparation was achieved by using different kits such as Sigma GenElute plasmid Midiprep Kit PDL35, Miniprep PLN70, Promega A2492, Qiagen MIDI 12143.

3.1.2 Synactive

Synactive consists of two constructs: pAAV-hSyn-rTTA-p2A-Tdtomato that works as a filler and pAAV-hSyn-TRE-SA-Venus. SynActive is a construct designed to detect activated synapses thanks to a molecular tag that becomes expressed at the post-synaptic side of glutamatergic synapses, after their potentiation. Using the SynActive tag the idea was to identify activated synapses after inducing a chemical LTP (cLTP) in *vitro* (Gobbo et al., 2017). SynActive expression is controlled by a Tet-responsive TRE promoter, and by the application of Doxycycline, the Tet-off blocking was removed, allowing the expression of the construct (Figure A below). Thanks to a collaboration with Lorena Zentilin in ICGEB-Trieste, pAAV-hSyn-TRE-SA-Venus construct was encapsulated in AAV-DJ viral vectors. Transduction transfection protocol and localization of Synactive will be analysed in further sections.

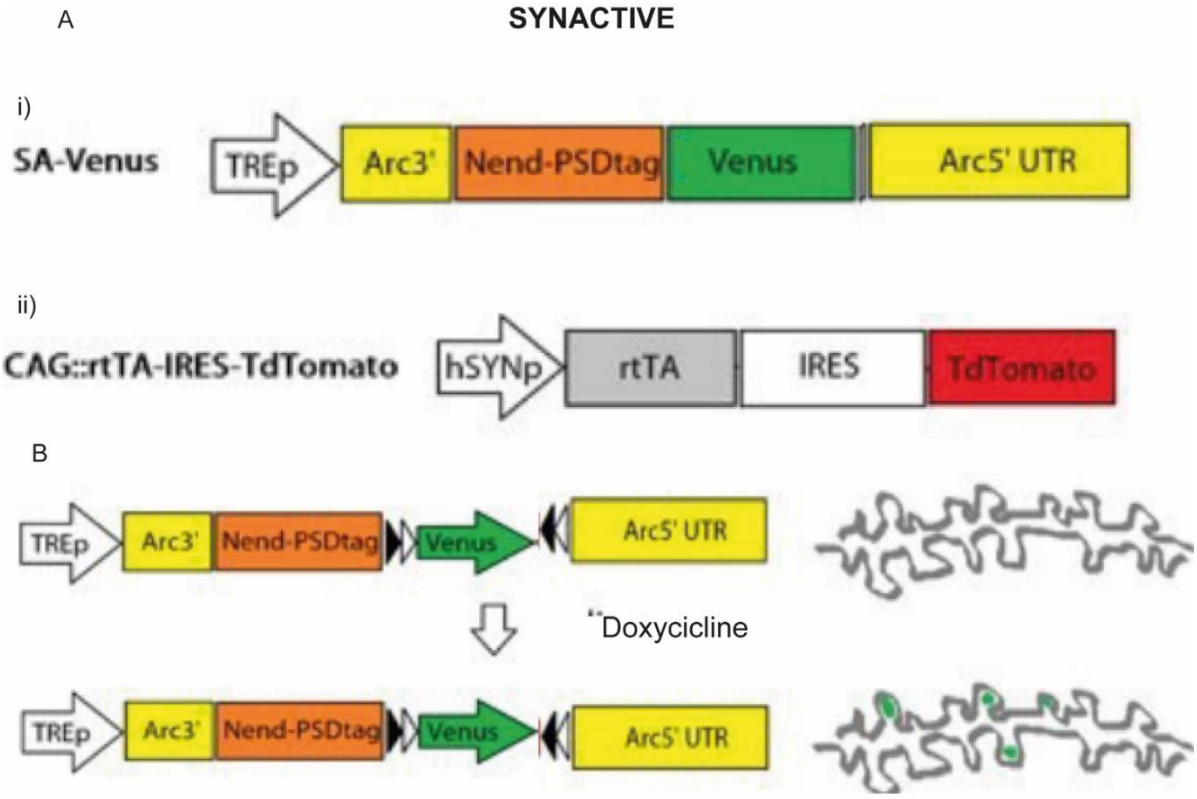

Figure A: SYNACTIVE constructs A) SYNACTIVE constructs i) SA-venus construct able to mark potentiated synapses as showed in B) after doxycycline and a potentiation protocol, synapse potentiated are marked in green ii) SYNACTIVE filler in TdTomato

3.2 Primers

Primers for the PCR on colony were designed and ordered from BMR genomics, the Tm, the content of GC, the self-dimerization were checked using different tools such as PrimerBLAST and Primer3. The primers for the PCR on colony were the following:

MS2Fw GGACGTCGACCTGAGGTAATT ™= 66°C

MS2 Rv GCGCAAATTTAAAGCGCTGATAT ™= 64°C

Primers for the cloning strategy to clone 24xMS2loops into the backbone of BDNF were

MS2_loop_SacII_FW atgtaa ccgcgg TAA cgacctgaggtaattataaccc ™= 66°C

MS2_loop_Not1_RV tatgta gcggccgc TGATATCGATCGCGCGCAG ™=73°C

Another pair of primers were designed for the cloning strategy:

FW: ATAAATCCGCGGTAAGGACGTCGACCTGAGGTA ™=68°C

RV: CTGCAGGCGGCCGCCATATGC ™=70°C

3.3 PCR

3.3.1 PCR on colony

The protocol for the PCR on colony was the following using the GRISP Xpert taq. The primers used were the ones reported on the section above. Between 5 and 8 colonies were screened per PCR: with a toothpick the colony was taken and then put in a small Eppendorf with 10µl of milliQ water. Then 1 µl of this water was then added to the PCR mix with Taq, 10µM primers, dNTPs and buffers.

Set-up PCR amplification as follows:

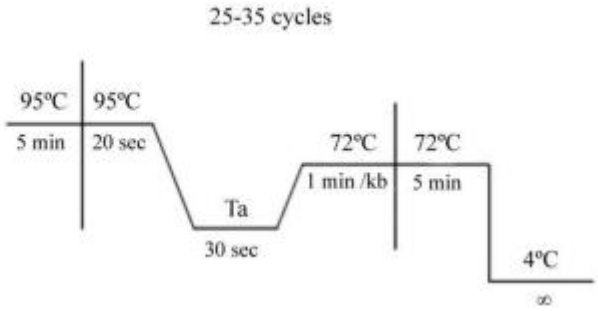

3.3.2 PCR for cloning

The primers used for cloning the 24xMS2loops into the backbone of BDNF were the following:

MS2_loop_SacII_FW atgtaa ccgcgg TAA cgacctgaggtaattataaccc

MS2_loop_Not1_RV tatgta gcggccgc TGATATCGATCGCGCGCAG

The Taq used was the Q5 enzyme from NEBcloner, 20 µM primer, dNTPs and the Q5 buffer were also added. In some trials DMSO 5% was put in order to resolve the loops. The 5X Q5 enzyme with high GC content was also added. The protocol for the PCR amplification was the following: 98°C x 30'' [98°C x 10'', 50-65°C x30''] * 32 times, 72°C x 45'', 72°C x 5 min, 4°C infinite. Different temperatures of annealing were chosen for each sample (62°C, 59.1°C,

55.7°C 52.9°C 59.0°C) thanks to the touchdown technique. Using a similar protocol for the amplification: 95°Cx 5', 95°Cx 20'' [61°C x30'', 72°Cx80''] * 5 times, 95°C x20'', [75°C x30'', 72°C x110''] *23 times, 72°C x 5 min the GoTaq (M7842, Promega) was used. Using the same primers and a similar amplification protocol also the Xpert Taq GRISP was tried.

Other primers were then designed in order to try again the strategy of the PCR cloning for the 24xMS2loops. They are the following:

FW: ATAAATCCGCGGTAAGGACGTCGACCTGAGGTA

RV: CTGCAGGCGGCCGCCATATGC

The Q5 enzyme, the GRISP Expert taq and the Gotaq from Promega were tried in order to achieve the fragment amplification. The protocol for the PCR amplification was:95°Cx 5', 95°Cx 20'' [61°C x30'', 72°Cx80''] * 5 times, 95°C x20'', [75°C x30'', 72°C x110''] *23 times, 72°C x 5 min the GoTaq (M7842, Promega), taking advantage of the two step PCR amplification. None of the strategies worked out.

3.4 Enzymes and reagents for cloning

Enzyme	Company	Catalogue #
AgeI HF	NEBcloner	R3552S
BamHI	NEBcloner	R0136L
BglII	NEBcloner	R0144S
EcoRI	NEBcloner	R0101S
HindIII	NEBcloner	R0104L
HpaI	NEBcloner	R0105L
NheI HF	NEBcloner	R3131S
NotI HF	NEBcloner	R31189S

PstI	NEBcloner	R014OT
SacII	NEBcloner	R0157S
XhoI	NEBcloner	R0146S
T4 DNA ligase	NEBcloner	M0202S
Antartic phosphatase	NEBcloner	B0289S
T4 polymerase	NEBcloner	M0203S
Klenow	NEBcloner	M0210L
Blunt/TA ligase	NEBcloner	M0367S

3.5 Competent cells

Different protocols were tried and optimized in order to have competent cells with a good efficiency for the cloning procedure. In addition, different bacterial strains were used in order to achieve the ligation of the cloned fragments. In addition to the DH5α, X-10G and Stbl3 were used for the cloning strategy. The first protocol used was the protocol using the TSS medium (10% w/v PEG 4000, 5% v/v DMSO, 35nM $MgCl_2$ and LB broth). The protocol consisted on the cold centrifugation of a bacterial growth with a O.D=0.3-0.35 and then the pellet was resuspended with the TSS medium. Another protocol used was the Calcium-Clorite protocol with small modifications from the Maniatis version. The maximum efficiency was obtained with the Rubidium-Chlorite protocol reaching 10^7 CFU/μg. The procedure was similar: pellet of a bacterial growth with a O.D=0.58 was resuspended two times in TfbI solution (1.18 g K-Acetate, 4.84 g RbCl, 0.59 g $CaCl_2$, 3.96 g $MnCl_2$, 60 ml glycerol). After the last centrifugation bacteria were resuspended in TfbII (0.21 g MOPS, 1.10 g $CaCl_2$, 0.12 g RbCl, 15 ml glycerol). The competency of the bacteria strains was evaluated each time.

3.6 Cloning protocol

Different strategies were tried in order to clone the 24xMS2loops into the backbone of BDNF. They are reported in the Result section. Here, the general protocol for cloning is reported. The starter DNA used for digestion with enzymes was between 3 and 5 µg. Then DNA together with the enzymes, and the specific buffer was put at 37°C for at least 3 hours. If the backbone was cutted, Antartic Phosfatase was added to phosphorylate the extremities, not allowing the self-annealing of the plasmid. The digestion mix was loaded in an agarose gel and then extracted through the gel extraction kit (GenElute, NA1111 Sigma). When the DNA was blunted using the T4 polymerase or Klenow fragment the DNA was then purified by the GenElute PCR Clean-Up Kit (NA1020). Each time in order to quantify the purified DNA, nanodrop quantification, or quantification by loading 1 µl of the sample in a gel was done. Once the fragmented DNA was ready to be ligated, different ratios between the backbone and the fragment were tried. The ligation step was tried at room temperature, at 16°C and at 4°C using the T4 Dna ligase or the Blunt/TA ligase. Between 1 hour and 3 hours for the ligation at room temperature was waited. At 16°C and 4°C DNA stayed for an O/N.

3.7 Heat shock protocol

Competent cells were heat shocked in order to introduce the ligation mix. Different bacterial strains were used (DH5α, X-10G, Stbl3), each of them has an optimised protocol for the heat shock treatment. The general protocol consisted in pre-chilled an aliquote of competent bacteria in ice, then when bacteria were defrosted, the DNA can be added carefully. Then the DNA remained between 20 and 30 minutes in ice. After a shock at 42°C for a few seconds (between 40'' and 60'') bacteria were shocked again in ice for a few minutes. Then LB medium was added and bacteria stayed for 1 hour in the shaker (200-300 rpm) at 37°C. After one-hour bacteria were plated on a selective antibiotic resistant LB agar plate. Plate stayed at 37°C O/N or over the weekend on the bench at room temperature.

3.8 Neuronal Cultures

3.8.1 Dissociated neuronal cultures

All animals were handled and killed according to European ethical rules. Dissociated mice hippocampal neurons were prepared from P0-P1 C57BL6/J pups. Hippocampi were dissected out in cold HBSS medium (Minimal Essential Medium, 0,2% MOPS, 20mM glucose, 1mM sodium pyruvate) and then incubated in 300µl of 0,25% Trypsin in HBSS at 37ºC for 8 minutes. After 5 min of centrifugation at 8000rpm, cells were mechanically dissociated by pipetting up and down with Pasteur pipette for 10 times in DMEM (DMEM 1x +5% of FBS). Cells were counted with the dye exclusion method using Trypan Blue (Sigma) in the Burker chamber (Eppendorf), containing 400 000–500 000 cells from each mouse. Cells were plated either on 12 mm cover slides coated with 0.1mg/ml poly-L-ornithine (Sigma), either on µ-Slide 8 Well Glass Bottom (#1.5polymer coating cat no 80806) from IBIDI company at a density of 130.000 cells/well. In order to reach this density having different coverslips per experiment, a pool of hippocampi from different animals were used for each preparation. After one hour from plating, DMEM was replaced with Neurobasal medium supplemented with 2% B-27 (Invitrogen), 1 mM L-glutamine (or Ala-Gn G1845, Sigma) and 0.45% Glucose and 1% penicillin-streptomycin. A final concentration of 1.25 uM Arac was added at DIV 4 to inhibit excessive glial proliferation. Neurons were cultured under a humidified 5% CO_2 atmosphere at 37ºC for 14 days. At DIV 4 half of the medium was replaced by adding Arac. Neurons stayed with that medium for 14 DIV.

3.8.2 Characterization of neuronal cultures

Neuronal cultures were fixed and stained for MAP2 and GFAP in order to evaluate the percentage of neurons and astrocytes present in the culture. Different concentrations of AraC (2µM, 1.25 µM, 0.83 µM, 0.62µM or not AraC) were used to evaluate the presence of glial cells. Images were taken with 10x objective using 7x10 field-images stitched in order to cover the maximum area of the coverslip. In addition to that, 10 fields (1636 x 1088 pixels) for each coverslip were acquired with a 10X objective in order to quantify manually the number of MAP2+

and GFAP+. To have a benchmark for the manual counting, I compared the value of DAPI+ cells obtained by me with that obtained by a NIS plugin available on the NIS software. As showed in the table below, the manual counting turned out to be relatively consistent with the automated counting, thus allowing me to apply the manual counting of MAP2+cells and GFAP+ to all the fields imaged. Furthermore, thanks to a custom ImageJ MACRO developed by me, a threshold was applied to the stitched images and the area covered by the GFAP+ cells and by MAP2+ cells was automatically evaluated for each condition.

3.8.3 Trials for different coating

Neurons were coated in parallel with poly-L-ornithine (0.1mg/ml) or poly-D-Lysine (50m g/ml) or Poly-L-ornithine+Laminin. The coating was tried for different time courses, resulting in better adhesion after 3 hours of coating. Cells were fixed and immunolabelled for MAP2 in order to evaluate differences in the network formation. Then the area covered was evaluated by a custom MACRO that consisted in a threshold application. The coated protocol chosen was the poly-L-ornithine (0.1mg/ml) for 3 hours at room temperature. Two washes with PBS 1x were necessary to remove the excessive coating, toxic for the cells.

3.8.4 Trials for Glutammine-Glutamax

For several months neurons grew with Neurobasal with 1mM L-glutamine. After many trials on cLTP induction were not successful, glutamine was replaced by the Ala-Gn (Sigma A8185), a more stable form of the glutamine. More details in the result section.

3.9 Transfection of neuronal cells

Different protocols and optimization were tried in order to reach a good transfection efficiency. Calcium phosphate protocol and Attractene (Qiagen) were tried. Then the Lipofectamine 2000 (ThermoFisher) was used. In 12 mm coverslip the protocol that worked better was to use 1 µg of DNA (2 µg of DNA for co-transfection) and 2µl of Lipofectamine 2000 per well. Instead of 50 µl of MEM, as suggested by the standard protocol, 100 µl of MEM was used. Small drops from

the mix DNA + Lipofectamine were used for each well. After one hour, the medium was changed with neurobasal. The protocol that works better for transfecting neurons in 8 µ-Slide 8 Well Glass Bottom IBIDI chamber slide was to use 1.2 µl of DNA and 1.2 µl Lipofectamine 2000 per well and 50 µl of MEM. The efficiency of the transfection decreases with the maturation of neurons. Neurons transfected with BDNF mRNA were transfected at DIV 11-12-13 with EX6-BDNFcds-12xMS2-3L and MS2-NLS-mcherry or Ex1-BDNFcfds-12xMS2-3L and MS2-NLS-mcherry or with CaMKIIa-12xMS2-3'UTR together with MS2-NLS-mcherry. Neurons transfected with Synactive filler tdTomato were transfected at 3, 5,7 and 9 DIV in order to evaluate which developmental stage was better for the survival of neurons.

The transfection of EX6-BDNFcds-gfp-3L or Ex1-BDNFcds-gfp-3L to see the protein were tried at different times at different stages as reported in the table below. However, few transfections were successful.

3.10 Transduction of neuronal cells

The serotype chosen for encapsulating the pAAV-TRE-SA-Venus was the DJ. Once the virus arrived, aliquots of 30-50 µl were done and the virus was stocked at -80°C. Neurons were infected using different MOI:10^1, 10^2, 10^3, 10^4. To calculate the µl of the virus needed for a specific MOI the following formula was considered: n of cells plated x MOI. In this way the particles of the viral genome were calculated. The concentration of the virus was $2*10^{11}$ vg/ml. The transduction was optimised at different stages of development. The medium was not changed after the transduction protocol.

3.11 cLTP protocols and solutions

Four different protocols were performed in order to obtain the cLTP stimulation. The first protocol used was a **glycinergic protocol** used in (Lu et al., 2001) with some modification:

FOR cLTP	Ecs Wang	ECS Wang +Glycine
NaCl	140mM	140mM
KCl	5 mM	5 mM
$CaCl_2$	1.3mM	1.3mM
HEPES	25 mM	25 mM
D-glucose	33mM	33mM
TTX	0.5 µM	0.5 µM
Picrotoxin	0.5 µM	0.5 µM
Strychinine	1 µM	1 µM
Glycine		200 µM

The osmolarity of the solution was reported to be between 310-325 mOsm and the pH was 7.4. Solution was pre-warmed before the experiments. In order to induce the stimulation, after 30 minutes of pre-conditioning with ECS, Glycine was added by substituting 250 µl of ECS conditioned with 245 µl of new ECS with 5 µl of Glycine 200 µM for 5 minutes. After 5 minutes, the ECS with glycine was replaced with the 250 µl of ECS conditioned and 250 µl of new ECS. After glycine treatment, ECS remained for different timepoints such as 15, 30, 60 and 180 minutes.

A second protocol used was the **Glutamate protocol** (Franceschi Biagioni et al., 2021):

FOR cLTP	Tyrode	Tyrode+Glutamate
NaCl	150 mM	150 mM
KCl	4 mM	4 mM
$MgCl_2$	1 mM	1 mM

FOR cLTP	Tyrode	Tyrode+Glutamate
$CaCl_2$	2 mM	2 mM
HEPES	10 mM	10 mM
D-glucose	10 mM	10 mM
Glutamate		50 µM

The pH was 7.4. Solution was pre-warmed before the experiments. In order to induce the stimulation, after 10 minutes of pre-conditioning with Tyrode, 50 µM Glutamate was added for 30 seconds. Then neurons stayed for 30 minutes in the Tyrode solution.

A third protocol used was **Forskolin+ Rolipram (**Sigma 557330)

FOR cLTP	Ctrl	Forskolin+Rolipram
NaCl	92.4 mM	92.4 mM
KCl	2.3 mM	2.3 mM
$MgSO_4$	0.8 mM	-
$CaCl_2$	1.3 mM	1.3 mM
Na_2HP0_4	0.35 mM	0.35 mM
$NaHCO_3$	4.2 mM	4.2 mM
K_2HPO_4	0.45 mM	0.45 mM
HEPES	7 mM	7 mM
D-glucose	5.5 mM	5.5 mM
Forskolin		10 µM
Rolipram		0.1 µM

The pH was 7.4. Solution was pre-warmed before the experiments. In order to induce the stimulation neurons stayed for 90 minutes in the solution with Forskolin and Rolipram.

A fourth protocol used was **Forskolin** (Sigma 344270)

FOR cLTP	Ctrl	Forskolin
NaCl	92.4 mM	92.4 mM
KCl	2.3 mM	2.3 mM
$MgSO_4$	0.8 mM	-
$CaCl_2$	1.3 mM	1.3 mM
Na_2HP0_4	0.35 mM	0.35 mM
$NaHCO_3$	4.2 mM	4.2 mM
K_2HPO_4	0.45 mM	0.45 mM
HEPES	7 mM	7 mM
D-glucose	5.5 mM	5.5 mM
Forskolin		10 µM

The pH was 7.4. Solution was pre-warmed before the experiments. In order to induce the stimulation, a time course at 30, 60 and 90 minutes was done.

3.12 KCl treatment

A positive control for the neuronal stimulation was the KCl. Different KCl solutions were used. As a positive control 50 mM KCl for 180 minutes was used (Baj et al., 2016). Then KCl was tried at 10 mM, 20mM and 50 mM for 90 minutes.

KCL	10mM	20 mM	50 mM
NaCl	131 mM	122 mM	93 mM
$MgS0_4$	0.8 mM	0.8 mM	0.8 mM
$CaCl_2$	1.3mM	1.3mM	1.3mM
Na_2HP0_4	0.35 mM	0.35 mM	0.35 mM
$NaHCO_3$	4.2 mM	4.2 mM	4.2 mM
K_2HPO_4	0.45 mM	0.45 mM	0.45 mM
HEPES	0.5 mM	0.5 mM	0.5 mM
D-glucose	5.5 mM	5.5 mM	5.5 mM

3.13 Live imaging protocol for the BDNF mRNA granules

Neurons coated in IBIDI chamber slides were transfected with BDNF mRNA+MS2 BP. After 17-18 hours from transfection were imaged. Nikon Eclipse Ti-E-epifluorescence using 40 X objective (1.0 NA oil PlanApo DICH) equipped with a DS-Qi2 Camera (NIKON) was used to acquire videos. Videos of 10 minutes at 1 frame/second for control condition and videos of 15 minutes at 1 frame/second for activated condition were acquired. During the 10 minutes of control neurons were in the control medium (as described above). Then a wash with the medium without MgSO4 was done. For stimulating neurons, 10μM of forskolin was added to the medium without MgSO4 and neurons were imaged for further 15 minutes.

3.14 BDNF protein transfection and visualization in live

Neurons coated in IBIDI chamber slides were transfected with ex1-BDNFcds-GFP-3'UTR long or ex6-BDNFcds-GFP-3'UTR long or BDNFcds-GFP. To better see the protein construct, neurons were co-transfected with an mcherry filler. After 17-18 hours from transfection were imaged. Nikon Eclipse Ti-E-epifluorescence using 40 X objective (1.0 NA oil PlanApo DICH) equipped with a DS-Qi2 Camera (NIKON) was used to acquire videos. Videos of 10 minutes at 1 frame/minute for control condition and videos of 60 minutes at 1 frame/minute for activated condition were acquired. During the 10 minutes of control condition neurons were in the control medium (as described above). Then a wash with the medium without MgSO4 was done. For

stimulating neurons, 10μM of forskolin was added to the medium without MgSO4 and neurons were imaged for further 60 minutes.

3.15 Video analysis for the BDNF mRNA and protein

After the acquisition, videos were opened on ImageJ and Kymographs were extracted by means of the Multi Kymograph plugin. The Kymograph analysis consisted in selecting a particular movement of the granules and drawing a segmented line over the corresponding track. Afterwards, thanks to a custom ImageJ MACRO developed by me, the position and the time coordinates (x and t), as well as the average and instantaneous velocities of the particle were extracted. Besides, the MACRO returned also the overall dynamical behaviour of the particle (anterograde, retrograde or confined), based on the total displacement. If the total displacement was lower than 0.5 μm, the selected particle was considered as confined. For the video of the BDNF protein, only neurons transfected with BDNFcds-GFP were analysed because with other constructs neurons were not well visible. The mean fluorescence of BDNFcds-GFP protein spots was measured every 10 minutes during the 60 minutes of Forskolin treatment. For each spot a mean fluorescence value of the untreated condition was also measured by doing an average on two time points (after 1 minute of imaging and after 10 minute).

3.16 Antibodies

TABLE I: Primary Antibodies

Antigen	species	dilution	company	Catalogue #
PSD95	mouse	1:200 1:500	Millipore	Clone k28/43 MABN68
GLUA1	rabbit	1:500	Alomone	AGC-004
vGLUT1	guinea pig	1:1000	MERCK Millipore	AB5905

c-Fos	Rabbit	1:1000	sigma	F7799
aGFP	chicken	1:1000	abcam	Ab13970
GFAP	mouse	1:1000	Sigma	G3893
MAP2	rabbit	1:100	Gentex	GTX133109
Synapsin I	Rabbit	1:1000	millipore	AB1243
BDNF	mouse	1:50	sigma	B5050
TGN38	mouse	1:500	US Biological	G2032-25F
GM130	mouse	1:500	BD transduction laboratories	610823
LMAN1	chicken	1:1000, 1500	Sigma	GW21589A

TABLE II: Secondary Antibodies

Antigen	**label**	**species**	**dilution**	**company**	**Catalogue #**
mouse	Alexa 488	goat	1:500	ThermoFischer Scientific	A11001
mouse	Alexa 568	goat	1:500	ThermoFischer Scientific	A11004
mouse	Alexa 647	donkey	1:500	ThermoFischer Scientific	A31571
rabbit	Alexa 488	goat	1:500	ThermoFischer Scientific	A11034
rabbit	Alexa 568	donkey	1:500	ThermoFischer Scientific	A10042
rabbit	Alexa 647	donkey	1:500	ThermoFischer Scientific	A31573

guinea pig	Alexa 568	goat	1:500	Abcam	Ab175714
chicken	Alexa 488	goat	1:500	ThermoFisher Scientific	A11039

3.17 Immunocytochemistry

Mouse hippocampal neurons, prepared as above were fixed for 15 minutes at room temperature with 4% paraformaldehyde, pH7.2. Cells were then permeabilized with 0.01% Triton X-100 in PBS for 15 minutes in order to detect intracellular proteins (PSD-95, Vglut1, c-Fos, SynapsinI, Map2). Non-specific binding sites were blocked with 2% BSA in PBS 0.01% Triton X-100 for 30 minutes. Then, primary antibodies as reported in the table above were used. Primary antibodies diluted in blocking solution were incubated for 120 minutes at room temperature or ON at 4°C. After three washes of 5 minutes in PBS, coverslides were incubated for 90 minutes in the proper combination of secondary antibodies (table II), diluted in blocking solution. Prior to incubation of secondary antibodies, the mix was centrifuged for 5 minutes at 20.000g to discard precipitates. After 90 minutes of secondary antibody incubation, three washes with PBS were done. Coverslips stay for 5 minutes with Hoechst 1:1000 in order to mark nuclei. Coverslips were then washed in water and mounted using Moviol.

3.18 Antibody optimization for the secretory pathway

Neurons were fixed at DIV 14 and TGN38, GM130 and LMAN1 were used. Different dilutions of the antibodies were used in order to define the best dilution. Dilutions 1:2000, 1:1000, 1:500 were done. Some explicative images were acquired at a confocal microscope and at Elyra 7. No further experiments or quantification were performed on the images.

3.19 Endogenous labelling of BDNF and analysis

14 DIV hippocampal neurons, after different time-courses (15, 30, 60, 180 minutes) from cLTP induction with Glycine 200 μM, were fixed following the protocol above. Together with BDNF (B5050), MAP2 was used to better visualize the structure of neurons and for normalization purposes. Images were acquired with a Nikon C1 confocal microscope using a 60X oil objective.

Images were acquired using the same settings for the first two experiments, then because of the laser 647 broke, a change in the secondary antibody (568) and in the laser (568) was necessary. 1048*1024 pixels images were acquired for each channel. Deconvolution of the images was done using Huygens software, choosing a high signal de-noise ratio. Once those images were deconvolved, a densitometric analysis was conducted. Regions were drawn by hand each time for each image to be more precise than possible. The regions considered were the soma, the primary dendrite (D1), the primary branching point (BP1), the secondary dendrite (D2), the secondary branching point (BP2), the tertiary and quaternary dendrites (D3&D4) and the tertiary branching point (BP3). For each region an approximate area was considered: for the soma (100µm²), D1 (100µm²), BP1 (10 µm²), D2 (45 µm²), BP2 (5 µm²), D3&D4 (20 µm²) and BP3 (3 µm²). Images were analysed with ImageJ. Once that the regions were drawn, the intensity and the volume of each region, and each channel was measured. In order to speed up the analysis two MACRO were designed: one for measuring the intensity, and another one to measure the volume. The MACRO applies a mask based on a fixed value of threshold (namely a minimum value of fluorescence intensity). Afterward, it calculates the average intensity and the total volume for each region. The volume is obtained by summing up the area above threshold in each frame of the z-stack. More details about the results of this procedure are present in the Result section.

3.20 GluA1 labelling and analysis

After different time points (15, 30, 60,180 minutes) from the LTP induction with Glycine 200 µM neurons were fixed with PFA 4%. Neurons were not permeabilized because GluA1 receptors on the surface wanted to be detected. After the blocking procedure, neurons were immunolabelled with GluA1 (1:500) O/N. Different dilutions were tried before performing the experiments (1:2000, 1:1000; 1:500; 1: 200) but taking in consideration the results and the literature the dilution 1:500 was then chosen. After the O/N neurons were then permeabilized and the VGLUT1 antibody was then added. Then the immunocytochemistry proceeded as in the section above. Images were acquired using the Nikon C1 confocal microscope with 488 laser (VGLUT1 channel) and 561 lasers for GluA1. Images were deconvolved using Hygens software and the high signal denoise program. Images were then analysed using Synapse counter, a plugin for ImageJ. Some parameters such as the dimensions of the images and the

area of the pre-synaptic and post-synaptic dots were adjusted, choosing the minimum and the maximum px^2 as 19 and 490 for the presynaptic dots, while 7 and 177px^2 for the postsynaptic dots.

3.21 VGLUT1-PSD95 labelling and analysis

After different protocols of cLTP induction VGLUT1-PSD95 immunolabeling was conducted (see the section cLTP protocols and solution). Neurons were fixed and immunolabeled for VGLUT1 and PSD95. Images were acquired using the Nikon C1 confocal microscope with 488 laser (PSD95 channel) and 561 lasers for VGLUT1. Images were deconvolved using Hygens software and the high signal denoise program. Images were then analysed using Synapse counter, a plugin for ImageJ. Some parameters such as the dimensions of the images and the area of the presynaptic and post-synaptic dots were adjusted. In order to validate the plugin, I created a MACRO on ImageJ that consisted of considering a thresholded image for VGUT1 and for PSD95, counting the dots and the area of the dots considered. Then the thresholded images were watershed and puncta were counted.

3.22 c-Fos labelling and analysis

After the cLTP induction with different protocols (see the section cLTP protocols and solution) neurons were fixed as the experiments above of immunocytochemistry. Once the immunostaining for c-Fos was concluded, images of neuronal cultures were acquired with Nikon Eclipse Ti-E-epifluorescence using a 20x objective equipped with PFS. Thanks to a specific MACRO created using the NIS software Element: between 6 and 10 fields of 1636*1088 pixels were acquired for each coverslip in two channels (DAPI and 488 for the c-Fos signal). The exposure time was the same for all the conditions (200ms). Images were then analysed using two different methods: the first method is based on counting c-Fos positive cells by eye, the other method consists of measuring the intensity of c-Fos by a MACRO created in Fiji. The MACRO consists of considering DAPI positive cells that are inside a specific range (between 5-10 µm), creating a mask on them and then exporting the mask on c-Fos channel in order to measure the intensity of the c-Fos. A detailed Figure representing the different steps of the MACRO is shown in the section Results.

3.23 Synapsin I labelling

Synapsin I labelling was used in two different experiments. In one experiment neurons at DIV 14 were transfected and infected with Synactive tool and then after a cLTP induction with Glycine were fixed and immunolabeled with Synapsin I to localize Synactive at post-synaptic side and Synapsin1 at presynaptic side.

3.24 Evaluate the distance between a granule and a synapse

After 17-18 hours from transfection with BDNF mRNA, neurons were stimulated with 10 μM Forskolin for 15, 30 and 60 minutes. Then neurons were fixed and labelled with Synapsin I. Images were acquired using Elyra 7 microscope using 63X objective using a filter combination: BP 420-480 and BF 405/488/561/642. SIM images were reconstructed through the Zen-black software. A Sim reconstruction followed by a Z-stack projection was performed using Zen-black software. A threshold for the channel of Synapsin I was applied, and a mask was created. The same was done for the BDNF mRNA channel. In this latter case, two thresholds were considered: one threshold for identifying the granules and a second threshold for delineating the structure of the neuron with the relative spines. A MACRO for speeding up the analysis was made. Once the thresholded and masked images were created, stretches of neurons between 30-50μm with visible spines were considered. Granules were counted between 3μm (away from the soma) and -3μm (closer to the soma) from an imaginary longitudinal axis that divides in two parts the spine. So, a total of 6μm were considered. Granules inside the spines were also counted. Stretches of 30-50 μm were considered of apical distal dendrites.

3.25 Evaluate the potentiation of synapse with Synactive

Once the neurons were infected and transfected with Synactive, the day before the cLTP induction 500ng of Doxycicline were added to the 500μl of Neurobasal medium, then the cLTP with Glycine was induced. After the 5 minutes with Glycine 200 μM neurons stayed for 3 hours in the conditioned Neurobasal medium. After that, neurons were fixed. Images were taken with the confocal (Laser 488 or Laser 514) and with the Elyra microscope. Anti GFP antibody that

recognizes the Venus tag was used in fixed cultures and images were taken with the epifluorescence microscope, to discriminate the mVenus (YFP) emission from the GFP emission detection of the YFP using bands a filter cube (Ex 500/24_DM 520_BA 542/27).

3.26 Statistical analysis

Data analysis was performed blind for all experiments. Statistical values are represented as mean ± S.E.M when data are parametric. When data are not parametric, median ± 95% confidence was chosen. The number of experiments and cells analysed for each situation is indicated in each figure. Statistical significance was calculated using GraphPad Prism version 8 (GraphPad Software, LaJolla, USA). Normality distributions test was done by Shapiro-Wilks test. If samples proved to have a normal distribution, then Student t-test (for two groups) or ANOVA with Tukey's post-test (for three or more groups) were used. When samples did not have a parametrical distribution, then for experimental conditions with two data sets the Mann-Whitney test was used or the Krustal-Wallis for three or more groups. χ^2 statistical analysis was also performed in order to identify independence between categories. Cumulative distribution of data was also used. Outliers were removed using the formula with the interquartile range rule. This required to calculate the first quartile Q_1 and the third quartile Q_3 and the difference between them. The difference was then multiplied by 1.5. It was necessary to add 1.5x (Q_3- Q_1) to the third quartile and to subtract 1.5x (Q_3- Q_1) any number greater or smaller than these values was a suspected outlier. Significance was set as *p<0.05; **p<0.01; ***p<0,001, **** p<0.0001. The p value is reported in each figure legend in the result section, as the statistics used for each experiment.

4. RESULTS

4.1 Development and validation of molecular tools for the BDNF trafficking in vitro

4.1.1 Cloning of MS2 loops in the backbone of BDNF-CDS

The first aim of my work was to create a suitable set of plasmids enabling the detection of BDNF mRNA in living neurons. The plasmids were supposed to encode the exon I, as an example of somatically localized mRNA, and exon VI, as an example of dendritic mRNA, ahead of a common backbone encoding the BDNF sequence followed by a 24xMS2 loops and either the 3'UTR-short or -3'UTR long sequence.

First of all, the 12xMS2 from the plasmid "pSL-MS2-12X" (Addgene) was nicked using EcoRI and BamHI. Afterwards, the 12xMS2 (600 bp) stem loops were cut using EcorI-BglII (Figure 1A) and cloned in the same vector, to obtain the plasmid with 24xMS2loops. This was possible because the two ends produced by the digestion with BamHI and BglII are compatible ends that can be ligated. Since the beginning of the experiments, the manipulation of plasmids showed some difficulties. Indeed, as bacteria seemed reluctant to accept the 24xMS2loops plasmid (4.6 kb). Accordingly, PCR on colonies was performed to identify the bacterial colonies containing the 24xMS2loops. Different kits (Promega, Qiagen, Sigma) and growing conditions (37°C O/N, 33°C O/N, 25°C O/N) were tested in order to get a good plasmid concentration. The different culture conditions were tested to establish if the growth of the bacteria was influenced by different values of temperature. Indeed, it was suspected that a possible recombination issue during the growing condition was occurring.

Once that the plasmid with 24xMS2 was isolated by PCR on colony (Figure 1B) and verified by sequencing (BMR genomics, Padova), I took advantages of three different strategies with the aim of cloning the 24xMS2 loops in the backbone encoding the BDNF coding sequence. The first strategy involved the PCR cloning. To amplify the 24xMS2, two sets of primers were designed (see section Materials and Methods). A Touchdown PCR method and different Taqs (Q5 NEBCLONER, Xpert Taq GRISP, GoTaq PROMEGA) were used with both sets of primers. PCR protocol was always adapted with the Taq manufacturer protocol. Changing the primers, the Taqs used, the protocol of PCR amplification, the presence or not of DMSO and the amount of DNA used did not produce any significant improvement and success in the outcome. Indeed,

different trials produced multiple bands or a smear so that it was impossible to clearly identify the band to extract for the cloning (Figure 1D). For the second strategy, I planned to cut the 24xMS2 using BamHI-Not1 and cloning it inside the BDNF backbone (8.8 kb) at the place of GFP, which was removed by AgeI-NotI (Figure 1C). AgeI and BamHI were filled-in by Klenow DNA polymerase to obtain blunt ends. This strategy did not produce positive clones with the 24xMS2 (Figure 1C, 1E).

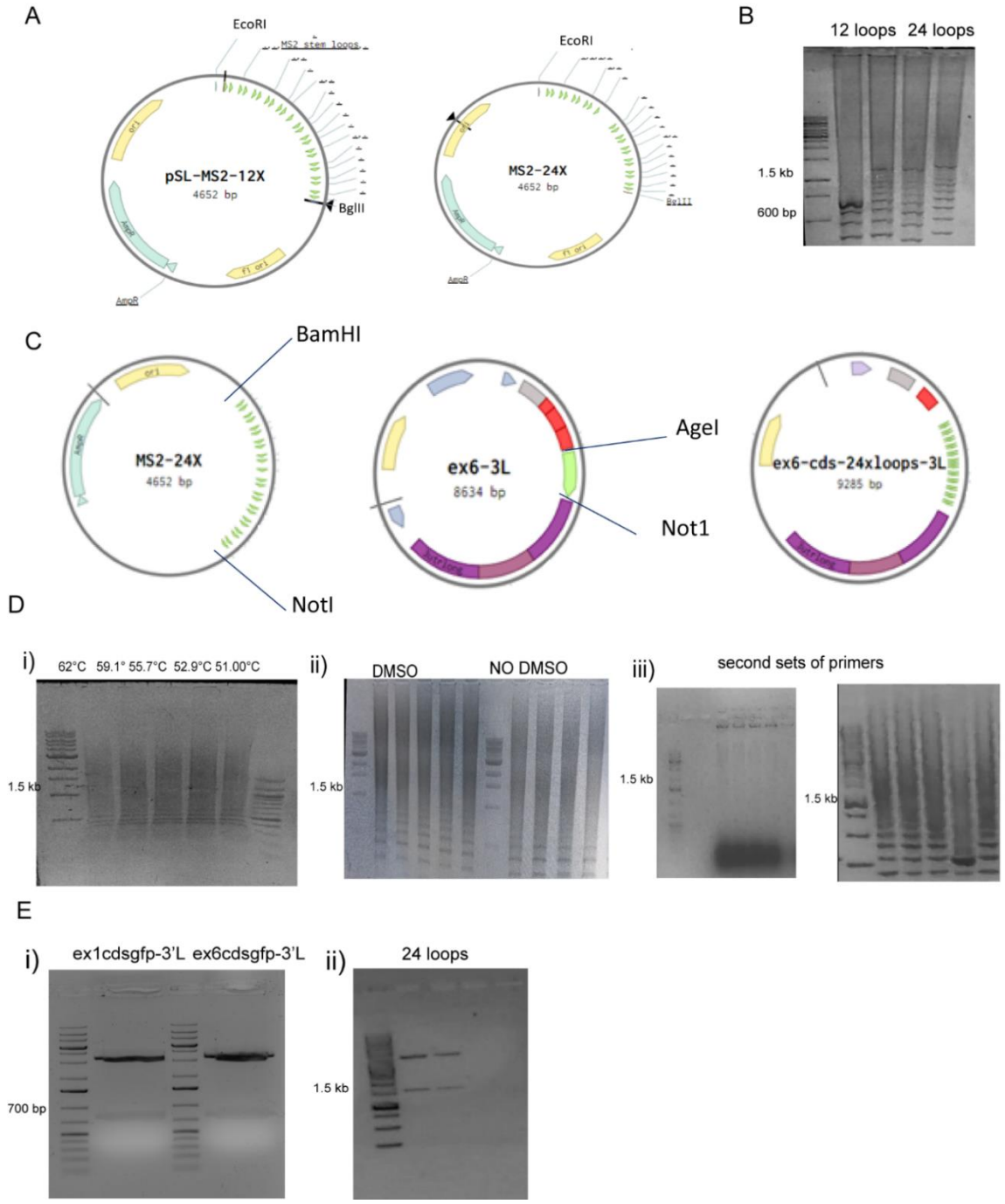

Figure 1: A) Cloning of the 24 MS2 loop plasmid by cutting with EcoRI and BglII the 12 MS2 loops. The fragment of the 12 MS2 loops was ligated into the backbone pSL-MS2-12x previously nicked by EcoRI and BamHI. B) Screening of bacterial colony containing 12 loops or 24 loops. The 12 loops fragment was about 600 bp, while the 24 fragment was around 1.5 kb. C) Strategy for cloning the 24 loops in the BDNF backbone through a PCR amplification strategy of the 24 loops (D) and through the restriction digest with BamHI and NotI for cutting the 24 loops and AgeI and NotI for cutting the GFP in the BDNF backbone. D) different PCR trials for the amplification of 24 loops: i) a touchdown PCR approach, using different annealing temperatures for the primers. A smear was visible at all temperatures ii) DMSO was added using the same temperatures as before iii) different primers were tried for the amplification of the 24 loops. E) Intermediates for the restriction digestion of the BDNF backbone and the 24 loops plasmids i) AgeI and NotI digestion for the GFP excision ii) 24 loops fragment cut by BamHI and NotI.

In the third strategy, the 24xMS2 was cut with (BamHI-XhoI) and cloned in a “passing” backbone (pcDNA3.1 HATRIM32, a kind gift from Prof.ssa Germana Meroni) cut with (BamHI-XhoI) thus allowing a sticky end cloning with the backbone of BDNF (Figure 2 A). This last strategy implied the cloning of the 24xMS2 closer to the CMV promoter at the 5’ UTR: in this condition there is a potential risk that the 24xMS2 insert might downregulate or prevent translation by hindering the initiation of translation. The first part of the cloning worked properly: I obtained the 24xMS2 cloned into the passing backbone of HA-TRIM32 (7.3 kb) (Figure 2 A). The second part of the cloning consisted in cutting the 24xMS2 (1.5 kb) from the HA-24xMS2 (7.3 kb) using NheI and XhoI and ligate that insert into the BDNF backbone, previously nicked with NheI and XhoI. This last strategy did not produce 24xMS2 BDNF clones (Figure 2 A).

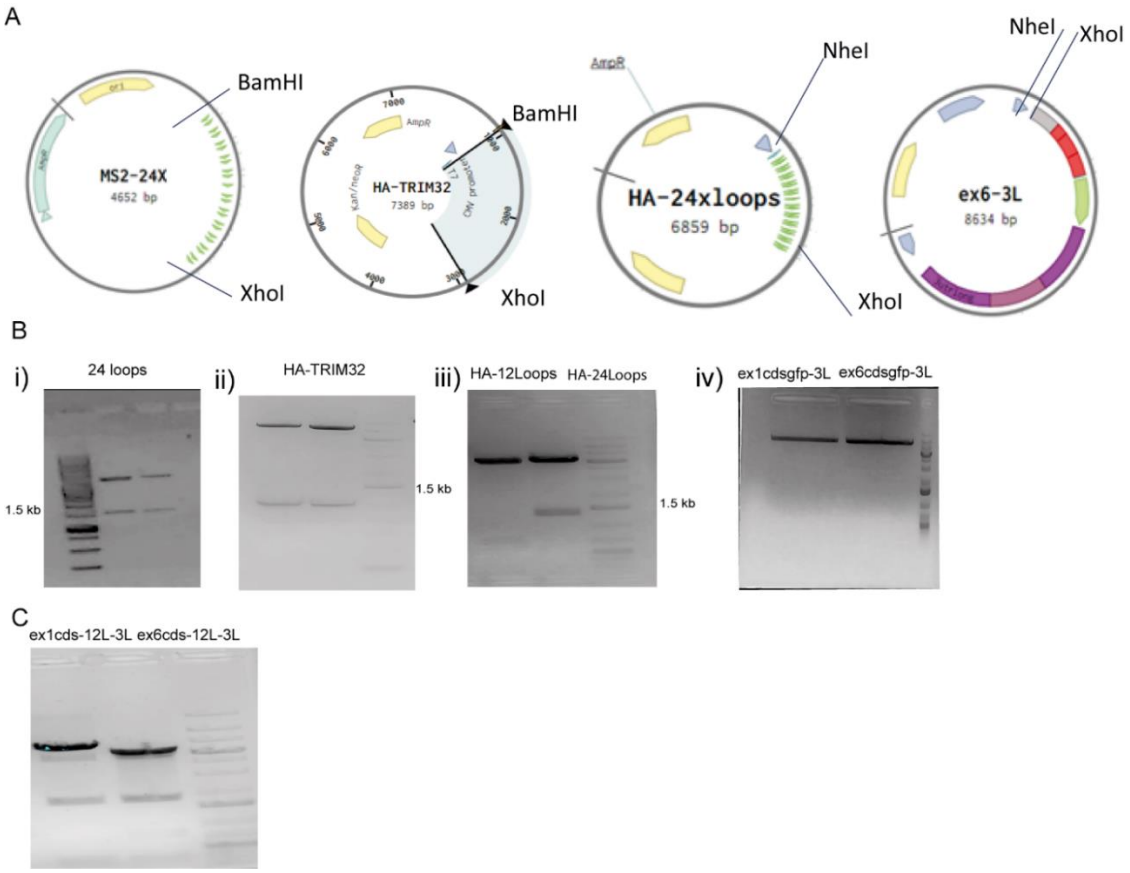

Figure 2: The third cloning strategy. A) The 24 loops fragment cut with BamHI and XhoI was cloned into the HA-TRIM32 backbone, previously cut with BamHI and XhoI. From the intermediate HA-24 loops, the loops were cut using the NheI and XhoI enzymes, this last fragment should have been cloned into the BDNF backbone, previously nicked using NheI and XhoI. B) Intermediates for the restriction digestion described above i) the fragment of the 24 loops cut with BamHI and XhoI ii) digestion of HA-TRIM32 with BamHI and XhoI ii) digestion with NheI and XhoI to cut the 12 loops or the 24 loops iv) digestion of the BDNF backbone with NheI and XhoI C) Verification of GenScript’s cloned plasmids using BamHI.

4.1.2 Verification of plasmids with 12 MS2 loops from GenScript

After testing the three strategies described before, a fourth strategy was considered. Ex1-cdsBDNF-3'UTR long and Ex6-cdsBDNF-3'UTR long plasmids were shipped together with the 12xMS2 and the 24xMS2 loops to two companies (GenScript and Genewiz). GenScript managed to clone the 12xMS2 in the backbone of either the Ex1-cdsBDNF-3'UTR long and the Ex6-cdsBDNF-3'UTR long. Once the plasmids arrived, plasmids were verified by a restriction digestion with BamHI, an enzyme that has different cutting sites (Figure 2 C) and then amplified. After this check, the plasmids were used to transfect neurons.

4.2 Validation of molecular tools for the visualization of potentiated synapses

4.2.1 Synactive verification

Synactive is a tool developed in Scuola Normale Superiore in Pisa. The purpose of the tool was to detect activated synapses thanks to a molecular tag, that after the potentiation, it became expressed at the post-synaptic side of glutamatergic synapses. Considering that Arc is an immediate early gene (Steward et al., 2015), the molecular tag in the Synactive construct is constituted by the 3'UTR and the 5'UTR Arc sequence. Using the Synactive construct I was supposed to be able to identify activated synapses after the induction of chemical LTP in vitro (Gobbo et al., 2017). Synactive consists of two different constructs: the first construct (tdTomato) that works as a filler and trough the rTTA trans-activator, allows the expression of the second construct (mVenus), that has a fluorescent synaptic tag followed by Arc RNA sequences. The expression of Synactive is controlled by a Tet-responsive TRE promoter: by application of Doxycycline, the Tet-off blocking is removed, and the expression of the construct is allowed. Initially I checked Synactive by means of a fingerprint digestion with Pst1, an enzyme with different cutting sites in the pAAV::TRE3g-SA-ChETA-Venus plasmid.

4.2.2 Optimization of SYNACTIVE tool

4.2.2.1 Synactive co-transfection/ transduction

First of all, a quantitative comparison between the co-transfection of the two plasmids: pAAV::syn-rTA-tdTomato and the pAAV::TRE3g-SA-ChETA-Venus and the transduction with pAAV::TRE3g-SA-ChETA-Venus in AVVDJ showed that the transduction /transfection protocol gave higher efficiency of tdTomato positive cells (Figure 3 C).

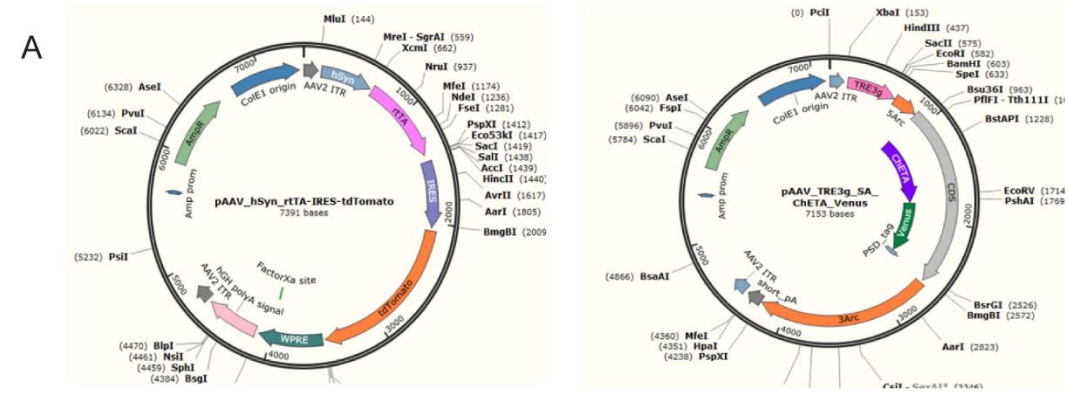

C

	co-transfection	infection/transfection
cells tdTomato+ (esp 1)	5	40
cells tdTomato+ (esp 2)	13	30
cells tdTomato+ (esp 3)	10	23

Figure 3: Synactive co-transfection/transduction optimization. A) Synactive is constituted by the Tdtomato filler (left) and the mVenus-Arc contruct (right). B) Representative images of co-transfection (using Lipofectamine 2000) and transduction/transfection protocol C) Number of tdTomato positive cells for each protocol. Scale bar of 20µm.

4.2.2.2 MOI for Synactive transduction

Once that the transduction/transfection protocol was established to be the optimal one, having the merit of a high efficiency of Tdtomato positive cells, I evaluated the optimal Multiplicity of Infection (MOI) to use in the cultures. By testing different values of MOI (10^1, 10^2, 10^3, 10^4), I evaluated the survival of neurons by measuring the DAPI+ cells (Figure 4B, n=3 independent cultures). Besides, I also evaluated the number of tdTomato positive, considering this parameter as the one to be optimized (Figure 4C). The plot in Figure 4B, shows that the survival rate at MOI 10^2, 10^3, 10^4 reaches a plateau, whereas the percentage of Tdtomato cells increases and reaches a maximum for MOI=10^4. Considering these results, the optimal MOI was established to be 10^4. Further experiments were conducted with this value, that is also reported in literature (Howard and Harvey, 2017; Schultz and Chamberlain, 2008).

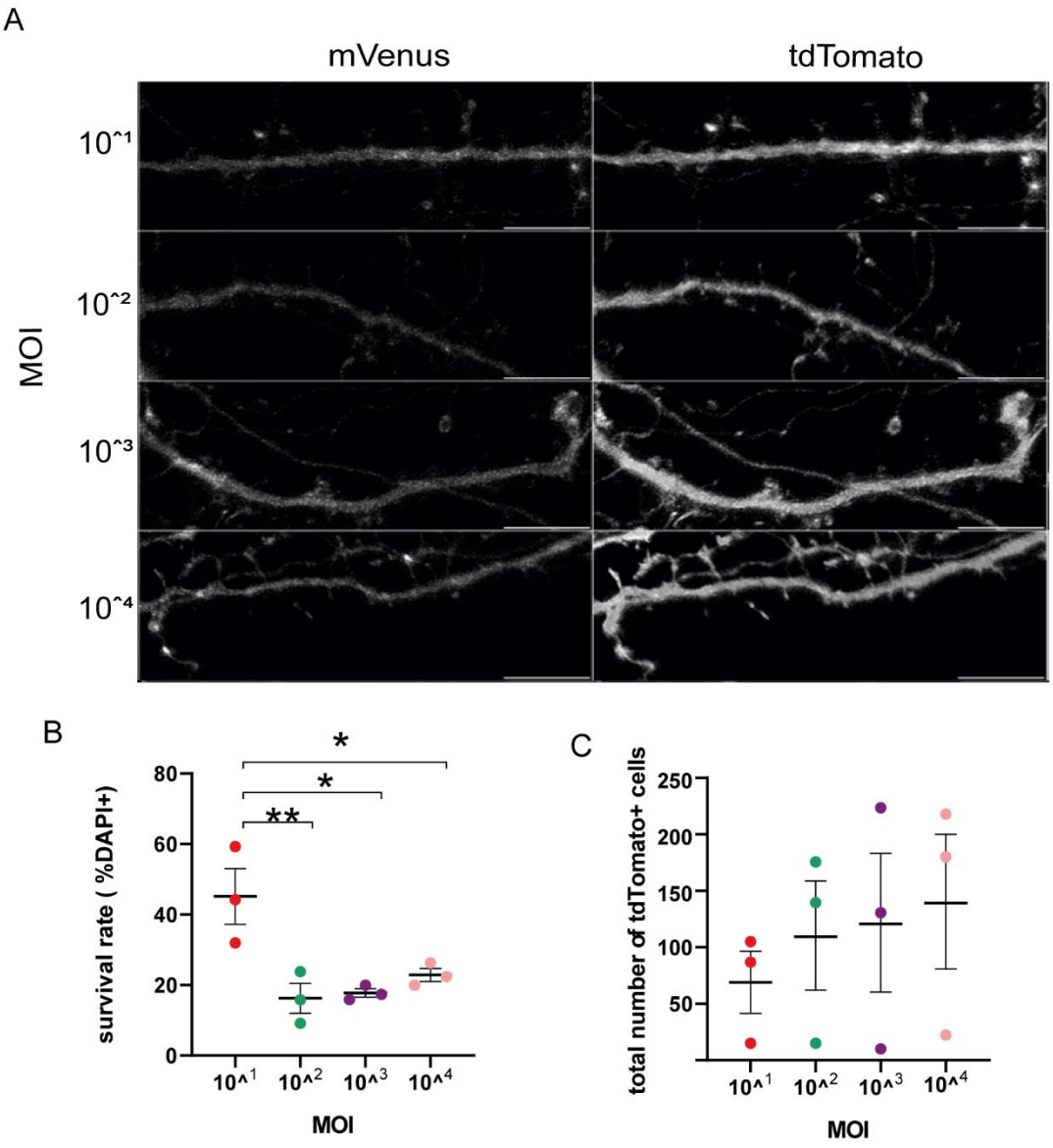

Figure 4: Optimization of the MOI A) Representative stretches of neurons infected at DIV 7 with different MOI values. Neurons were imaged at 14 DIV B) Quantification of DAPI positive cells for each MOI used. With 10^2, 10^3, 10^4 a plateau was reached. Data are expressed as mean ± sem. One way ANOVA using Tukey's post hoc test was used (** p=0.0095, 10^1 versus 10^3 p=0.0128, 10^1 versus 10^4 p=0.0372) C) The number of tdTomato transfected cells counted for each MOI used. Using 10^4 MOI the number of Tdtomato+ cells was higher. Scale bar 10*μm,* n=3 independent experiments.

4.2.2.3 Synactive transduction at different days in vitro

Once that the MOI was defined, it was necessary to establish the optimal neuronal developmental stage in which perform the transduction and transfection. For this purpose, I measured the total number of TdTomato positive cells at various stages during the development (Figure 5, n= 2 independent cultures). The best conditions turned out to be the transduction at late stages 6-7 days in vitro (DIV) and the transfection at early stages as 3-5 DIV.

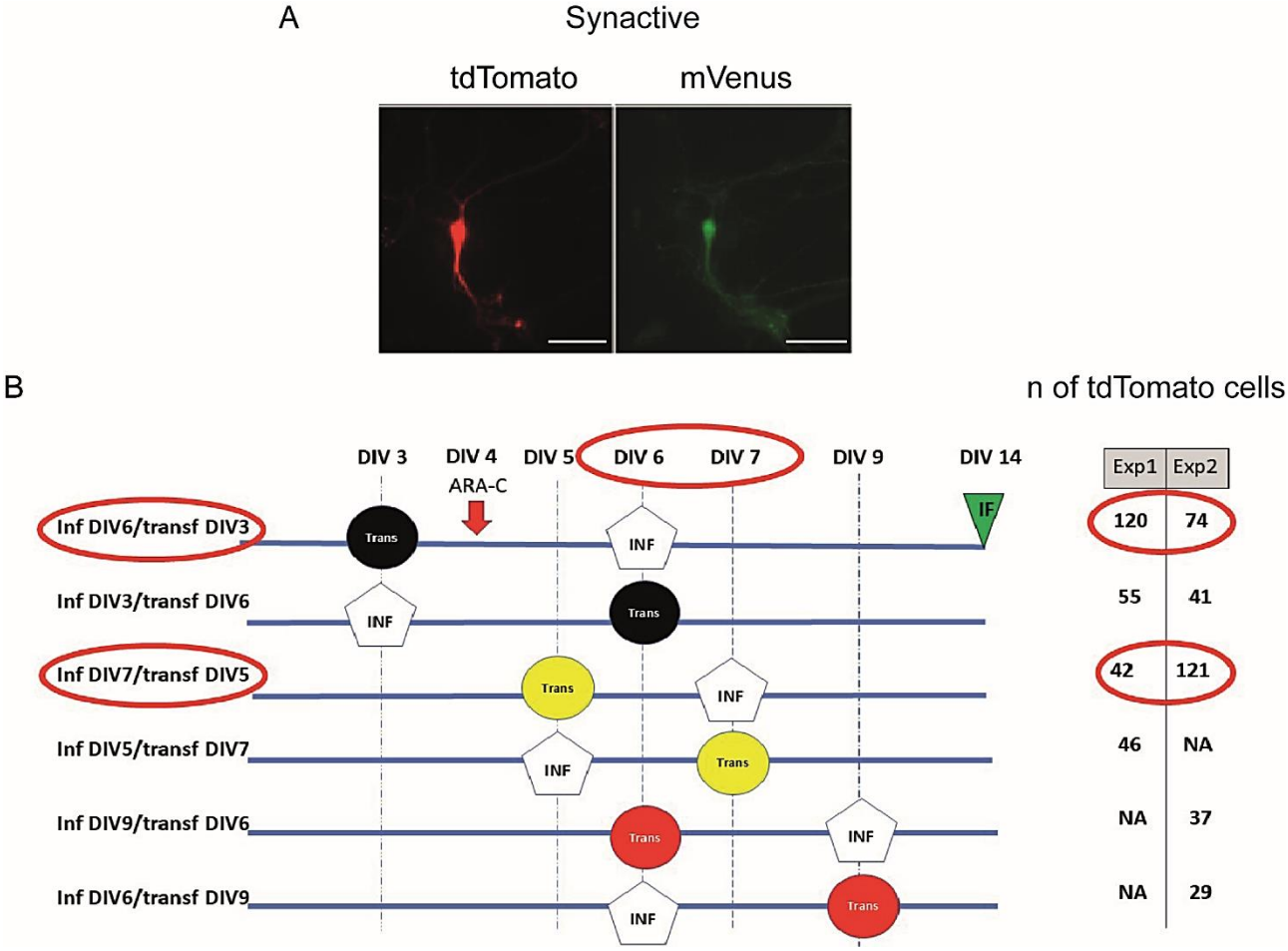

Figure 5: Transduction at different developmental stages A) Representative infected/transfected neurons with Synactive B) Different trials at which the transfection and the transduction were tested, in red the two conditions that showed the higher number of tdTomato positive cells. Scale bar 50µm, n= 2 independent cultures.

4.2.2.4 Qualitative analysis of Synactive positive neurons in control and potentiated condition

First, I performed a qualitative approach on Synactive. Neurons infected and transfected with Synactive were immunolabelled with PSD-95 to define the subcellular localization of Synactive.

Because of the post-synaptic tag present in the Synactive mVenus construct, Synactive was reported to be at the post-synaptic side (Gobbo et al., 2017). Synactive appeared to be expressed in the post synaptic side also in my system. Some dots of Synactive seemed to co-localize with PSD95 and some others not (Figure 6 A, n= 2 independent cultures). Indeed, I expected that only a sub-set of spines were potentiated, whereas others not. The dots of Synactive that seemed to co-localize with PSD95 could indicate the activated synapses, while the others could be the non-potentiated synapses. However, these analyses are qualitative (Figure 6 A). Neurons transduced and transfected with Synactive were also treated with different stimuli to evaluate if the pattern of fluorescence and/or the localization of Synactive changed (Figure 6 B, n=2 independent cultures). Neurons were treated with TTX for 2 days before the cLTP induction. Neurons activated with the glycinergic LTP stayed for 3 minutes in 200µM glycine and then 3 hours in neurobasal medium before being fixed. Neurons activated with KCl stayed for 3 hours with 50mM KCl. As showed in the panel B in Figure 6, the pattern of Synactive was not changed after these different stimuli while an enrichment at spines after cLTP and KCl treatment was expected.

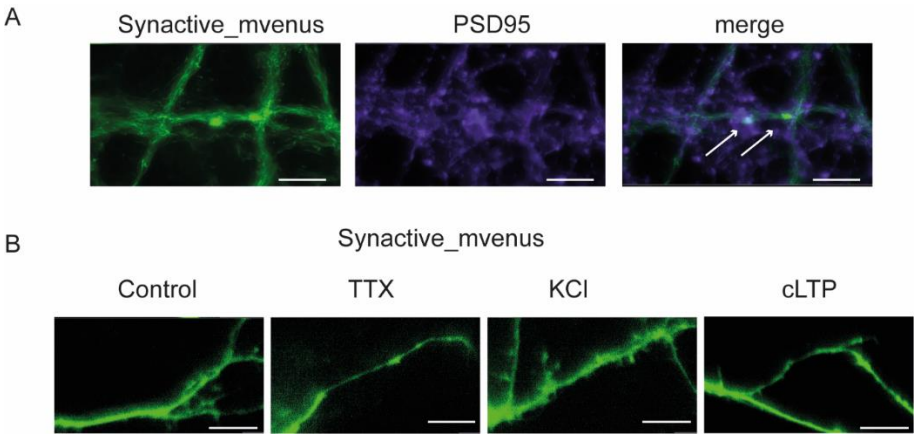

Figure 6: Qualitative evaluation of Synactive neurons. A) Neurons infected and transfected with Synactive, after the potentiation protocol, were fixed and immunolabeled with PSD95. Arrows indicate some PSD95 dots that seemed to colocalize with Synactive dots and some other PSD95 dots that did not colocalize with Synactive. Images taken with confocal microscope 60x objective B) Representative dendrites stretch of neurons activated with different stimuli such as: TTX (0.5 µM), 50mM KCl for 180' and 200µM glycine for 3' for the cLTP protocol. Images taken with epifluorescence microscope with a 60x objective. Scale bar 20 µm.

4.2.2.5 Quantitative analysis of Synactive infected neurons in control and potentiated conditions

After the first qualitative evaluation of the tool, a quantitative analysis was performed. Neurons infected and transfected with Synactive were activated with glycinergic cLTP (Materials and Methods) and then leaved for 3 hours in the conditioned medium. To evaluate if the Synactive tool allows to see a difference between activated and not activated spines, I measured the fluorescence of spines. I expected to see an enrichment of fluorescence after cLTP induction at potentiated spines. As showed in Figure 7, the fluorescence of Synactive was measured in spines and along the dendritic shaft, through a line scanning approach (Figure 7 B). The quantification was performed on neurons that stayed in Neurobasal, and on neurons activated with the glycinergic cLTP protocol, or neurons activated with 50 mM KCl were considered (Figure 7 A). The fluorescence at activated spine (green line panel C) was not higher than the fluorescence of the control (red line, panel C) or the KCl (black line, panel C) spines. Indeed, it seemed that the fluorescence of the control neurons was higher than the two potentiated conditions (cLTP and KCl) for the spine intensity (panel C, ctrl versus KCl $p=0.0003$, n= 50-60 spines analysed for each condition in approximately 10-13 neurons for each condition) and also for the shaft (panel D, ctrl versus KCl and ctrl versus cLTP $p<0.0001$). Indeed, this result showed that the expected enrichment at activated spines was not visible neither after glycinergic cLTP protocol, nor after the KCl treatment was visible. When the fluorescence of the spine and the shaft was compared (as showed in panel E, F, G in Figure 7) the fluorescence of the shaft was significantly higher for the ctrl ($p=0.0022$) and the KCl ($p=0.0022$). The fluorescence of cLTP spines was slightly higher than the shaft, but still not statistically significant (Figure 7, panel F).

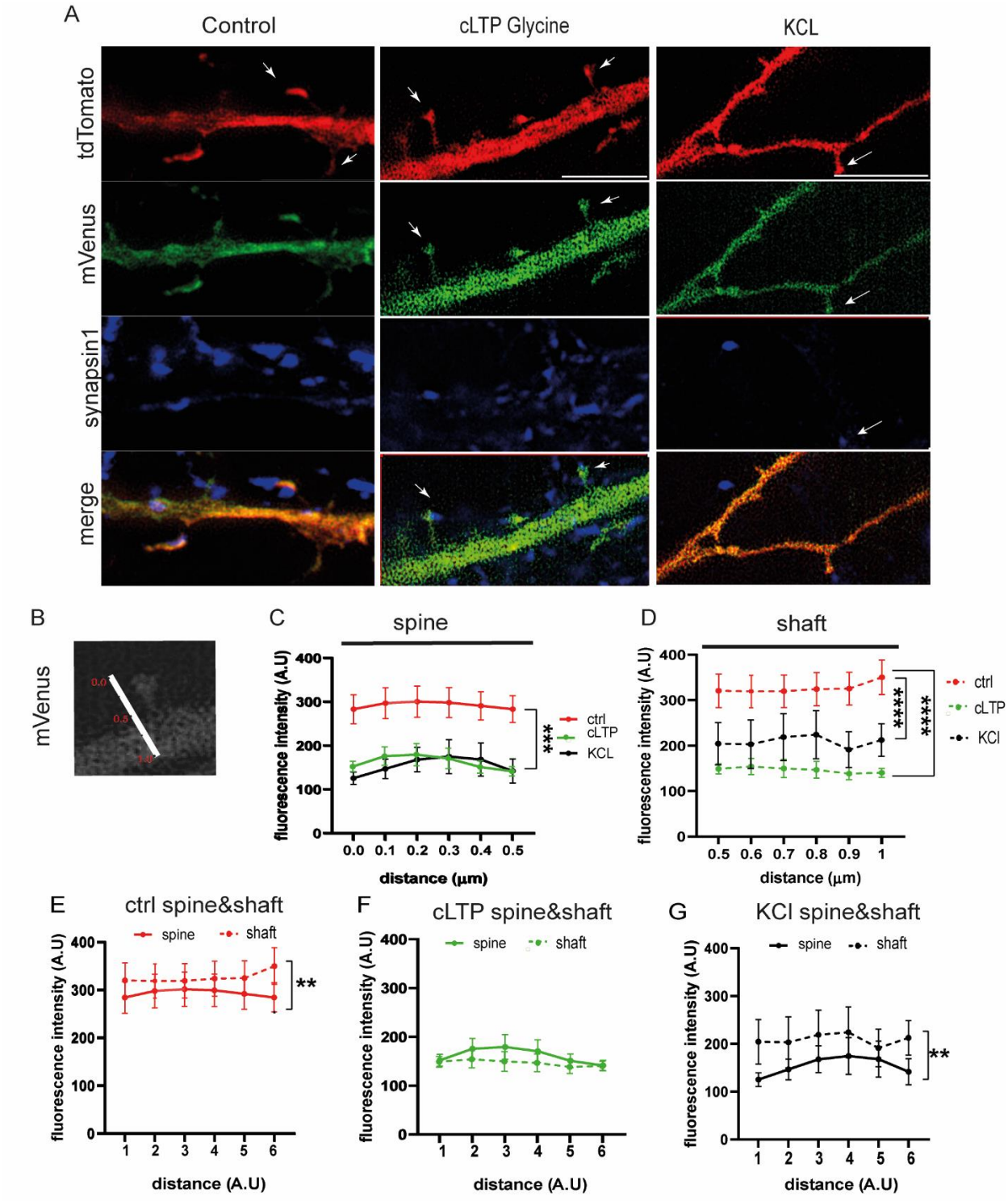

Figure7: Quantitative analysis of Synactive A) Representative images of control neurons and activated neurons with cLTP glycinergic protocol and with 50mM KCl for 180'. Spines were detected and examined in a further analysis, scale bar 20 µm B) Representative spine: a line scanning approach was used to measure the fluorescence along each spine. Starting from the top of the spine, a line of length 1 µm was drawn and the fluorescence was measured C) Fluorescence of spines in control, cLTP and KCl conditions. Data plotted as mean ± sem. ANOVA followed by Dunn's post hoc test was pursued for panel C and D. Panel E, F, G

represent the fluorescence intensity in spine and along the shaft for each condition, Mann-Whitney test between shaft and spine fluorescence was conducted.

4.3 Validation of chemical LTP protocol

4.3.1 Glycinergic protocol

4.3.1.1 Increment of endogenous BDNF protein levels after Glycinergic cLTP

As a read out for the cLTP activation, I measured the endogenous BDNF protein at different time points after the induction of cLTP. To ensure that neurons were mature enough to have fully active synapses, I performed all the experiments at 14-15 div. I performed two sets of experiments that differed in the medium used after the treatment with 3 minutes with 200µM glycine. In the first set of experiments (Figure 8 panel A), neurons after Glycine were incubated in Neurobasal, whereas in the second set, after glycine treatment, neurons were transferred in ECS. In the first case I considered the following time points 15 minutes, 30 minutes, 1 and 3 hours after cLTP induction, whereas with ECS I settled the last time course at 1 hour, since neurons did not survive at 3 hours. Then, neurons were stained for BDNF and MAP2 (Figure 8 B). Confocal images were acquired and a quantification of the average intensity of BDNF along different compartments of apical dendrites (primary, secondary and tertiary dendrites and primary and secondary branching points) were performed in order to understand where BNDF increased after cLTP induction (Figure 8 C). Densitometric analysis of BDNF immunofluorescence was performed in each condition. For each considered ROI, the average intensity of BDNF was normalized to the MAP2+ average intensity. As showed in Figures 8 D (i) and E (i), in all the conditions, for both data sets, the BDNF fluorescence turned to be not higher than the basal level in all the tested cLTP conditions. Besides, I also evaluated the total volume occupied by BDNF and MAP2. This was obtained by considering the area above a fixed threshold value of intensity and summing these values over the full z-stack. However, also in this case BDNF did not show any significant increment upon cLTP stimulus (Figure 8 D ii and E ii, n=4 independent cultures for each of them 10-13 neurons were analysed). In addition, the same analysis was conducted with a positive control given by neurons treated with 50mM KCl for a time of 180'. Indeed, a work published by our laboratory (Baj et al., 2016) reported that this condition can give a significant increase of BDNF protein in all the neuronal regions

analysed (soma, d1, bp1, d2, bp2, d3). Repeating the experiments using KCl, I did not identify the expected increment of BDNF (Figure 8 F, n=3 independent cultures, 10-13 neurons analysed in each culture). I also evaluated the BDNF fluorescence intensity and volume without the MAP2 normalization, since the MAP2 expression turned out to be not enough constant to be used as a proper reference value (see Figure 9). However, as reported in Figure 9, I did not detect any significant increment of BDNF neither in mean intensity nor in the volume for both the settings: Neurobasal and ECS.

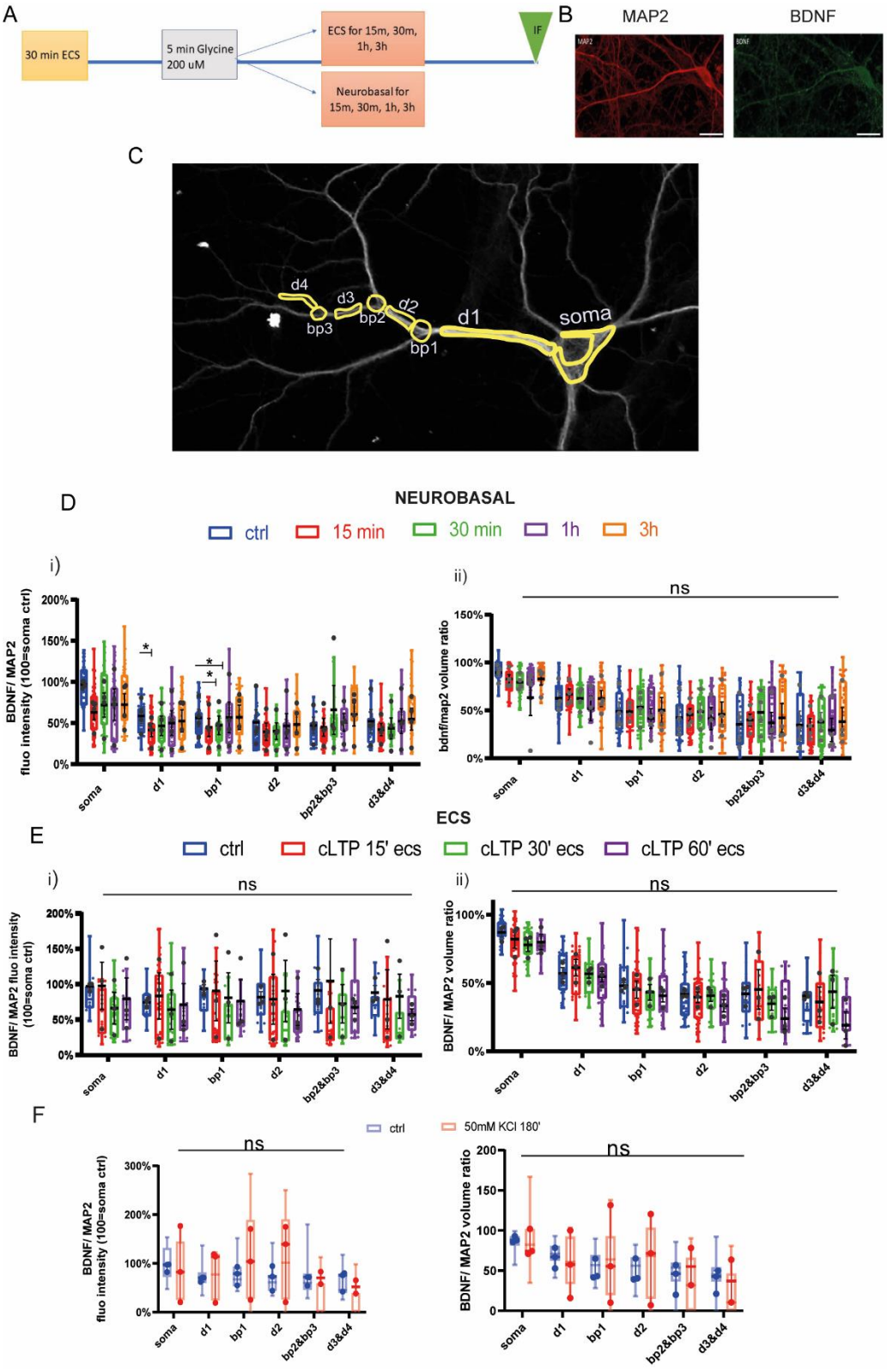

Figure 8: Endogenous BDNF quantification. A) Experimental outline of the glycinergic cLTP protocols: neurons after the 3 minutes of 200 µM Glycine, were incubated either in Neurobasal or in ECS for different time courses. B) Fixed and immunolabeled neurons for BNDF and MAP2 C) Representative

regions used in the quantification: soma, primary dendrite (d1), primary branching point (bp1), secondary dendrite (d2), secondary branching point (bp2), tertiary dendrite (d3), tertiary branching point (bp3), quaternary dendrite (d4). D) Experiments conducted with neurons that after glycine were incubated in Neurobasal: i) BDNF/MAP2 intensity ratio, data from n=4 independent experiments were plotted together, statistical analysis was conducted on the mean of each experiment (black dots) using the ANOVA followed by Dunnett's post hoc test. A decrement of BDNF/MAP2 intensity ratio was visible between ctrl and 15 min cLTP in d1 and in bp1 regions. Viceversa, BDNF increment was not reported in any condition ii) BDNF/MAP2 volume ratio did not show any increment upon cLTP stimulation E) Experiments conducted with neurons that after glycine stayed in Neurobasal: i) BDNF/MAP2 intensity ratio. The data of n=3 independent experiments have been merged and plotted together; statistical analysis was conducted on the mean of each experiment (black dots) using the ANOVA followed by Dunnett's post hoc test ii) BDNF/MAP2 volume ratio did not show any increment upon cLTP stimulation F) As a positive control, neurons were incubated for 180' with KCl 50 mM, the same analysis was conducted and no increment in the BNDF/MAP2 intensity ratio, or in BDNF/MAP2 volume ratio was detected. Dots represent n=3 independent experiments. ANOVA followed by Dunnett's post hoc test was used.

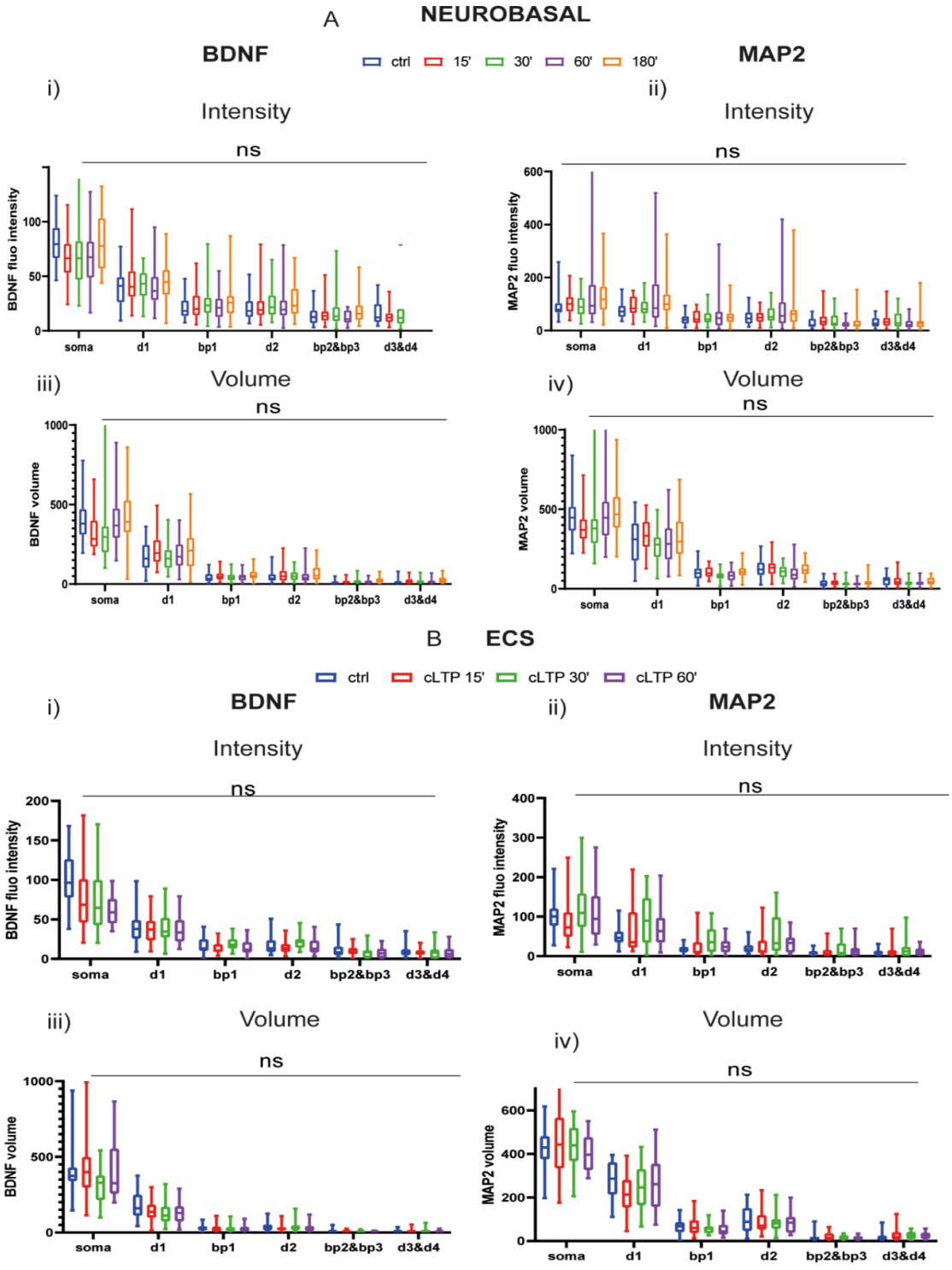

Figure 9: Endogenous BDNF quantification, without normalization to MAP2. A) Experiments conducted with neurons that after glycine stayed in Neurobasal: i) BDNF fluorescence intensity, ii) MAP2 fluorescence intensity. All the data of n=4 independent experiments were plotted together. Statistical analysis was conducted using the ANOVA followed by Dunnett's post hoc test. iii) BDNF volume and iv) MAP2 volume B) Experiments conducted with neurons that after glycine stayed in Neurobasal: i) BDNF intensity ii) MAP2 fluorescence intensity all the data of each experiments n= 3 independent experiments were plotted together, statistical analysis using the ANOVA followed by Dunnett's post hoc test iii) BDNF volume iv) MAP2 volume.

4.3.1.2 GluA1-vGLUT1 and PSD95-vGLUT1 quantification of Glycinergic cLTP

During LTP the steady state of AMPA receptors at the synapses is very mobile and this induces a dynamicity in the pool and trafficking of receptors (Huganir and Nicoll, 2013). Different working models have been proposed to explain the dynamics of the system. In the insertion model: exocytosis of AMPA receptors is the mechanism that leads to an increase of glutamate receptors containing vesicles onto the surface (Huganir and Nicoll, 2013; Lu et al., 2001). Considering this aspect, an antibody for the GluA1 subunit (Materials and Methods) of the AMPA receptors that recognizes an extracellular epitope of the receptor was used. Control cultures and cLTP cultures were fixed and immunolabeled with VGLUT1, a marker of pre-synaptic terminals, and GluA1. The time-course for the cLTP induction was the same used in previous experiments. The number of presynaptic puncta and the presynaptic puncta area were evaluated (Figure 10 panel B i) and ii)), showing that after cLTP 15' ($p=0.0090$) and 60'($p=0.0011$) there was an increment in the VGLUT1 puncta number, whereas no significant change was detected for the area of VGLUT1 (ii). Surprisingly, the number and the area of GluA1 puncta were not increased after cLTP induction (Figure 10 panel C i) and ii)), suggesting that the cLTP was not induced. The colocalization of VGLUT1 and GluA1 was not changed upon cLTP induction (D,E). Considering that the GluA1 antibody did not produce the expected dotty pattern, to determine whether cLTP was induced or not, I evaluated the colocalization of VGLUT1 with PSD95 (Figure 11). The same glycinergic protocol was applied. These experiments were conducted considering just a time point: after the 3 minutes of glycine, neurons stayed for 30' in ECS (indicated as the cLTP in Figure 11). This timing was chosen considering the results of a previous analysis on neurons in which cLTP was induced with a similar protocol (personal communication with Dr. Elisa Pati, PhD's at SISSA). The same parameters: the number and the area of presynaptic and postsynaptic sites were considered. However, neither the presynaptic (VGLUT1, panel C) and the postsynaptic (PSD95, panel B) puncta showed an increment in the size, neither in their number (panel B). The colocalization between VGLUT1 and PSD95 did not show any significant increment after cLTP induction (panel D, n=2 independent cultures, ROI from 8-10 neurons were analysed for each condition in each culture).

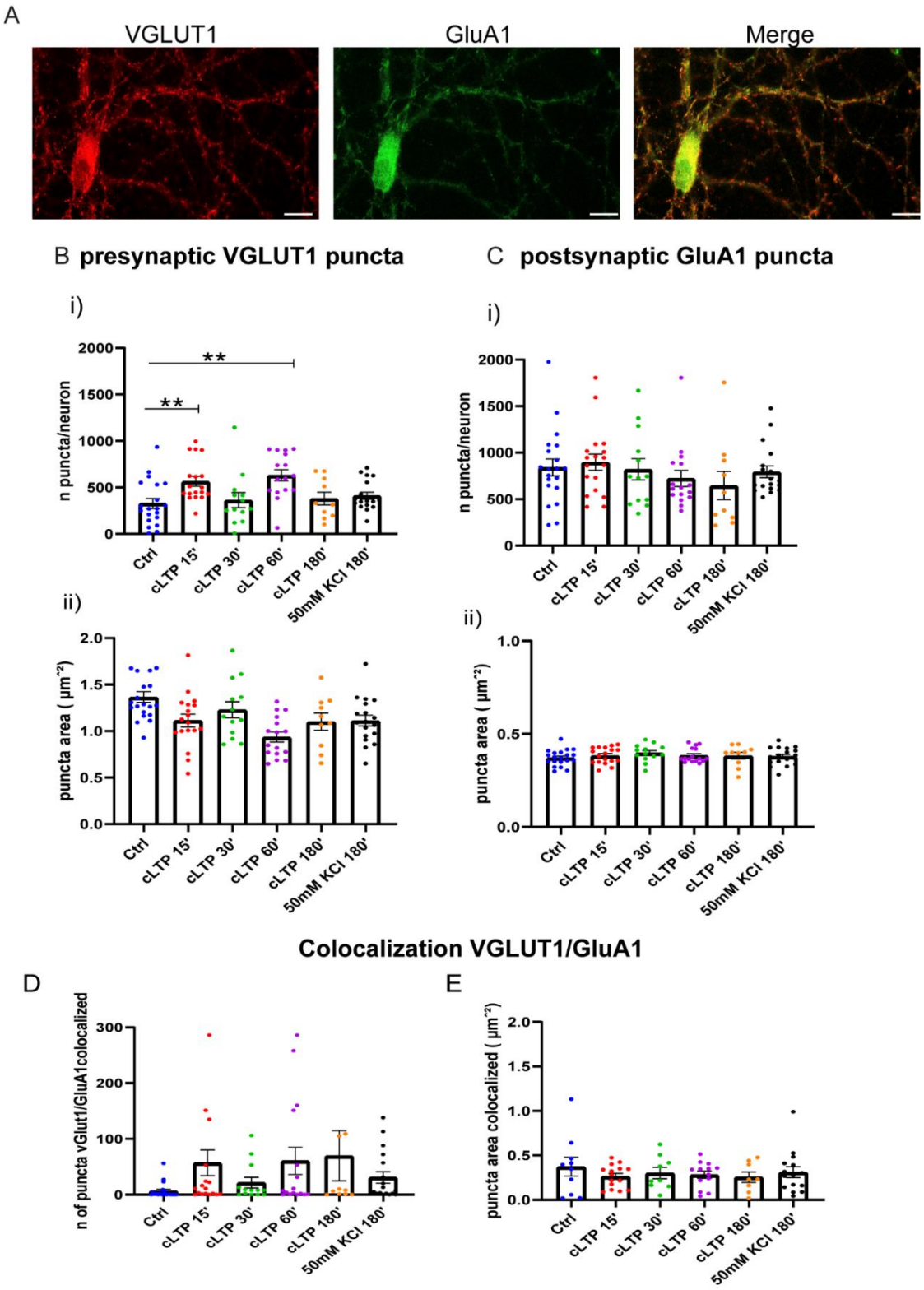

Figure 10: GluA1 and VGLUT1 quantification A) Representation of immunolabeled neurons with VGLUT1 and GluA1, scale bar 10 µm B) Presynaptic VGLUT1 quantification i) n of VGLUT1 puncta in each neuron analysed by ANOVA test followed by Dunnett's post hoc test showed significance p=0.0090 for 15 minutes and p=0.0011 for 60 minutes ii) area of the VGLUT1 puncta C) postsynaptic GluA1 puncta i) puncta in each neuron, ii) GluA1 puncta area D) colocalization of VGLUT1 and GLuA1 puncta E) area of VGLUT1 and GluA1 colocalized.

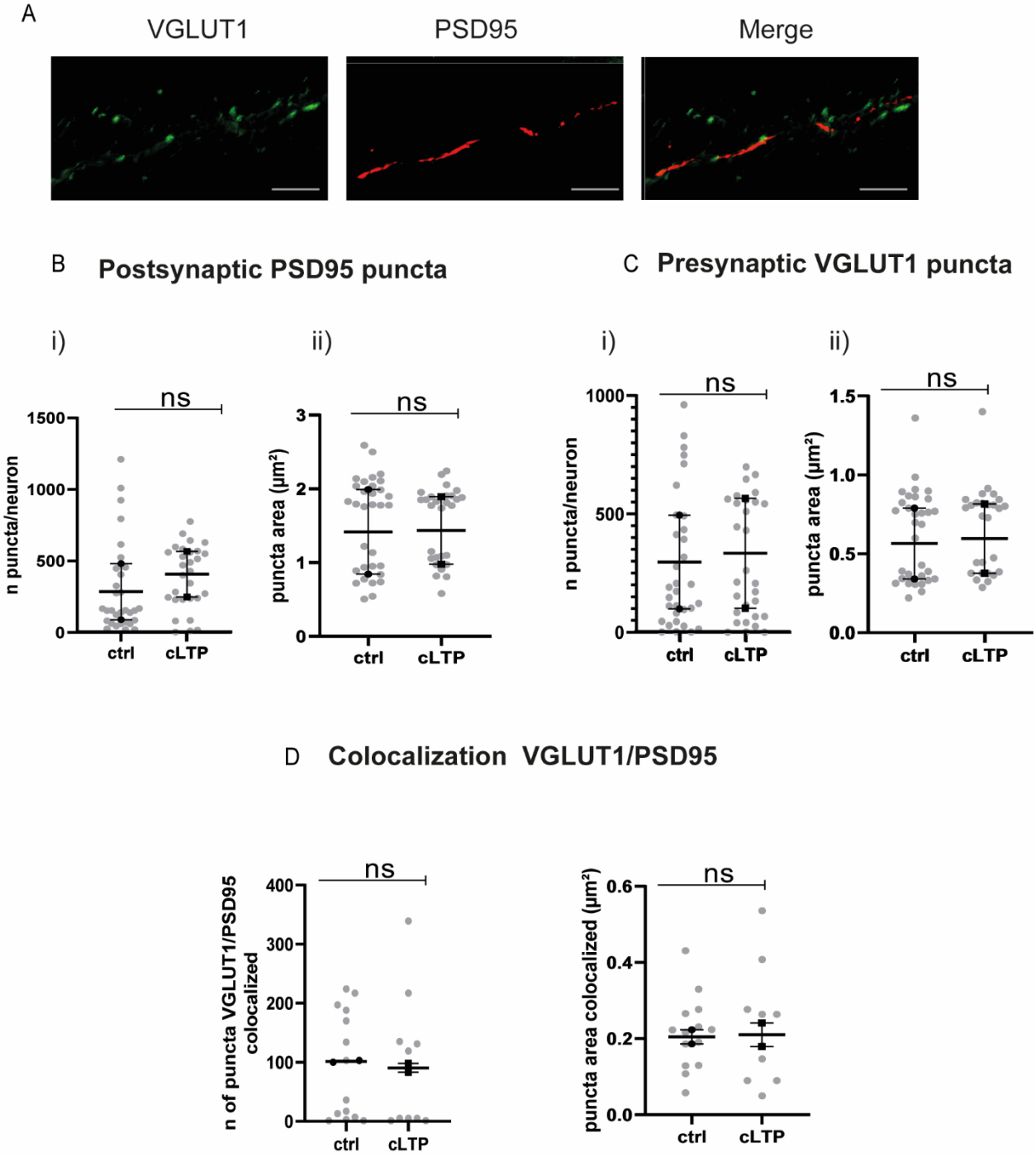

Figure 11: PSD95 and VGLUT1 quantification A) Representation of immunolabeled neurons with VGLUT1 and PSD95, scale bar 10 µm B) Presynaptic VGLUT1 quantification i) n of VGLUT1 puncta in each neuron analysed by t-test test showed not statistical difference in the two conditions ii) area of the VGLUT1 puncta C) postsynaptic PSD95 puncta i) number of puncta in each neuron, ii) PSD95 puncta area D) colocalization of VGLUT1 and PSD95 puncta on the left the number of puncta colocalized and on the left the area of VGLUT1 and GluA1 colocalized. Data are showed as median with 95% CI and unpaired t-test has been used, n=2 independent cultures in each of them ROI from 8-10 neurons were considered.

4.3.1.3 cFOS evaluation of glycine-cLTP induction

As a third read out for the cLTP induction, I used C-fos immunostaining to determine whether the induction of cLTP was successful. *C-fos* is an immediate early gene that is commonly used to assess neural activity (Bullitt, 1990; Ferhat et al., 1993; Herdegen and Leah, 1998). The *C-fos* expression was analysed by means of the immunocytochemical detection of Fos, the nuclear phosphoprotein encoded by the *c-fos* gene. First of all, cultures activated with the cLTP glycinergic protocol were immunolabeled with C-fos at various time intervals: 15 minutes, 30 minutes, 60 minutes and 180 minutes after cLTP activation: the time point considered were the same for the quantification of endogenous BDNF. As showed in Figure 12 panel A, the C-fos mean intensity was evaluated using a customed MACRO created and developed by me in order to analyse the C-fos positive cells (details on Materials and Methods). Results of three independent experiments showed that after the cLTP induction an increase of C-fos protein expression in the nucleus was not detected (Figure 12 E, n= 3 independent cultures, in each coverslips hundreds of cells were analysed). Our data suggested that the C-fos intensity in control condition (Neurobasal) was high and it was difficult to detect a difference with the activated ones. A possible explanation for this behaviour was that the Neurobasal medium contained 0.8mM magnesium, a possible cause for the high excitability of the control neurons. Considering this aspect, a second trial of experiments were made: neurons were incubated in ECS (composition in materials and methods) and not in neurobasal for the control condition. However, data did not show any increment after cLTP induction (Figure 12 F, n= 2 independent cultures, between 1000 and 2000 analysed cells).

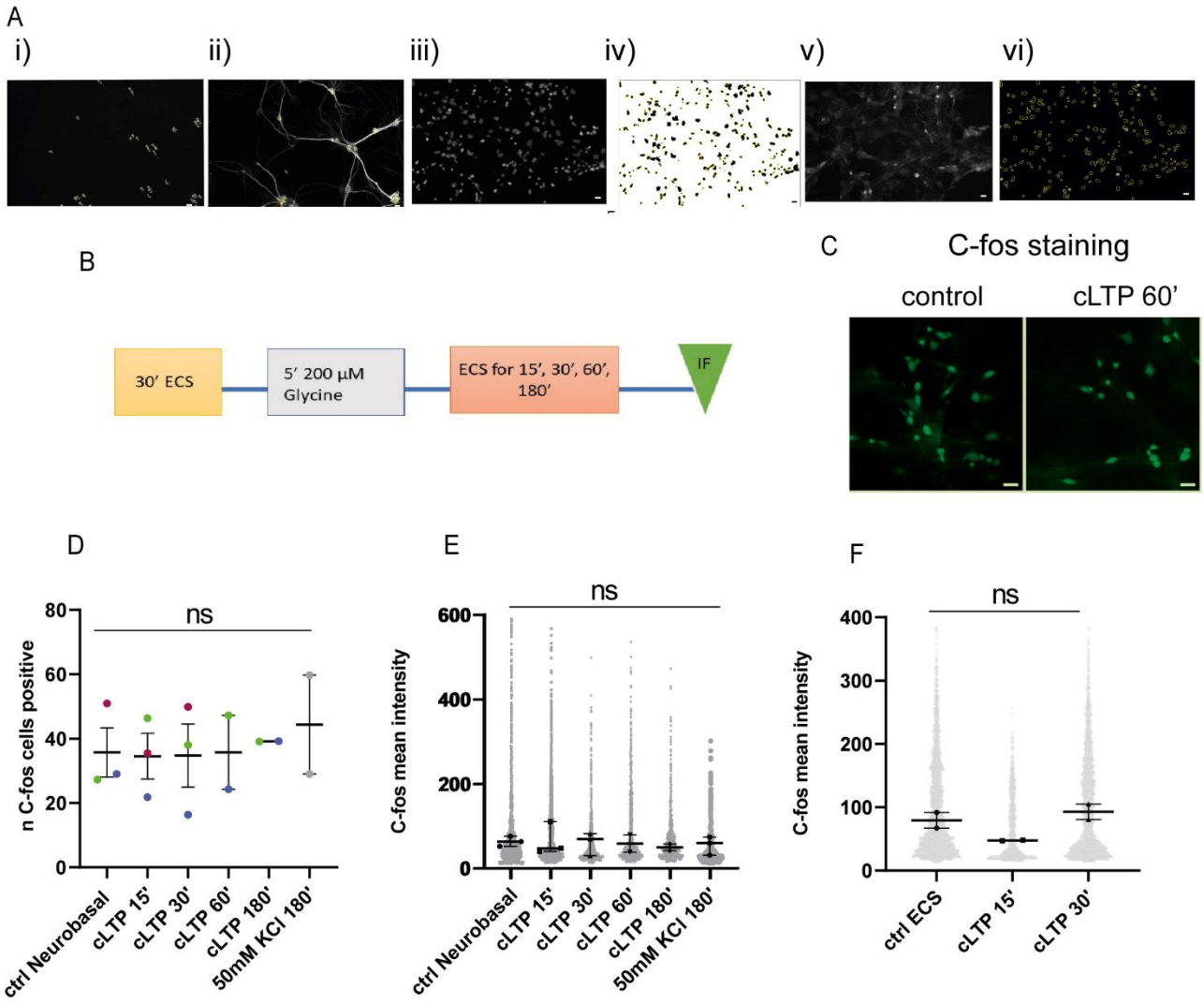

Figure 12: C-fos evaluation after the glycinergic cLTP induction A) Representative images used to validate the MACRO created for the detection of C-fos positive cells. In i) DAPI+ cells are showed, After the application of a threshold, only the DAPI+ cells of area within the range 5-10 µm² were taken into account, these DAPI+cells were verified to be neuronal cells because the thresholded DAPI+ cells were super-imposed to a MAP2 staining (ii); a mask of DAPI+ cells was created iii), iv) the mask was then applied to C-fos channel image B) Experimental outline for the C-fos experiments C) C-fos staining of control cultures and cultures in which the cLTP was induced. Scale bar 10 µm D) Quantification of C-fos cells by eye was performed for the three independent experiments, this analysis was no further considered E) Analysis of the C-fos mean intensity using the MACRO, each grey dot represents a cell, the median of each experiment was showed in black. ANOVA followed by Kruskal-Wallis test on the median of n=3 independent experiments showed no significant differences upon cLTP induction F) C-fos mean intensity quantification with control neurons in ECS medium, same analysis using the Kruskal-Walllis test was performed.

4.3.1.4 KCl as a positive control

As showed with the previous analysis, the increment of endogenous BDNF was not higher even when cultures were treated with KCl following a protocol reported in literature (Baj et al., 2016). In order to define the optimal time point and the KCl concentration, I evaluated the C-fos intensity of cultures that were treated with 50 mM KCl for 30',60' and 90' minutes. Cumulative plots showed in Figure 13 indicated that 90' minutes was the time in which the population of cells showed the higher C-fos fluorescence intensity (panel A iii). Once that the time of 90' was selected, different concentrations of KCl were tested: 10mM, 20mM and 50mM. This latter concentration turned out to be the one having the largest increment in C-fos intensity fluorescence (p=0.0351, panel B, n= 4 independent cultures, between 1000 and 2000 analysed cells).

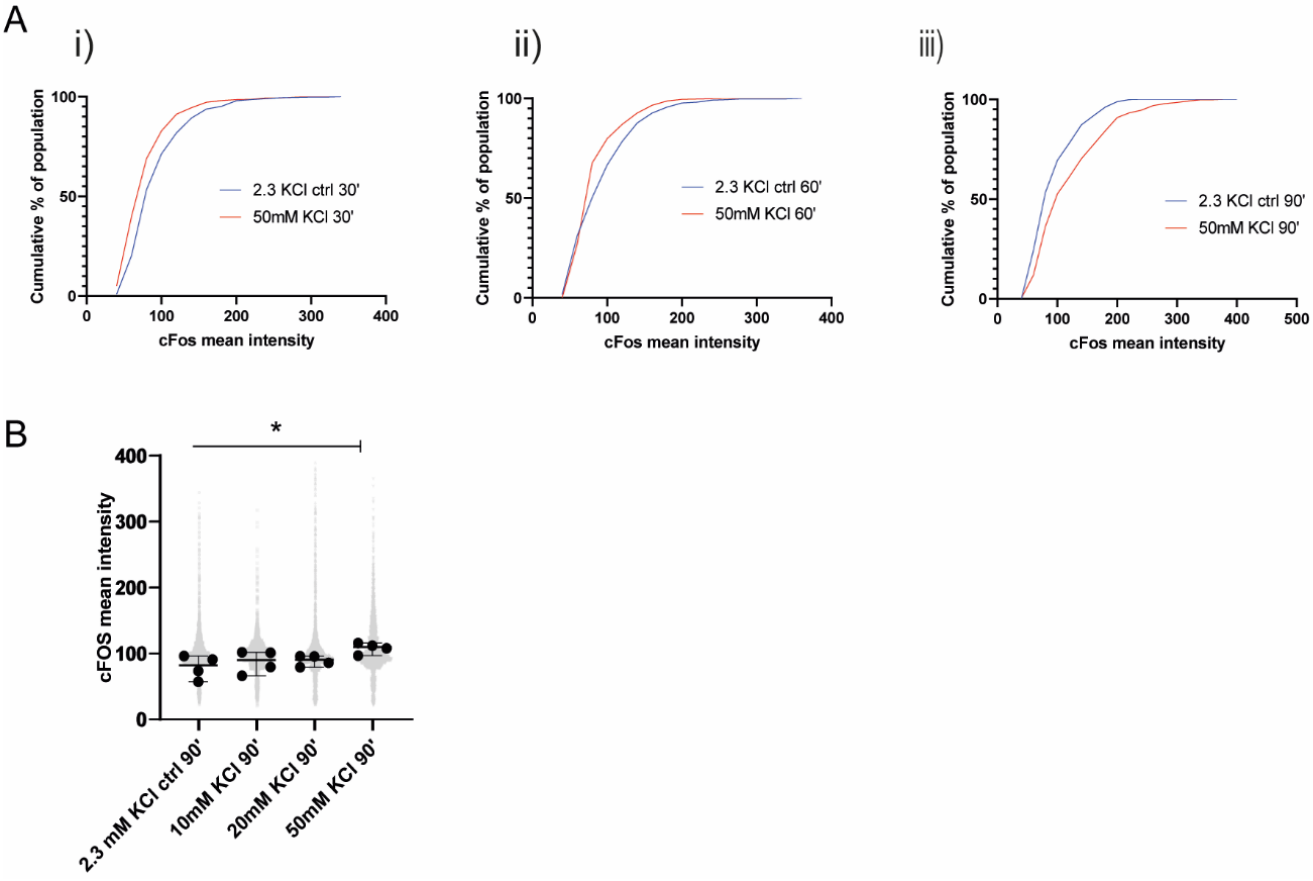

Figure 13: KCl as a positive control. A) Cumulative plots of the fluorescence intensity of neurons for control and KCl 50 mM at different time-points: i) KCl 30 minutes. The cumulative curve of KCl is shifted to left, showing that the population of neurons has lower fluorescence intensity compared to the control. Ii) KCl 60 minutes shows a similar behaviour iii) KCl 90 minutes, the cumulative curve of KCl is shifted to right showing that the population of neurons has higher fluorescence intensity compared to the control. B) Neurons activated with different concentration of KCl 10 mM, 20 mM and 50 mM. ANOVA followed by Holm Sidak's multiple comparison revealed a significant increment of cFos intensity after 90' with 50 mM KCl. n=4 independent experiments.

4.3.1.5 Characterization of neuronal cultures using different AraC concentrations

Evaluating the difficulties faced with the induction of cLTP in neuronal cultures, I considered the glia impact in cultures, supposing that in my model glia was not enough for the cLTP induction. First of all, I characterized neuronal hippocampal cultures using different AraC concentrations. The used concentration in the laboratory was 1:2500 (2µM) my starting concentration, then I tried different dilutions such as 1:4000 (1.25 µM), 1:6000 (0.83µM), 1:8000 (0.62µM) of AraC adding a condition in which AraC was not added (Figure 14). For each condition, the total number of neurons, astrocytes and DAPI+ cells were manually counted in all the 10 fields imaged from each coverslip per condition. The data revealed that there was a significant increment of DAPI+ cells in the absence of AraC if compared with all the other conditions (Figure 14 B NO AraC vs. 0.62µM p=0.0103; NO AraC vs. 0.83µM p=0.0130; NO AraC vs. 1.25µM p=0.0082; NO AraC vs. 2µM p=0.0072, n= 3 independent cultures). Together with the increment of DAPI+ cells, also GFAP+ cells increased as expected (Figure 14 C; NO AraC vs. 0.62µM p=0.0024; NO AraC vs. 0.83µM p=0.0008; NO AraC vs. 1.25µM p=0.0006; NO AraC vs. 2µMp=0.0005, n= 3 independent cultures). The ratio between MAP2+/GFAP+ cells increased with the concentration of AraC (Figure 14 D, NO AraC vs.1.25µM p=0.0191; NO AraC vs. 2µM p=0.0004; 0.62µM vs. 2µM p=0.0122; 0.83µM vs. 2µM p=0.0090, n=3 independent cultures), suggesting, as expected, an increment of MAP2+ when the GFAP+ cells diminished. Together with the total number of cells, the area of the coverslip covered by the GFAP+ and MAP2+ was measured by applying a threshold (details on Materials and Methods). With lower concentration of AraC, the area occupied by GFAP+ increased, whereas the area of MAP2+ decreased (Figure 14 E). Specifically, the percentages are reported in the table in panel D. At this point, cLTP induction through Glycine 200 µM was tried again in order to evaluate the involvement of glia in cLTP. However, as showed in panels F and G of Figure 14, cFOS intensity at different time points from the cLTP activation was not statistically different from the control condition, suggesting that the cause for the cLTP induction failure is not related with the quantity of glia present in the cultures (n= 2 independent cultures, between 1000 and 2000 analysed cells). Data showed that even using the higher AraC concentration, astrocytes occupied the 30% of coverslip area.

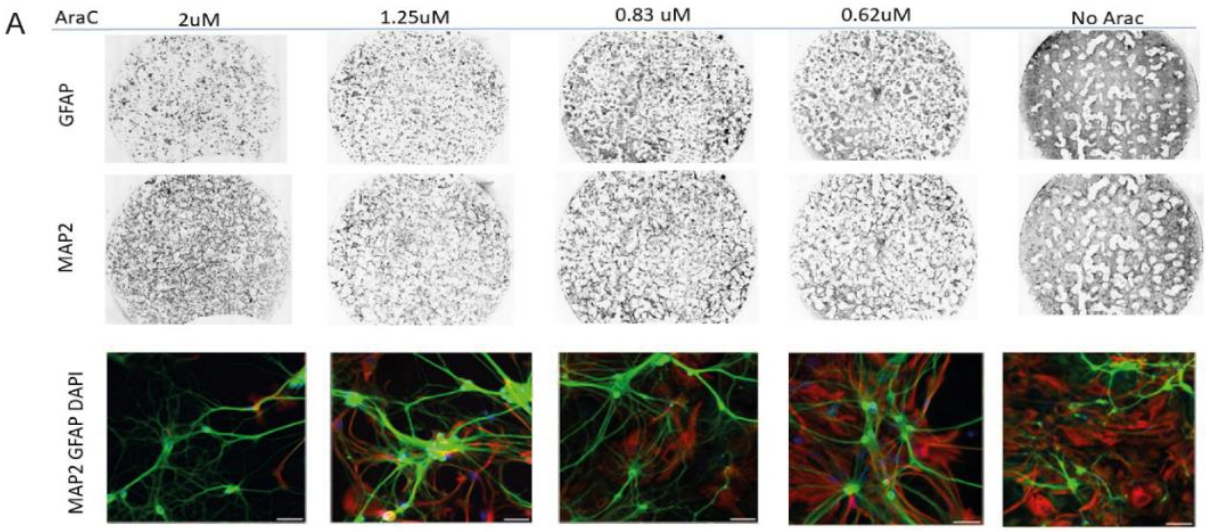

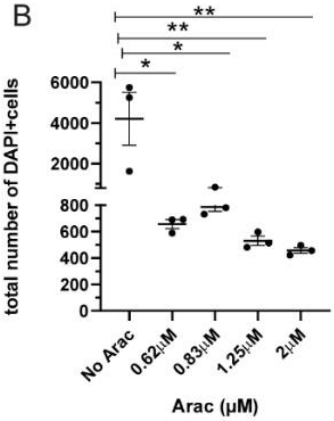

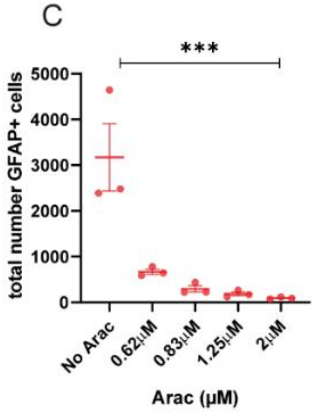

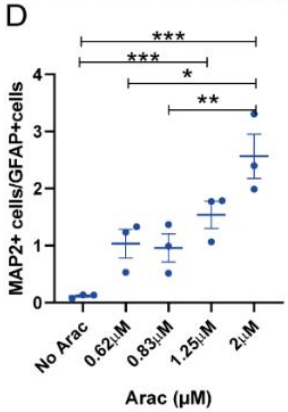

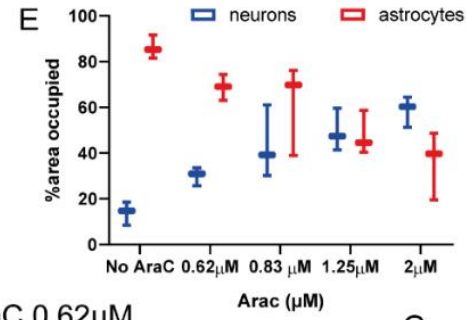

AraC conc.	Neurons %	Astrocytes%
2µM	58.6944	35.96935
1.25µM	49.4805	47.83943
0.83µM	43.49396	61.62818
0.62µM	30.04808	68.79585
NOARAC	13.86557	86.13443

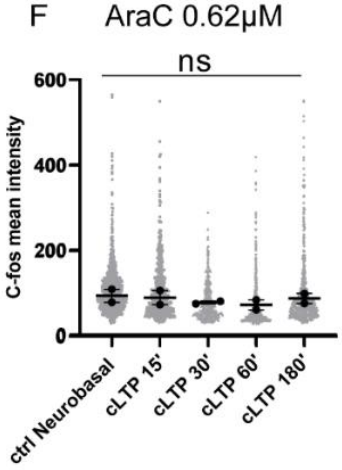

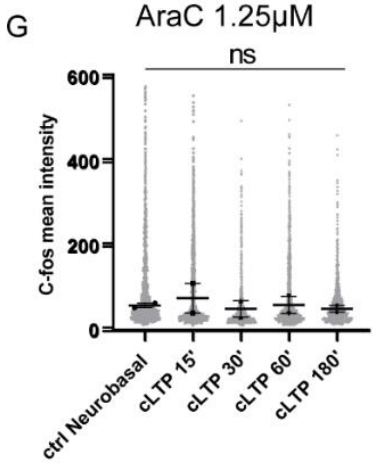

Figure 14: Characterization of neuronal cultures using different AraC concentration A) Representative panel of area covered by GFAP+ and MAP2+ at different AraC concentration. B) Total number of DAPI+ cells counted at different AraC concentration. ANOVA followed by Tukey's post hoc test revealed that the condition without AraC has the higher number of DAPI+ (No Arac vs 0.62 µM p=0.0103, no AraC vs 0.83 µM p=0.0130, no AraC vs 1.25 µM p=0.0082, No AraC vs 2µM p=0.0072) C) Total number of GFAP+ cells at different AraC concentration. The condition without AraC shows significantly higher number of GFAP+ cells, as expected (NO AraC vs. 0.62µM p=0.0024; NO AraC vs. 0.83µM p=0.0008; NO AraC vs. 1.25µM p=0.0006; NO AraC vs. 2µMp=0.0005) D) The ratio MAP2+/GFAP+ increase with the AraC concentration (NO AraC vs.1.25µM p=0.0191; NO AraC vs. 2µM p=0.0004; 0.62µM vs. 2µM p=0.0122; 0.83µM vs. 2µM p=0.0090) E) Area of MAP2+ and GFAP+ covered, the percentages are reported in the table on the right. Data are reported as mean±sem, n=3 independent experiments F) and G) After cLTP induction the cFos mean intensity is measured in cultures with different AraC concentration. ANOVA followed by Kruskal-Wallis test on the median of n=2 independent experiments showed no significant differences upon cLTP induction.

4.3.2 Glutamate LTP protocol

After the glycinergic LTP, the glutamate protocol for the activation of cLTP was tested, following the protocol published by (Franceschi Biagioni et al., 2021). Neurons at DIV 14 were activated for 30 seconds with Glutamate (50 µM, materials and methods). As read-outs of the cLTP induction, C-fos intensity and colocalization of VGLUT1 with PSD95 were evaluated. Both of them showed that the cLTP was not induced in neuronal cultures. The intensity of the C-fos was not higher for the cLTP (ctrl vs cLTP p>0.9999, n=2 independent cultures, between 900 and 2500 analysed cells). Considering the same analysis conducted for the glycinergic protocol, the analysis on the VGLUT1 and PSD95 puncta was conducted, showing that the number and the area of presynaptic and postsynaptic sites did not change upon cLTP induction (Figure 15). On the other hand, neither the presynaptic (VGLUT1) and the postsynaptic (PSD95) puncta showed an increment in the size, or in their number (panels D e E). The colocalization between VGLUT1 and PSD95 did not show any significant increment after cLTP induction (panel F).

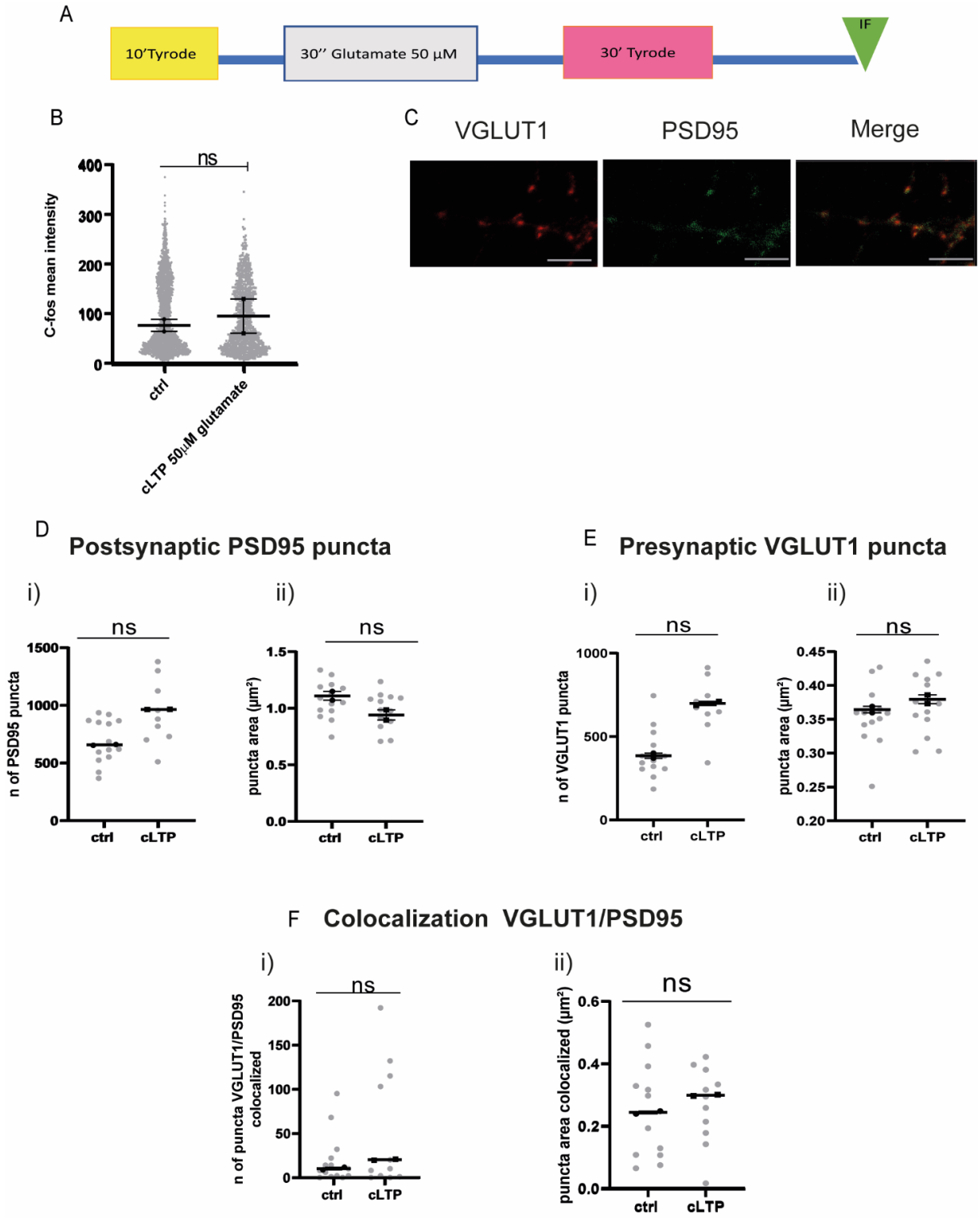

Figure 15: Glutamate cLTP protocol. A) Experimental outline of glutamate cLTP induction B) C-fos mean intensity after cLTP induction. Statistical analysis performed by unpaired t-test C) Representative images of VGLUT1 and PSD95 labelled neurons. Scale bar 10 µm D) Quantification of postsynaptic puncta: i) number of PSD95 puncta ii) PSD95 puncta area E) Quantification of presynaptic puncta: i) number of VGLUT1 puncta ii) VGLUT1 puncta area F) Quantification of colocalization of VGLUT1/PSD95: i) number of VGLUT1/PSD95 puncta colocalized ii) puncta area colocalized. Data are analysed by unpaired t test and median with 95% CI is represented. n=2 independent experiments

4.3.3 Forskolin LTP protocol

I considered, as the last protocol for the cLTP induction, the Forskolin cLTP. Neurons were treated for 90 minutes with 10 μM of Forskolin following the protocol reported in Lam et al., 2009. In the first set of experiments, the expected increase of C-fos intensity compared to not activated cultures, was not detected. Thus, a second set of experiments was tried adding 0.01% Rolipram to the Forskolin (Figure 16, panel B ii). However, even in this case the expected fluorescence increase was not detected. At this point, the protocol of neuronal cultures was further optimized. Instead of glutamine 200μM, GlutaMAX (Sigma, Ala-gn) was used in the Neurobasal medium. By a comparison of glutamine and GlutaMAX cultures, it was clear that cultures with GlutaMAX were significantly activated after 90 minutes with 10 μM of Forskolin (ctrl vs cLTP p= 0.04, Figure 16 C). Thus, neurons were always cultured with GlutaMAX in the following experiments. A time-course with Forskolin 10 μM was performed. Neurons were treated with Forskolin 10 μM for 30', 60' and 90'. The same time points were considered also for neurons in control medium. As showed in Figure 16, the C-fos intensity turned out to be significantly higher after 90' (ctrl vs cLTP p=0.0379, n=4 independent cultures, between 900 and 3000 analysed cells in total), while at 30' I found a statistical tendency (ctrl vs cLTP p=0.0649). In parallel, a quantification of the VGLUT1 puncta was performed at all the time points after the cLTP induction. For each time point, unpaired t test was performed comparing the control to the corresponding activated condition. A slight statistical tendency for the increase in the number of VGLUT1 puncta as well as in the average area of puncta was found after 90' cLTP ii) ctrl vs 90' cLTP p=0.11 iii) ctrl vs 90' cLTP p=0.10, panel E (n=2 independent cultures in each of them ROI from 10-15 neurons were analysed). In conclusion, among the three different methods for the induction of chemical LTP (glycine, glutamate, forskolin), only forskolin was able to induce a significant change in C-fos, indicating activation of cLTP plasticity.

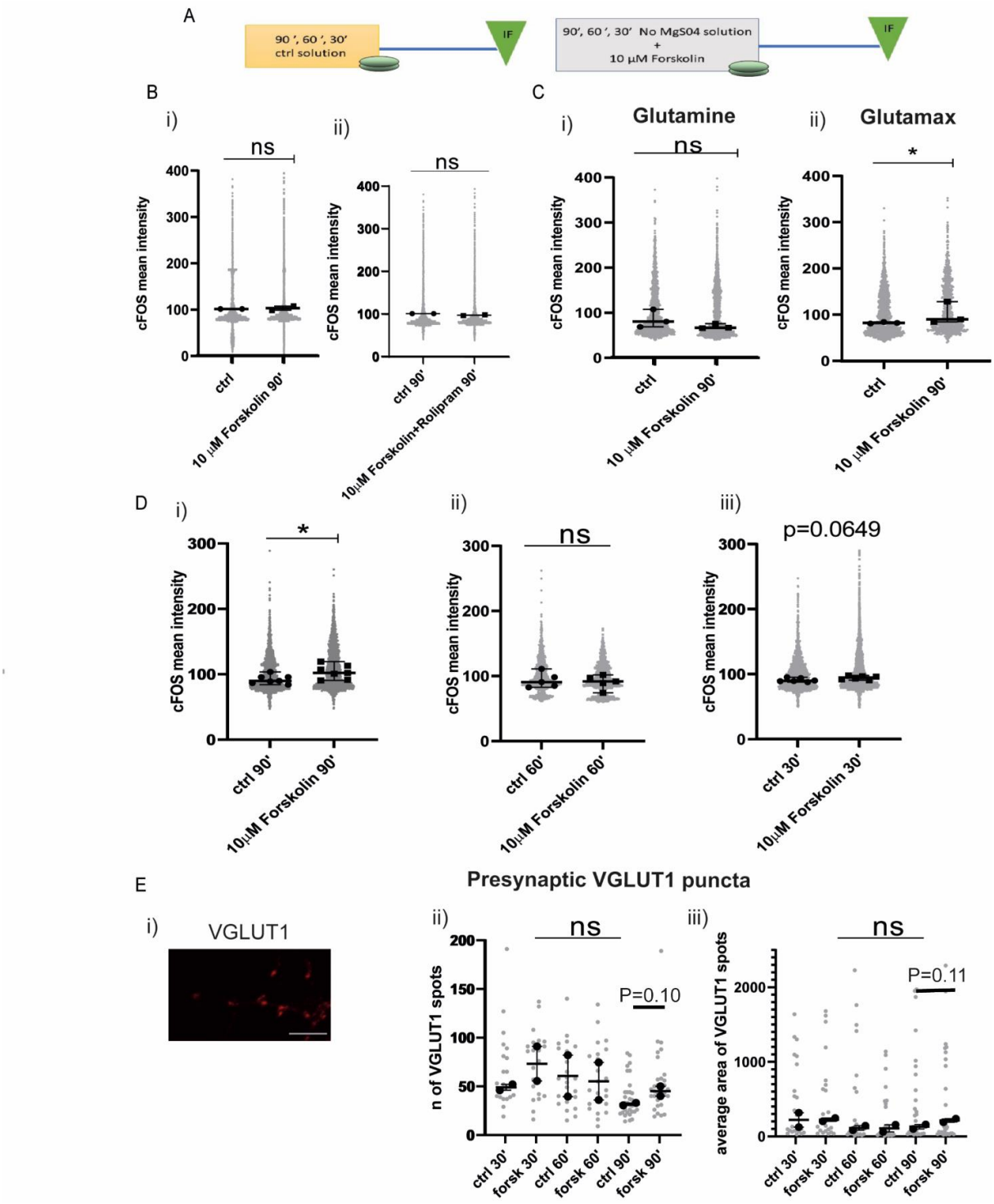

Figure 16: Forskolin induced cLTP A) Experimental outline for the time-course analysis using 10 µM Forskolin. B) C-fos mean intensity quantification i) using 10 µM Forskolin, ii) using 0.01% rolipram+10 µM Forskolin C) Comparison of cultures grew with glutamine and glutamax. ii) Cultures grew with glutamax showed (p=0.04) higher C-fos intensity after cLTP. D) Time-course of 30',60',90' 10 µM Forskolin showed an increment in cFos intensity after 90' (p=0.0379) and a tendency at 30'(p=0.0649) N= 4 independent experiments E) Quantification of VGLUT1 puncta: ii) number of spots iii) area of VGLUT1 spots. Unpaired t test was performed comparing inside each timepoint the respective control and the activated condition, showing a tendency (p=0.10) between ctrl and 90'cLTP, n=2 independent experiments.

4.4 Settings for live imaging of mRNA

4.4.1 Time-course for the visualization of exogenous mRNA after transfection

The imaging of live neurons with the MS2 loop system is a well-known method, reported in several works (Bauer et al., 2019; Dahm et al., 2008; Yoon et al., 2016). In a first set of experiments, I conducted a time point analysis to find the optimal time point to image the neurons in order to avoid possible artifacts. For this purpose, I co-transfeted (DIV 11-12) neurons with the CamKII-8L-3'UTR with the MCP-mcherry as a positive control, and the MCP-mcherry alone as a negative control. Neurons where imaged after different time points from the transfection, i.e.10-12, 17-18, 22-24, 36, 68 hours. In all the conditions, I recorded videos of 10 minutes for each neuron to evaluate the granules movement dynamics. Concerning the transfection with MCP-mcherry alone, my initial expectation was to not detect mRNA granules, since the stem loops to which MCP-mcherry is supposed to bind were not transfected. However, I detected some MCP-mcherry granules after 22-24 hours from transfection, but not before (Figure 17 B). A possible interpretation is that these observed granules could be an aggregation of MCP-mcherry proteins themselves. Besides, the number of neurons with granules considerably increased: 15% of transfected neurons showed granules after 22-24h, 40% of neurons after 36 hours and 100% after 68 hours from transfection. A statistical analysis with Wilcon t test showed that the number of neurons with granules was significantly different from zero (Figure 17 C ## = 0.0015; ###= 0.0002; ####=<0.0001, n=5-15 neurons for each of the 3 independent cultures). However, each data set is statistically significant compared to each other by ANOVA Tukey's multiple comparison test (see Table 1 below for MCP_alone)

Tukey's multiple comparison test	Significance	Adjusted p value
10-12 vs. 17-18	ns	>0.9999
10-12 vs. 22-24	***	0.0002
10-12 vs. 36	****	<0.0001
10-12 vs. 68	****	<0.0001
17-18 vs. 22-24	***	0.0002
17-18 vs. 36	****	<0.0001
17-18 vs. 68	****	<0.0001
22-24 vs. 36	****	<0.0001
22-24 vs. 68	****	<0.0001
36 vs. 68	****	<0.0001

Table 1

The number of granules detected in each neuron (Figure 17 D) increased from an average of 1.68 granules/neuron (22-24 hours), to 2.83 granules/neuron (36 hours), till 4.18 granules/neuron (68 hours). ANOVA test followed by Tukey's multiple comparison reveals: 22-24 vs. 36 p=0.0910, ns; 22-24 vs. 68 P= 0.0002 ***; 36 vs. 68 p=0.0056 **. I evaluated the dimensions of the granules considering the diameter, finding no significant change, as showed in Figure 17E (22-24 vs. 36 p= 0.89; 22-24 vs. 68 p=0.88; 36 vs. 68 p=0.64). However, it has to be mentioned that these measurements were conducted with an epifluorescence microscope equipped with 40X (Materials and Methods, section live imaging), presumably with higher resolution I could detect a change in the dimensions. Indeed, different size and shape of the granules after prolonged overexpression were reported in literature (Dahm et al., 2008). An evaluation of the granule's dynamics showed that the vast majority of them were confined: 100% of confined granules at 22-24 h, 76% confined, 21% anterograde, 3% retrograde at 36 h; 75% confined, 20% anterograde and 5% retrograde at 68h. The χ^2 test suggested a differential granule distribution (confined, anterograde and retrograde) at different time points (22-24 with 36 h F, n=5-15 neurons for each of the 3 independent cultures). All these data together suggested that if the imaging of neurons is conducted before 22-24 hours from transfections, granules caused by the MCP protein alone were not visible. Suggesting that 10-12 or 17-18 hours post transfection were the preferable time points to image neurons. For neurons transfected with the CamKII-8L-3'UTR with the MCP-mcherry the same analysis was conducted. Figure 17 G showed that neurons with granules considerably increased after transfection: 26% of neurons transfected showed granules after 10-12 h, 34% of neurons after 17-18 hours, 42% of neurons after 22-24 hours, 68% after 36h and 97% after 68 hours after

transfection. Statistics was conducted using Wilcon t test, evaluating how samples are different from zero (Figure B ## = 0.0063 10-12 h; ## = 0.0037 17-18 h; ## = 0.0030 22-24h; ###= 0.0002 36h; ###=0.0007 68 h). However, each data set is statistically significant compared to each other one by ANOVA Tukey's multiple comparison test (table 2 below for CamkII granules).

Tukey's multiple comparision test	significant?	adjusted p value	Tukey's multiple comparision test	significant?	adjusted p value
10-12 vs. 17-18	ns	0.1231	17-18 vs. 36	****	<0.0001
10-12 vs. 22-24	**	0.0021	17-18 vs. 68	****	<0.0001
10-12 vs. 36	****	<0.0001	22-24 vs. 36	****	<0.0001
10-12 vs. 68	****	<0.0001	22-24 vs. 68	****	<0.0001
17-18 vs. 22-24	ns	0.1231	36 vs. 68	****	<0.0001

The number of granules detected in each neuron (Figure 17 H) increased from an average of 2.33 granules/neuron (10-12 hours); 5.3 granules/ neuron (17-18 hours); 6.3 granules/ neuron (22-24 hours) to 8.3 granules/ neuron (36 hours) till 9.11 granules/neuron (68 hours). ANOVA test followed by Tukey's multiple comparison showed the followed statistics:

Tukey's multiple comparision test	significant?	adjusted p value
10-12 vs. 17-18	****	<0.0001
10-12 vs. 22-24	****	<0.0001
10-12 vs. 36	****	<0.0001
10-12 vs. 68	****	<0.0001
17-18 vs. 22-24	ns	0.3484
17-18 vs. 36	****	<0.0001
17-18 vs. 68	****	<0.0001
22-24 vs. 36	***	0.0004
22-24 vs. 68	****	<0.0001
36 vs. 68	ns	0.3199

Considering these data and the previous ones from the MCP alone, the optimal time point to image neurons resulted to be 17-18 hours post transfection, since the number of CamkII granules was large (5 granules/neuron) if compared with the 10-12 hours (2 granules/neuron, 10-12 hours vs 17-18 hours, $p < 0.0001$), without artifacts for the MCP alone. Also, for the CamKII, I evaluated the dimensions of the granules considering the diameter, but as showed in Figure 17 I, it did not change (n= 3 independent cultures, n=5-15 neurons for each of the 3 independent cultures) Considering the dynamics of the granules the vast majority of granules was confined: 100% of confined granules at 10-12 h, 81% confined, 5% anterograde, 14% retrograde at 17-18 h; 80% confined, 13% anterograde, 7% retrograde at 22-24 h; 65% confined, 20% anterograde and 25% retrograde at 36h; 55% confined, 36% anterograde and 9% retrograde at 68h (L). The χ^2 test was conducted in order to evaluate the different distribution between 10-12 hours and 17-18 hours ($p<0.0001$). These two time points were evaluated to be better for setting the live imaging of mRNA because I did not detect MCP-mcherry alone granules. This additional analysis corroborated the 17/18 h as best time point because, not only I could see more granules per neuron, but also granules were moving in anterograde and retrograde directions.

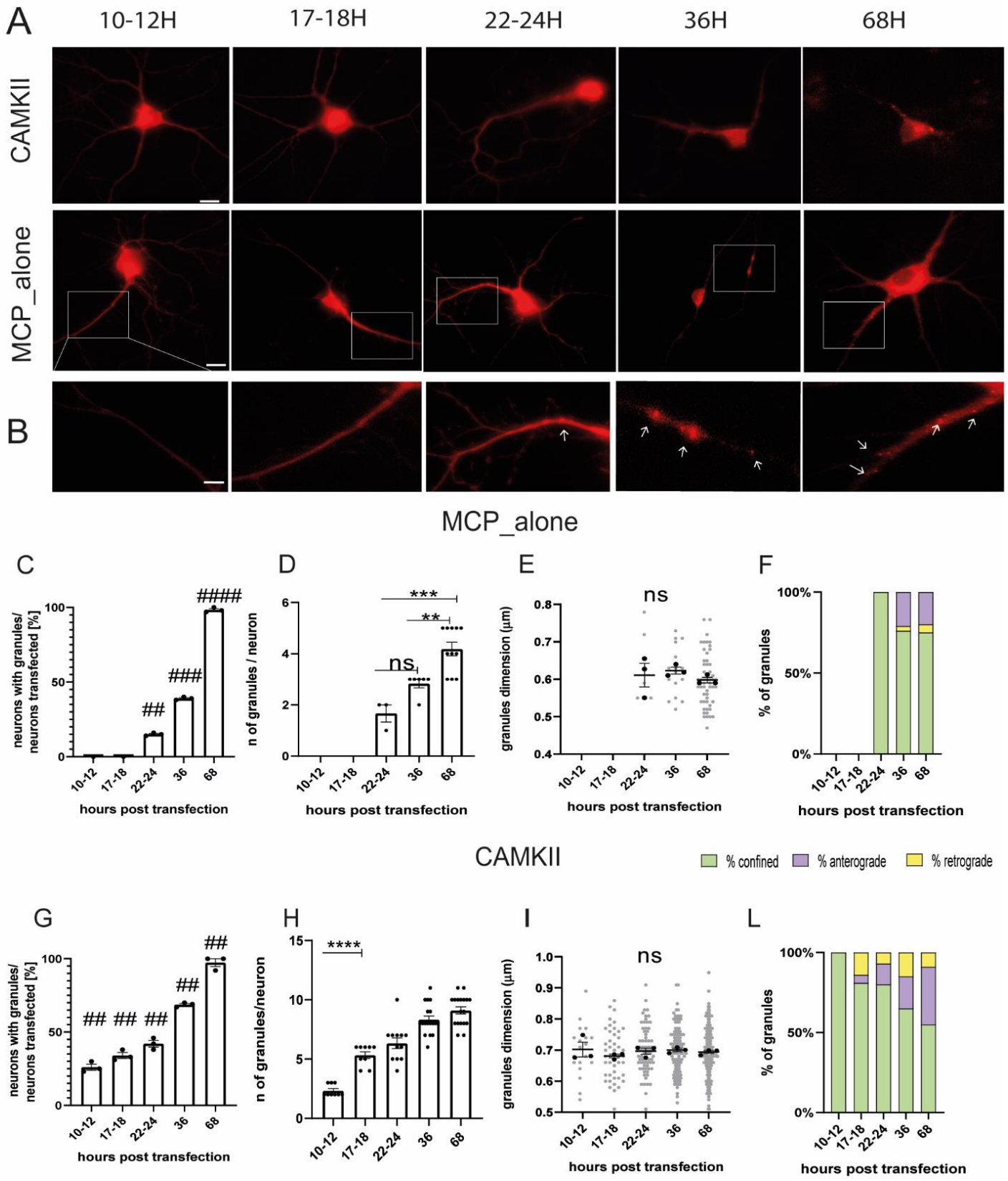
A
10-12H
17-18H
22-24H
36H
68H
CAMKII
MCP_alone
B
MCP_alone
C
neurons with granules/ neurons transfected [%]
hours post transfection
D
n of granules / neuron
ns
***
**
hours post transfection
E
granules dimension (µm)
ns
hours post transfection
F
% of granules
hours post transfection
CAMKII
% confined
% anterograde
% retrograde
G
neurons with granules/ neurons transfected [%]
hours post transfection
H
n of granules/neuron
****
hours post transfection
I
granules dimension (µm)
ns
hours post transfection
L
% of granules
hours post transfection

Figure 17: Settings for in live imaging analysis A) Representative images of MCP_ alone and CamkII neurons imaged after different times post transfection B) Zoomed images at each time point of neurons transfected with MCP alone. Arrows indicate granules. C) Number of neurons with granules after different times post transfection statistical analysis was performed through the one sample t test, evaluating how different are the 22-24, 36 and 68 timepoints from zero (##) D) Number of granules present in the neurons transfected after different time, before 22-24 hours neurons with granules were not detected. ANOVA followed by Tukey's post hoc test was performed E) Dimension of the MCP_granules analysed by the ANOVA followed by Tukey's post hoc test. F) Movement dynamics of granules. A χ^2 test revealed significant difference in the distribution of granules dynamics. G) Number of neurons with granules after different times post transfection statistical analysis was performed through the One sample t test, evaluating how different is each timepoints from zero (##) H) Number of granules present in the neurons transfected after different time I) Dimension of CamkII granules analysed by the ANOVA followed by Tukey's post hoc test. L) CamkII movements dynamics after different hours post transfection. The χ^2 test was performed ($p<0.001$ was establish the different distribution of granules at 10-12 and 17-18 hours post transfection. n= 3 independent experiments.

4.4.2 Tracking of BDNF mRNA in living neurons

Once that the settings for visualizing exogenous mRNA were settled, hippocampal neurons were transfected with BDNF mRNA and the MCP-mcherry at 11 DIV. The day after (17-18 hours post transfection) neurons were live imaged. The same neuron was imaged in control solution (see Materials and Methods) for 10 minutes to establish the baseline and then was imaged for 15 minutes in a solution containing Forskolin 10 µM. Video with 1f/sec were acquired using a 40X oil objective. To assess BDNF mRNA dynamics, we focused on the Ex6-bdnfCDS-12L-3UTR, Ex1-bdnfCDS-12L-3UTR and, as controls, CamkIIa-8L-3'UTR and 12L (12 stem loop plasmid). This last plasmid does not have the BDNF mRNA, nor the 3'UTR sequence, but just the same bacteriophages stem loops which were cloned in the BDNF and in CamkIIa constructs. First, I evaluated the transport dynamics with the extraction of the Kymograph in ImageJ and then, thanks to a MACRO that I developed, the type of movement that granules showed: anterograde (away from the cell body), retrograde (toward the cell body) or confined. Confined movements were defined as movements in which the granules total displacement within the dendrite is <0.5 µm. Data showed were acquired from three independent experiments and a total of almost 20 neurons per condition were imaged.

4.4.3 Localization and nature of granules

During the analysis of the videos, I observed that granules were present in both apical and basal dendrites. The majority of visible granules were found in dendrites in which the signal to

noise ratio is high and the fluorescence of the granule was higher in comparison with the background fluorescence. A representative image of granules analysed in dendrites is showed in panel A, Figure 18. In the same figure, in panel B the percentage of granules that were present in basal and apical dendrites is showed. All the four constructs showed similar percentages of the apical and basal localization of granules: 65% apical and 34% basal for CamKII, 56% apical and 44% basal for Ex6, 47% apical and 52% basal for Ex1 and 71% apical and 29% basal for the 12L. By extracting the kymographs of the granule's movement (panel C), I defined the percentage of the type of movements (confined, retrograde, anterograde) that these granules showed. The percentage of confined movements is the largest for all the constructs, indicating that the high majority of the granules were quite oscillatory. Basal and apical granules showed similar percentages of the movements: confined, anterograde and retrograde. I verified by a χ^2 test if being basal or apical (for a granule) could influence on the type of movement that the granule displayed. By the χ^2 test, the statistical analysis confirmed that for all the constructs the distribution was not statistically significant for the type of movement they showed (panel E, F, G, H Figure 18). Considering this, apical and basal granules were pulled together for further analysis. For all the constructs I evaluated the localization of the granules detected within the dendrites. As showed in Figure 19, a histogram for the four constructs was represented. The majority of granules for the constructs was present in the proximal dendrites: between 20-60 µm from the cell soma. This localization turned out to not change after the induction of cLTP upon Forskolin treatment (data not showed). Previous results (Baj et al., 2011) indicate that Ex1 is located mainly at proximal dendrites, whereas Ex6 has been identified up to 70 um from the cell soma. Ex1 has been reported mainly at proximal dendrites, while Ex6 has been identified up to 70 µm from the cell soma. Surprisingly, upon stimulation with Forskolin, I could not detect the distal localization for the EX6-bdnfCDS-12L-3UTR, already reported with *in situ* analysis (Baj et al., 2011). This could be most likely due to the timing and nature of the stimulus. Indeed, after 3 hours of stimulation with KCl 10mM, the reported distal localization was achieved. In our system, 15 minutes of Forskolin 10 µM might not be enough for mRNA targeting to the distal compartments of the dendrites. The localization of the granules with 12 L showed more proximal localization in comparison with all other constructs with the 3'UTR sequence. This result was in accordance with results already published by the group: in the 3'UTR sequence, DTE signals such as AU-rich regions, ELAV binding sites and a G-quartet-like structure were reported to be important for the dendritic

transport along the dendrite (Vaghi et al., 2014). Interestingly, the number of granules detected for the 12 L construct was much less than all the other numbers of granules (panel G).

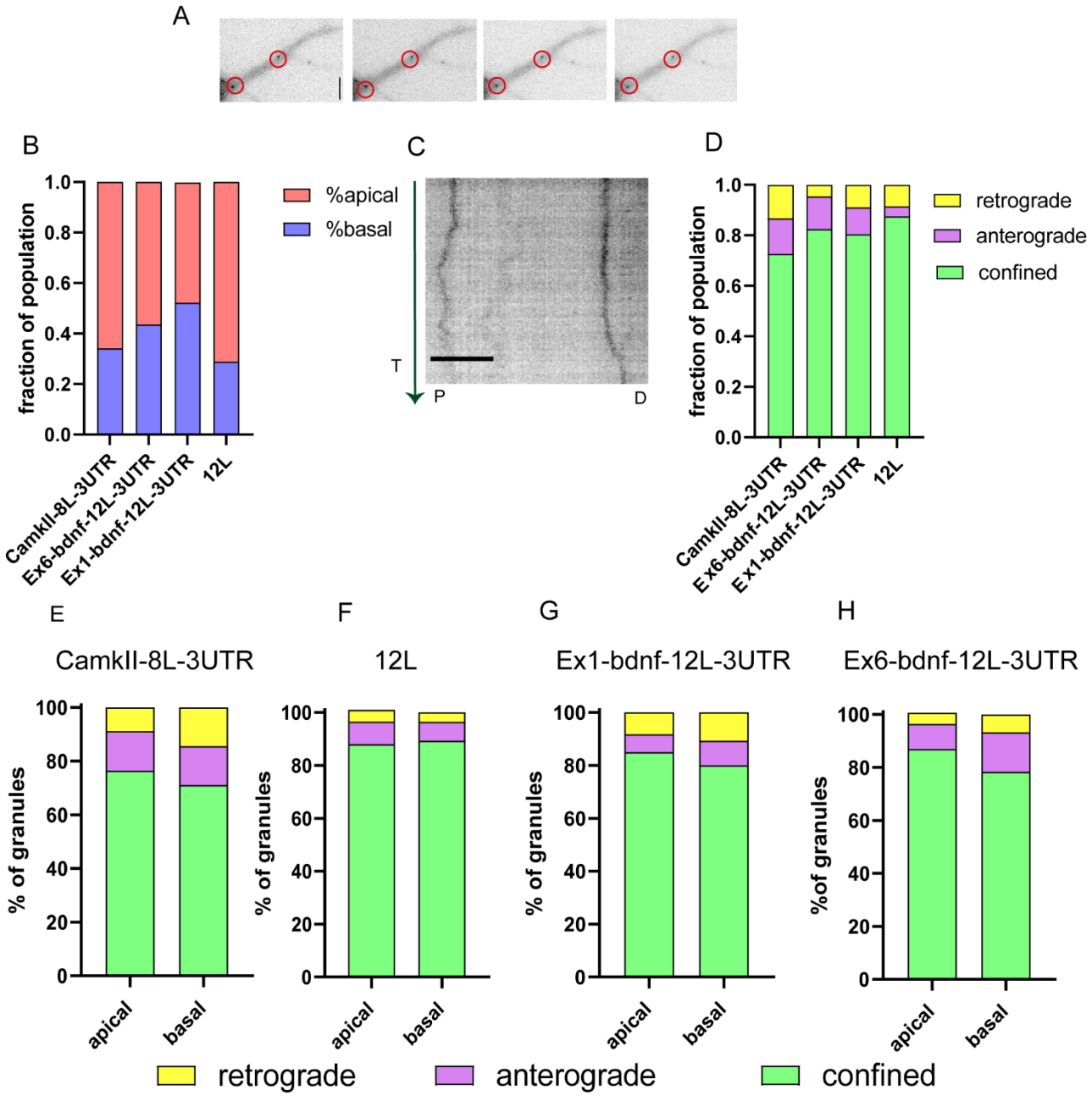

Figure 18: Tracking mRNA granules in live neurons A) Representative dendrites with granules underlined by a red circle. B) Fraction of population of granules present at apical and basal dendrites. The percentages of apical and basal granules are similar for all the four constructs. C) Representative kymograph of a granule movement: the green vertical line represents the time (T), while P and D represent respectively the Proximal and Distal part of the dendrite. D) Fraction of granules population showing the movement dynamic: the vast majority of granules show confined behaviour. E) apical and basal granules of CamkII show similar distribution of anterograde, retrograde and confined granules behaviour without any statically difference by the χ^2 test, the same test was applied for F) 12 L apical and basal granules and G) Ex1-bdnf-12L-3 UTR and H) Ex6-bdnf-12L-3UTR showing that apical and basal granules for each construct behave similarly without any significant statistical change.

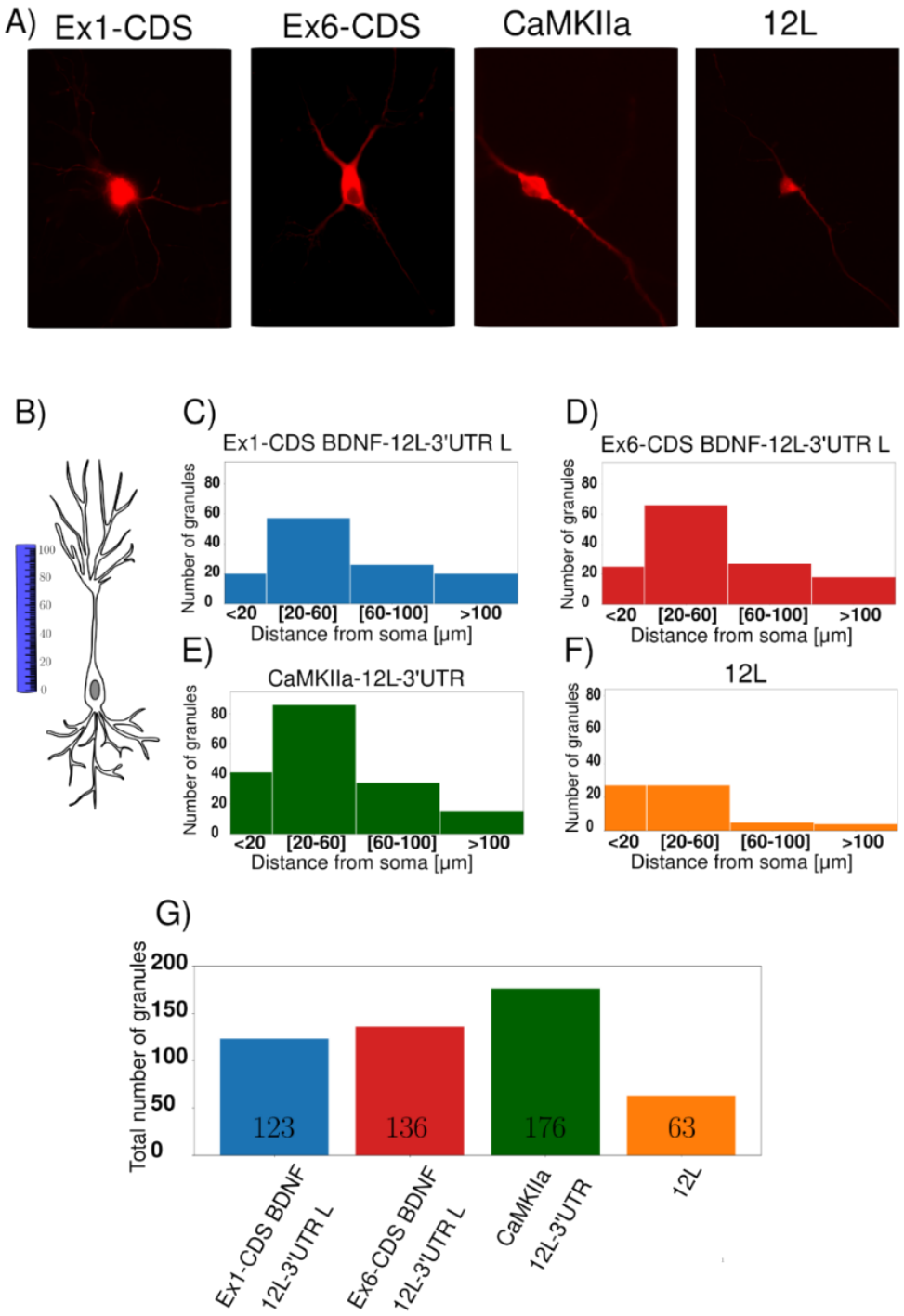

Figure 19: Subcellular localization of mRNA granules. A) Representative neurons transfected with the BDNF mRNA construct and MCP_mcherry, or CamkII and MCP_mcherry or the 12 L construct B) Graphical representation showing how the distance from the soma was calculated C) Ex1-cdsBDNF-12L-3UTR histogram with the number of granules detected at proximal (20-60 µm) distal (60-100 µm) dendrites, the majority of granules is at 20-60 µm D) Ex6-cdsBDNF-12L-3UTR histogram E) CamkIIa-12L-3UTR histogram even in this case the majority of granules is at proximal dendrites F) 12L histogram G) Total number of granules detected in almost 20 neurons for each construct.

4.3.4 Analysis of the movements of granules

Similar to previous reports (Doyle and Kiebler, 2011; Yoon et al., 2016), I found that all the four constructs were mostly confined, as represented in Figure 20 panel A. The plot shows the fraction of granules having confined, anterograde, retrograde movements within the total granule population for each analysed neuron (CamKII median: 0.75 upper limit 1 and lower limit 0.125; Ex1-bdnf-12L-3UTR median:0.88 upper limit 1 and lower limit 0.33; Ex6-bdnf-12L-3UTR median: 1 upper limit 1 and lower limit 0.36; 12L median: 1 upper limit 1 and lower limit 0.4 median with upper and lower limit, n= 20-21 neurons for each construct were considered). A statistical comparison between the constructs suggested no significant differences, except for a tendency between CamKII vs 12 L p=0.13, suggesting a higher confined population for the 12L granules (Figure 20 panel B, n= 20-21 neurons for each construct were considered). For the population of anterograde and retrograde there was not significant difference between the four constructs. Regarding the active movements, the three constructs, with the exception of 12 L, displayed a slight bias, not statistically significant, for anterograde transport (fraction of population, anterograde vs. retrograde: CamKII: 0.075 upper limit 0.57 and lower limit 0 vs 0.09 upper limit 0.5 and lower limit 0; Ex1-bdnf-12L-3UTR: 0 upper limit 0.5 and lower limit 0 vs 0 upper limit 0.25 and lower limit 0; Ex6-bdnf-12L-3UTR: 0.5 upper limit 0 lower limit 0 vs 0.45 upper limit 0 lower limit 0). For the construct 12L, the anterograde and the retrograde transport showed similar results (median:0 upper limit 0.25 and lower limit 0 for the anterograde; 0 upper limit 0.5 and lower limit 0 for the retrograde). The constructs showed also similar velocities for anterograde movements: CamKII: -0.153 µm/sec, Ex1-bdnf-12L-3UTR: -0.133 µm/sec, Ex6-bdnf-12L-3UTR: -0.189 µm/sec, 12L: -0.125µm/sec; for retrograde movements: CamKII: 0.234 µm/sec, Ex1-bdnf-12L-3UTR: 0.195 µm/sec, Ex6-bdnf-12L-3UTR: 0.143 µm/sec, 12L: -0.176 µm/sec. The observed values of velocity are consistent with similar values already reported in literature (Vaghi et al., 2014). As in Figure 20 F significant difference (Ex6 vs Ex1 p =0.035) was showed for anterograde velocity between Ex1-bdnf-12L-3UTR and Ex6-bdnf-12L-3UTR, whereas for the retrograde transport there was not a significant difference. All the mRNA constructs have been observed to travel for similar distances for the anterograde movement, in average: CamKII: -3.5 µm, Ex1-bdnf-12L-3UTR: -3.9 µm, Ex6-bdnf-12L3UTR-3.4 µm, 12L: 5.3µm. For the retrograde movement in average: CamKII: 10.790 µm, Ex1-bdnf-12L-3UTR: 2.9 µm, Ex6-bdnf-12L-3UTR: 3.1 µm, 12L: 2.8 µm (panel K,L,M).

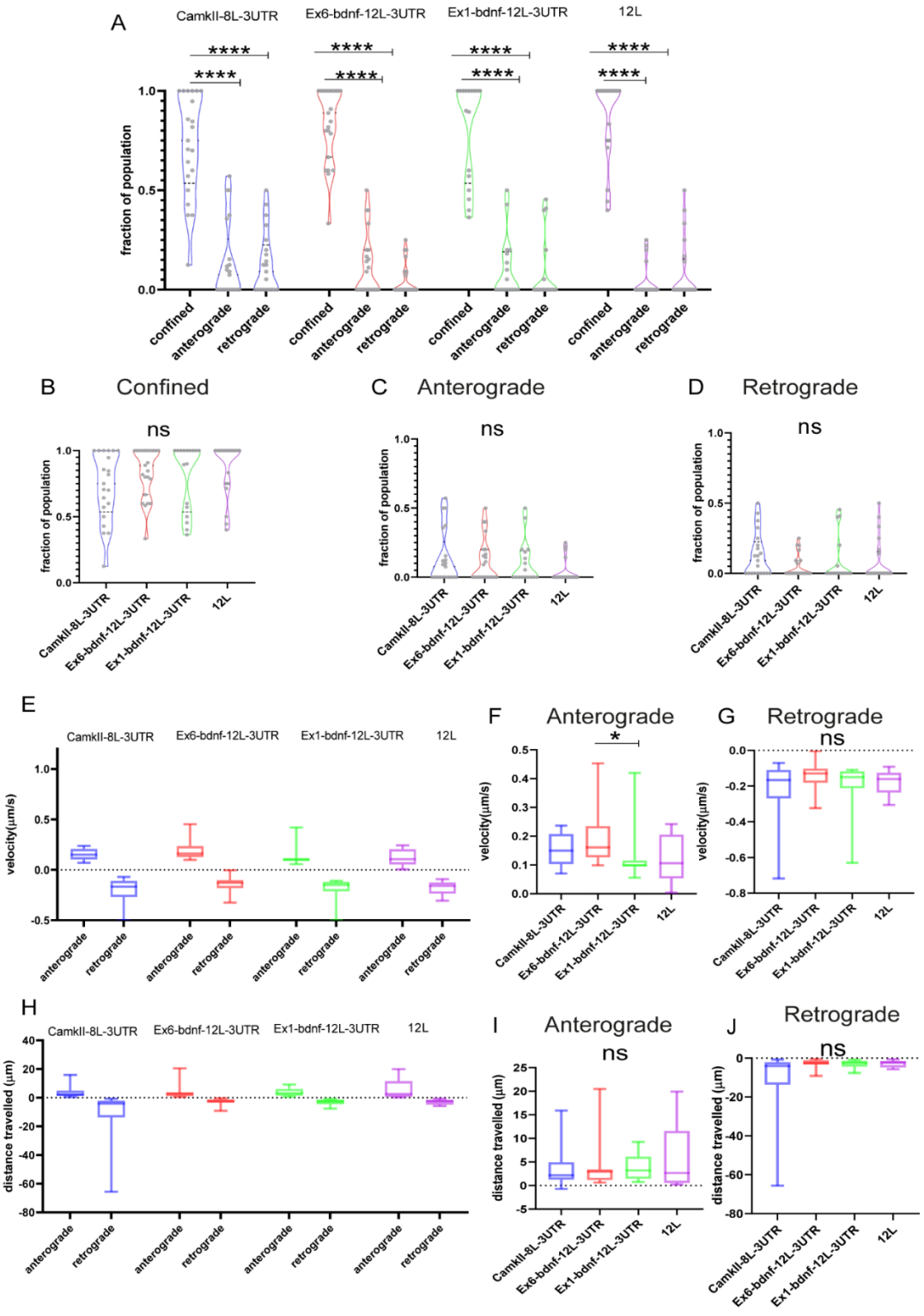

Figure 20: Type of movements of mRNA granules A), B), C) D) Confined, anterograde and retrograde fraction of population. The vast majority of granules were confined. ANOVA followed by Kruskal Wallis post hoc test did not show significant difference between the different constructs E), F), G) Anterograde and retrograde velocity for the four constructs F) Significant difference between Ex6 and Ex1 for anterograde velocity (P=0.035) ANOVA followed by Kruskal Wallis. H) I) J) Total displacement of anterograde and retrograde movements. Data are represented by the median with 95% CI.

4.4.5 What happens after cLTP stimulation?

After 10 minutes of baseline imaging, I added forskolin, and each neuron was imaged for an additional 15 minutes. Granules exhibited a considerable arrest following the forskolin administration, as seen in Figure 21. The granules confined in control condition remained confined, whereas the granules that showed anterograde and retrograde movements in control conditions after cLTP froze and showed confined behaviour (Figure 21 panel B, C, D, E, representing the granule population for each analysed neuron, n= 20-21 neurons). A statistical analysis showed that, comparing ctrl and cLTP condition, the confined population was always statistically higher for the cLTP condition: p= 0.0234 (Ex6, panel B); p=0.0156 (ex1, panel C); p=0.0084 (CamkII panel D); p=0.0156 (12 L, panel E). For the anterograde population there was a significant decrement between ctrl and cLTP as: p=0.0156 (Ex6, panel B), p=0.0313 (Ex1, panel C), and a tendency for p=0.11 (CamkII, panel D), p=0.12 (12l, panel E). After the cLTP induction, the retrograde population was significant different p=0.0020 (CamkII,panel D); p=0.0313 (12L, panel E) while there was a tendency p=0.0625 (Ex1, panel C). The construct with the 12 L exhibited a similar behaviour to the CamkII mRNA. This outcome was surprising because the 12 L construct was not expected to have a biological significance after the induction of cLTP. However, regarding the number of mRNA granules after cLTP induction, the χ^2 test between CamkII and 12 L on the data showed in panel F showed that the number of neurons with less granules after cLTP was significant higher for the CamkII construct while there was no significant difference between the BDNF mRNA and the CamkII and the BDNF mRNA and the 12 L.

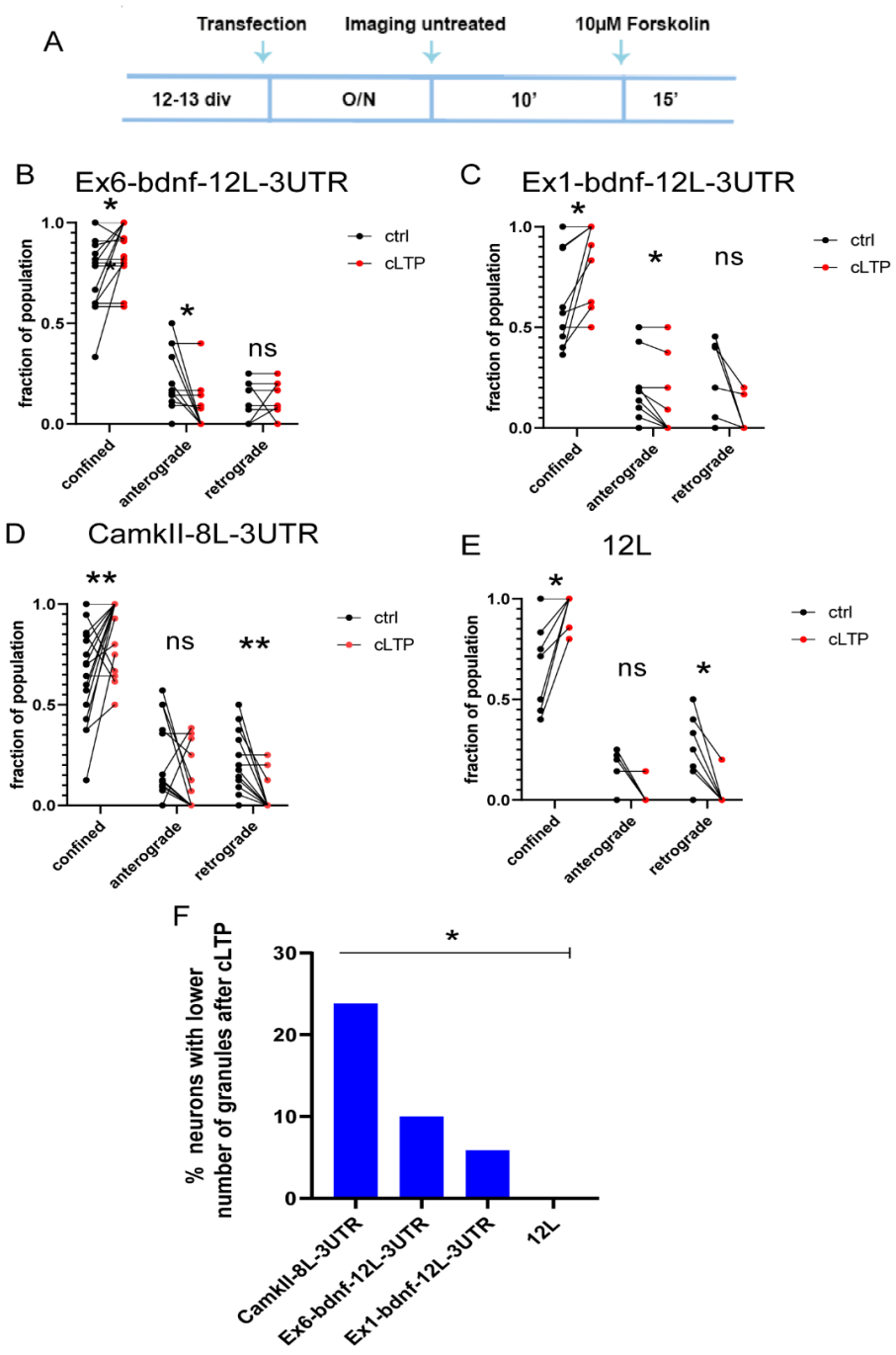

Figure 21: Granules after cLTP induction A) Experimental outline: neurons after an overnight from the transfection were imaged with 10' of control medium, the same neurons were then imaged for 15' with Forskolin 10 μM B) Ex6-bdnf-12L-3UTR granules showed an increase of confined population (p= 0.0234), and a decrease in the anterograde movement (p=0.0156) after cLTP induction C) Ex1-bdnf-12L-3UTR showed an increase of confined population (p=0.0156) and a decrease in the anterograde movement (p=0.0313) D) CamkIIa-8L-3UTR showed an increase (p=0.0084) and a decrease in the retrograde (p=0.0020); E) 12L showed an increase of confined population (p=0.0313) and a decrease in the retrograde(p=0.12) Statistical analysis was performed by paired t-test. F) Percentage of neurons with lower number of granules after cLTP CamkII vs 12 L p=0.05.

4.5 BDNF mRNA in proximity to a spine

From the live analysis, mRNA granules resulted to be mostly confined and that after cLTP stimulation most of them remained confined. However, because of resolution limitations, it was not clear if these granules were in proximity to a spine or not. For this purpose, neurons transfected with the same constructs as before (Ex6-bdnfCDS-12L-3UTR, Ex1-bdnfCDS-12L-3UTR and as controls CamkIIa-8L-3'UTR and 12L) were analysed with the super-resolution Elyra 7 SIM microscope after cLTP induction. Neurons were fixed at different time points such as 15 minutes, 30 minutes and 60 minutes from the cLTP induction. They were then immunolabelled with Synapsin I and images were acquired with Elyra7 (see Materials and methods). During post-processing analysis, thresholded images of the mRNA granules and Synapsin I were created (panel A Figure 22). After detecting the spines along the dendrites, I evaluated the number of granules located within +3 µm (granules more distant to the soma) and -3 µm (granules closer to the soma) from each spine considered. For this purpose, I identified an orthogonal axis dividing in two the spine as a reference line (see Figure 22 panel A). For each spine, the head diameter and the neck were measured in order to identify mushroom and stubby spines. Both were considered for the analysis. Each time a ROI of 30-50 µm was drawn and all the spines in it were considered. Panel i) shows the density of granules counted in each ROI for all the four constructs. The density is obtained as the number of granules per unit of length (granules/ µm). The density did not change after different time points from the cLTP induction in all the four constructs, suggesting that the number of mRNA granules did not increase or decrease after the cLTP induction. This is in accordance with the analysis in living neurons: the number of granules detected was similar. Some granules disappeared and some other appeared during time lapse videos but because of technical issue (focus and photobleaching) I could not be sure about the biological significance of this event. The analysis of the granule's density suggested that the number of granules did not increase or decrease significantly after cLTP. The plot ii) of B, C panels in Figure 22 and in A e B panels in Figure 24 represents the granules detected near a spine, considering the range +3 µm, -3 µm. Particular relevance was given to the granules inside, in the spine head, or below, in dendritic shaft in correspondence to the spine neck, a spine (see Figure 23). In panel iii) of B, C in Figure 22 and A e B in Figure 24 granules inside and under a spine were plotted together. For the CamkIIa-

8L-3’UTR (B, iii), after 15’ and 30’ minutes from cLTP induction there was a significant increment of granules inside and under a spine (ctrl vs cLTP 15’ p=0.0311, ctrl vs cLTP 30’ p=0.0180); considering the 12 L, the negative control, in control and after cLTP stimulation granules did not distribute differently inside and under a spine. Considering the BDNF constructs, for Ex1-bdnfCDS-12L-3UTR (Figure 24, panel A) iii) there was a significant increment of granules inside and under a spine after 30’ from cLTP (ctrl vs cLTP 30’ p=0.0266), while there was a tendency for the 15’ and 60’ cLTP (ctrl vs 15’ p=0.22 and ctrl vs 60’ p=0.13). For the Ex6-bdnfCDS-12L-3UTR the increment was significant between cLTP 15’ and cLTP 60’, while there was a tendency between ctrl vs cLTP 15’ p=0.0785. When the granules inside a spine were separated from the granules under a spine as showed in panels iv) and v) for all the constructs (B;C figure 22 and A e B figure 24), it was possible to see for CamkII a significant increase of the granules under a spine (ctrl vs cLTP 15’ p=0.0140 and ctrl vs cLTP 30’ p=0.0204), and for granules inside a spine (ctrl vs 15’ p=0.03369 and ctrl vs cLTP 60’ p= 0.00336), for the 12 L construct, no significance was reported inside the spine, not even under a spine after a cLTP activation. Considering the BDNF constructs, Ex1-bdnfCDS-12L-3UTR (A, iv) showed an increment of mRNA granules under a spine after 15’ from cLTP (ctrl vs cLTP 15’ p=0.0047), while there was an increment of BDNF mRNA granules inside the spine after 30’ from cLTP (ctrl vs 30’ p=0.0253) panel v, figure 24. For Ex6-bdnfCDS-12L-3UTR (B, iv, figure 24) there was an increase of granules under a spine after 15’ from cLTP induction (ctrl vs 15’ cLTP p=0.0005), while there was a tendency for an increment of granules inside the spine (B, (v), ctrl vs cLTP 60’ p=0.1271). All these results suggest that the distribution of BDNF mRNA granules changes significantly after cLTP induction. A possible interpretation of this phenomenon is provided in the Discussion section.

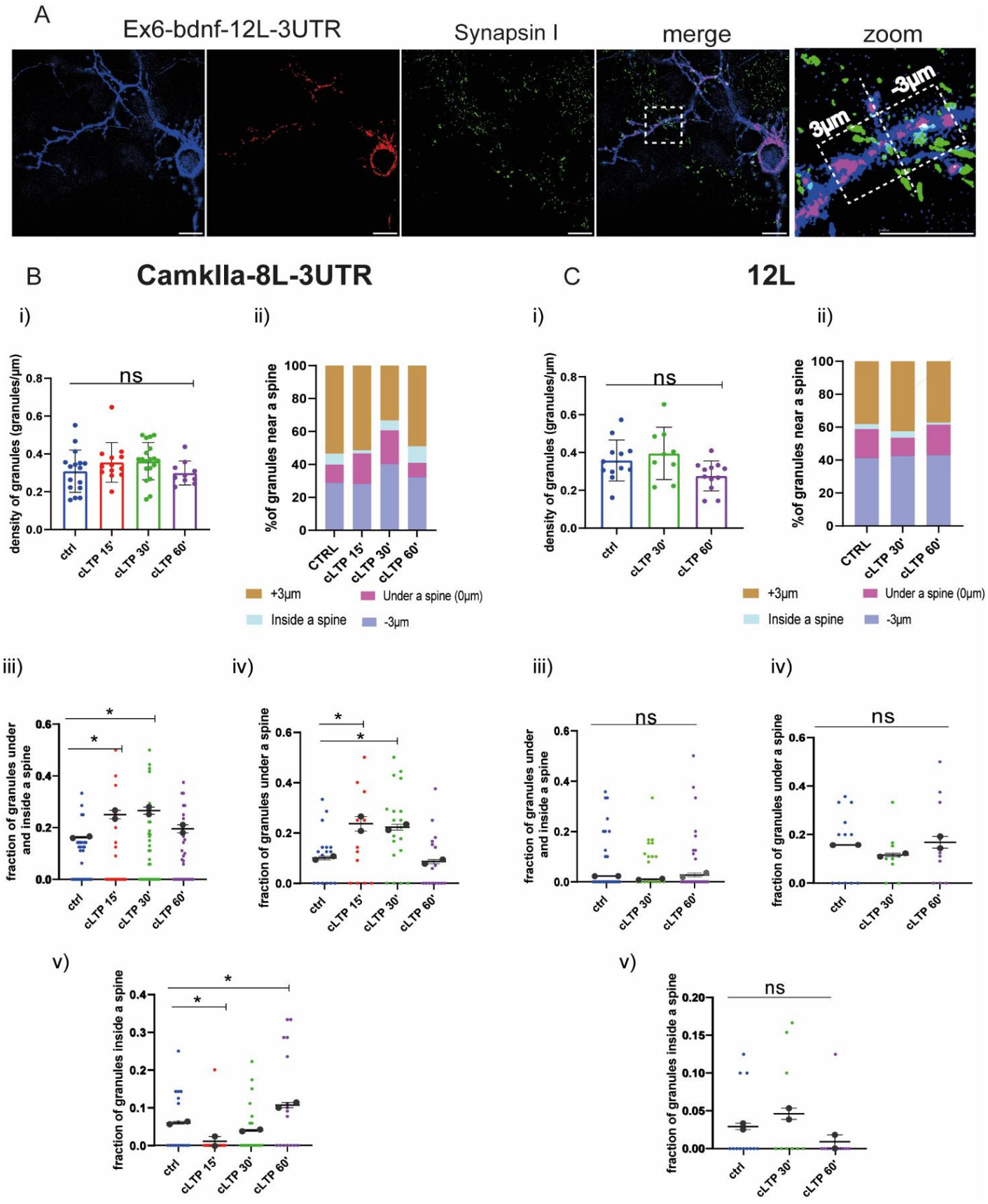
A
Ex6-bdnf-12L-3UTR
Synapsin I
merge
zoom
-3µm
3µm
B
Camklla-8L-3UTR
C
12L
i)
ii)
density of granules (granules/µm)
ns
ctrl
cLTP 15'
cLTP 30'
cLTP 60'
%of granules near a spine
CTRL
+3µm
Under a spine (0µm)
Inside a spine
-3µm
iii)
iv)
v)
fraction of granules under and inside a spine
fraction of granules under a spine
fraction of granules inside a spine
*

Figure 22: mRNA granules near a spine A) Representative thresholded images of Ex6-BDNF-12L-3UTR and Synapsin I. From the zoom section a spine is visible, granules found in the range of +3 µm and -3 µm were considered. Scale bar 5 µm. **B) CamkIIa-8L-3UTR granules** i) CamkII mRNA granules counted in each dendrite streches of 30-50 µm. ANOVA followed by Dunnett's post hoc test revealed no significant difference in the density of mRNA CamkIIa granules after cLTP stimulation ii) mRNA granules distribution near a spine after cLTP induction. Granules under a spine and inside a spine were considered iii) CamkII granules under and inside a spine were considered at different cLTP induction. After 15' and 30' from cLTP induction there is an increase in the granules present under and inside a spine (ctrl vs cLTP 15' p=0.0311, ctrl vs cLTP 30' p=0.0180) iv) CamkII granules under a spine were significantly higher after 15' and 30' from cLTP induction (p= ctrl vs cLTP 15' p=0.0140 and ctrl vs cLTP 30' p=0.0204) v) CamkII granules inside a spine were significantly higher after 60' from cLTP ctrl vs 15' p=0.03369 and ctrl vs cLTP 60' p= 0.00336) **C) 12 L granules** i) 12L mRNA granules counted in each dendrite streches of 30-50 µm ANOVA followed by Dunnett's post hoc test revealed no significant difference in the density of 12L granules after cLTP stimulation ii) mRNA granules distribution near a spine after cLTP induction iii) 12 L granules under and inside a spine were considered at different cLTP induction. iv) 12L granules under a spine were not significantly higher after cLTP induction v) 12 L granules inside a spine were not significantly higher after cLTP.

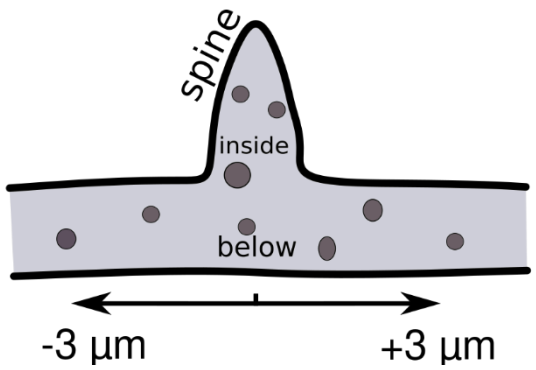

Figure 23: a representative sketch of the analysis performed on the granules close, inside or below a spine.

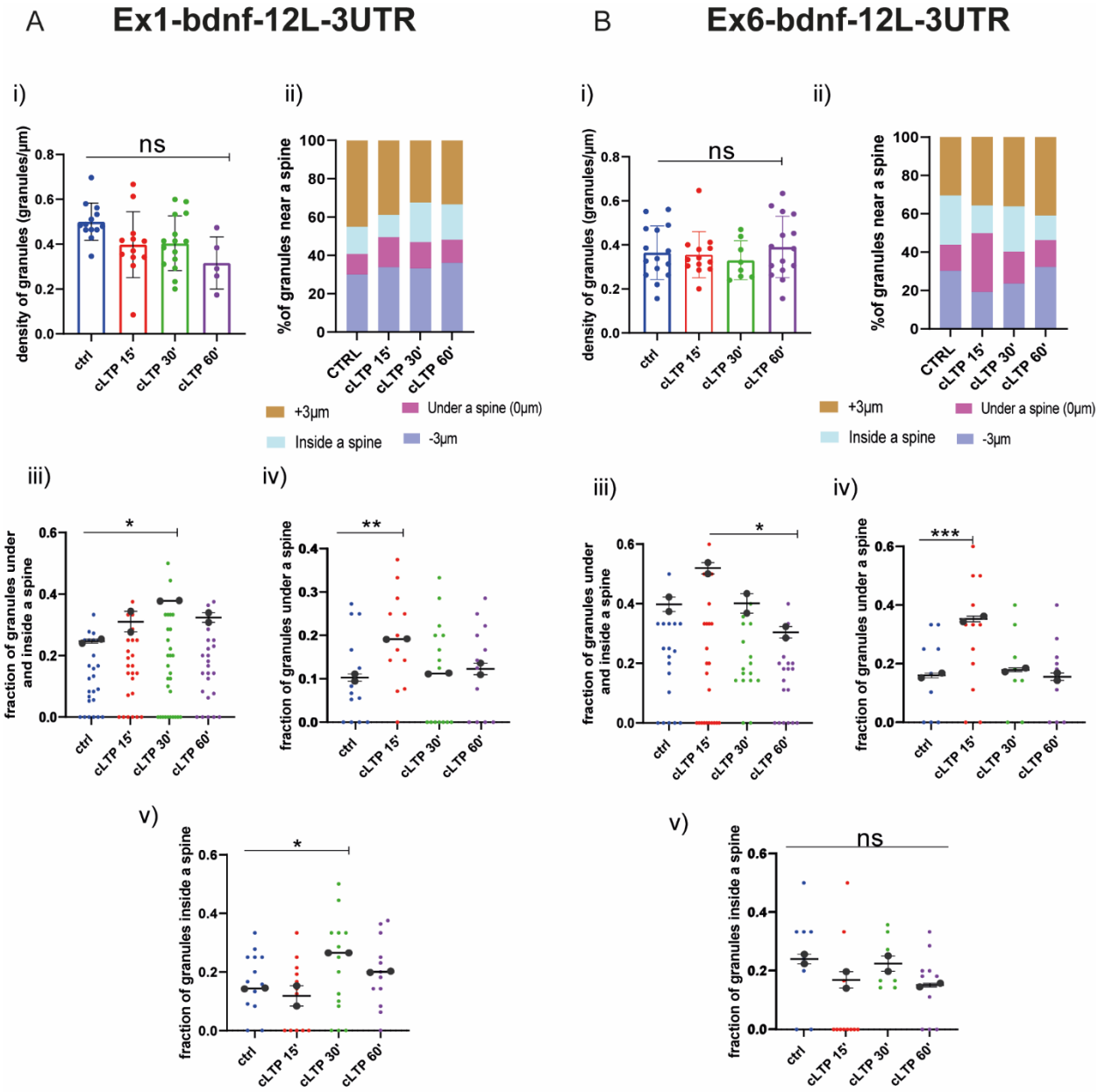

Figure 24: BDNF mRNA granules near a spine **A) Ex1-bdnf-12L-3UTR** i) mRNA granules counted in each dendrite streches of 30-50 µm ANOVA followed by Dunnett's post hoc test revealed no significant difference in the density of Ex1-bdnf mRNA granules after cLTP stimulation ii) mRNA granules distribution near a spine after cLTP induction. Granules under a spine and inside a spine were considered iii) Ex1bdnf granules under and inside a spine were considered at different cLTP induction. After 30' from cLTP induction there is an increase in the granules present under and inside a spine. iv) Ex1bdnf granules under a spine were significantly higher after 15' from cLTP induction ctrl vs cLTP 15' p=0.047 v) Ex1bdnf granules inside a spine were significantly higher after 30' from cLTP ctrl vs 30' p=0.0253 **B) Ex6-bdnf-12l-3UTR** i) mRNA granules counted in each dendrite streches of 30-50 µm ANOVA followed by Dunnett's post hoc test revealed no significant difference in the density of mRNA CamkIIa granules after cLTP stimulation ii) mRNA granules distribution near a spine after cLTP induction. Granules under a spine and inside a spine were considered iii) Ex6bdnf granules under and inside a spine were considered at different cLTP induction. There is a tendency (ctrl vs cLTP 15' p=0.0785), while there is a significant increase between 15' and 60' from cLTP induction iv) Ex6bdnf granules under a spine were significantly higher after 15' from cLTP induction p= ctrl vs 15' cLTP p=0.0005 v) Ex6bdnf granules inside a spine were not significantly higher after any time from cLTP. Statistical analysis was done by ANOVA followed by Tukey's post hoc test.

4.6 Tracking the BDNF protein in living neurons

Once that the mRNA of BDNF was tracked thanks to the loops in live neurons, I investigated what happens to the BDNF protein in living neurons after the cLTP induction. I used similar constructs that I used for the detection of mRNA with, instead of the MS2 loops, a GFP protein fused to Ex6 and Ex1: Ex6-CDSbdnf-GFP-3'UTR long and Ex1-CDSbdnf-GFP-3' UTR. As a control I used the CDS-bdnf. Neurons were co-transfected, using the BDNF construct together with a filler in mcherry, at div 9-10 and imaged after 2 days, as already reported in literature (Baj et al., 2011). As showed in Figure 25 A, neurons transfected with Ex1 or Ex6 were not visible, while I could detect mcherry transfected neurons. Unfortunately, this compromised the live imaging analysis on those constructs. However, neurons transfected with the CDS of BDNF were detected and protein granules spots were analysed taking in consideration their localization and the type of movements (n= 21 neurons, n=3 independent cultures). The vast majority of spots were detected at proximal dendrites: 15 spots at a distance less than <20 µm from the cell soma, 60 spots at 20-60µm from the cell soma, 25 spots at 60-100 µm from the cell soma and 15 spots were detected at a distance further than 100 µm from the cell soma. Protein spots were detected in both apical (59%) and basal dendrites (41%) and the vast majority of them were confined (99.40%) panel C. The confined population was statistically significant compared to the anterograde and retrograde population (panel D) in control condition and after cLTP. Protein spots did not show any significant change in their behaviour before and after cLTP, as the confined population was always very high (D) ($p<0.0001$). Even if a comparison between the dynamics of the mRNA and the protein for the same construct was not possible, it could be noted that the CDS-bdnf showed the highest percentage of confined movements. In order to evaluate the protein synthesis after cLTP activation, the fluorescence intensity of single spots was measured every 10 minutes from the Forskolin treatment, up to 60 minutes of recording. A total of 7 fluorescence measurements per each spot were therefore considered. Fluorescence of every spot was also measured before the Forskolin treatment (2 measurements at time=0 and time=10 minutes in control medium). Considering all the fluorescence intensity values of each single spot together, I obtained the cumulative curve distribution showed in panel F. The curve corresponding to control condition appears considerably shifted to higher values of fluorescence intensity with respect to the other activated time points. This suggested that the fluorescence intensity measurements could not easily

detect an increment of the protein synthesis, at least with the available tools. Analysing the recorded videos, focusing on BDNF protein spots, I observed some “new-born” spots. Indeed, within a total population of 115 detected spots, 10 (the 8.69%) were considered as new-born, because they were not previously detected in the first 10 minutes of control recording. In other cases, the spots, instead, disappeared after the 10 minutes of control recording. This happened with 5 spots: the frequency of this phenomenon was 4%. The biological significance behind these two events could be that: the new-born spots were the newly synthesized BDNF proteins caused by the cLTP induction, whereas the spots that were not detected after the 10 minutes control, they could represent a physiological turnover of the protein. However, these conclusions were not supported so far with additional experiments. Further analysis was conducted for measuring the distance between a protein spot and a closest spine. This analysis was therefore similar to the already presented for the mRNA constructs.

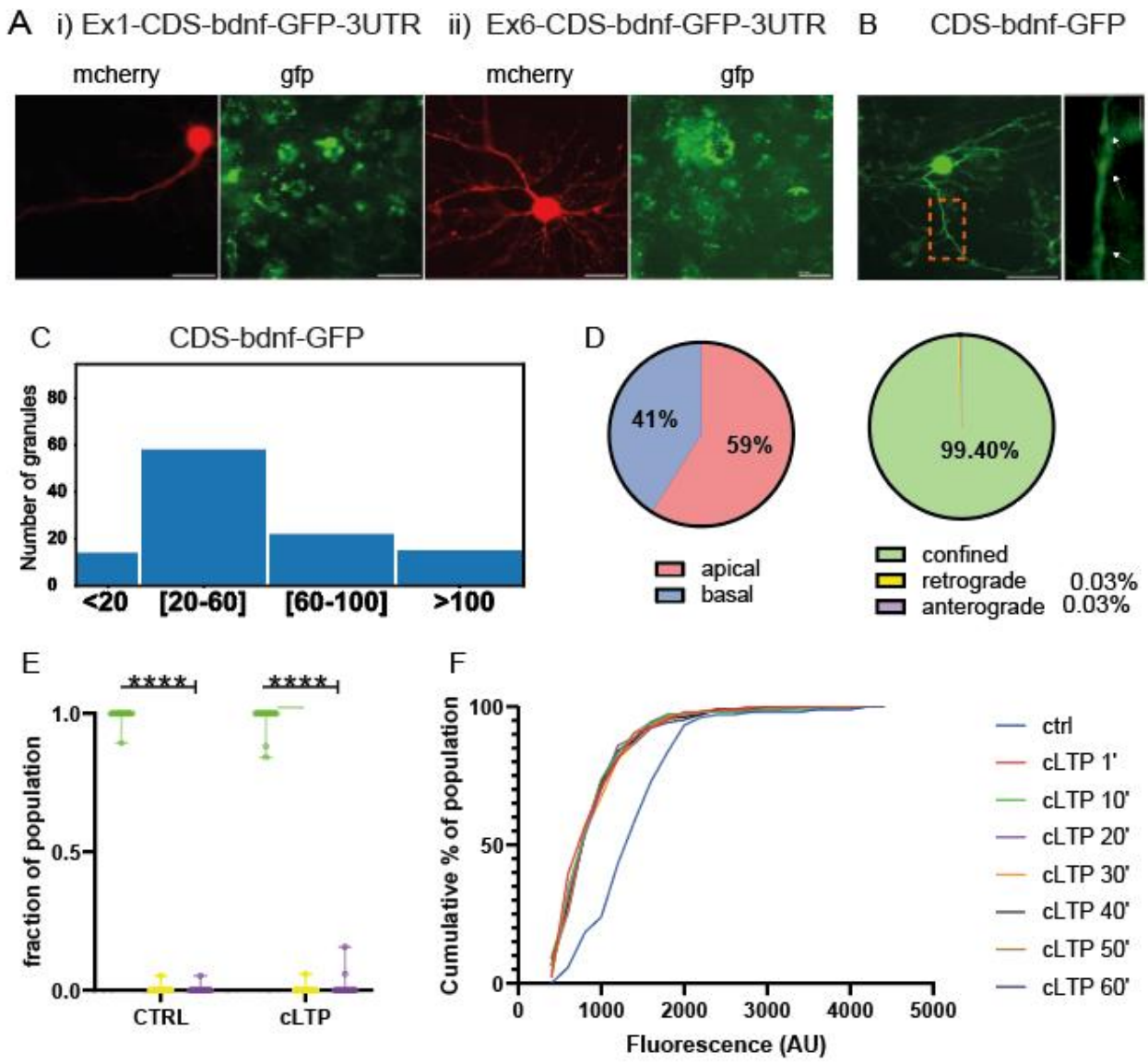

Figure 25: BDNF protein spots in dendrites. A) Representative images of neurons transfected with Ex1-bdnf-gfp-3UTR and Ex6-bdnf-gfp-3UTR, neurons were mcherry positive, but none of them were found to be transfected also with the Ex1-bdnf-gfp-3UTR or Ex6-bdnf-gfp-3UTR Scale bar 10 μm B) transfected neuron with CDS-bdnf-GFP. Arrows indicate the protein spots detected for the analysis C) histogram of the CDS-bdnf-GFP protein spots, the vast majority of spots is at proximal dendrite D) Percentage of CDS-bdnf-GFP spots granules at apical and basal dendrites and the percentage of spots confined, anterograde and retrograde. Almost all the protein spots resulted to be confined. E) Fraction of spots protein confined, anterograde and retrograde in control condition and after cLTP stimulation F) Cumulative distribution of the fluorescence of CDS-bdnf- GFP protein spots in control and every 10 minutes from the cLTP induction. The curve of control is shifted to right showing that the population of protein spots has higher fluorescence intensity compared to the activated cLTP condition

4.7 BDNF protein in proximity to a spine

The same analysis on mRNA granules in fixed samples was conducted also in neurons transfected with the protein constructs in order to see BDNF spot proteins at subcellular level. Neurons were transfected again with Ex6-CDSbdnf-GFP-3'UTR long and Ex1-CDSbdnf-GFP-3' UTR, fixed and immunolabelled with anti-GFP antibody to have a corroboration of what already observed in living neurons. As showed in panel A Figure 26 Ex1-CDSbdnf-GFP-3' UTR is somatic, I was not able to detect immunolabelled green neurons with Ex1-CDSbdnf-GFP-3' UTR in which dendrites were labelled. For Ex6-CDSbdnf-GFP-3'UTR just few neurons were detected with a very dotty pattern as showed in the representative panel A. It was difficult to address if the dotty pattern detected in some dendrites for Ex6-CDSbdnf-GFP-3'UTR was a background signal considering that it was similar to unspecific signal. Therefore, quantification of spot proteins was conducted only on CDS-bdnf-GFP transfected neurons. Preliminary results showed that the density of BDNF protein was not changed after 60 minutes from the induction of cLTP (panel B, n= 8-10 neurons). As mentioned in Section 4.6, in the live imaging I detected new-born spots, with a frequency of 8.64% within the total spot population. However, these events seemed to not significantly affect the density of protein spots after 60 minutes from cLTP induction, possibly because of a physiological turnover of the protein. The distribution of the granules was plotted in C) as well as the fraction of granules inside and under a spine was plotted in D) showing a tendency (ctrl vs cLTP 60' p= 0.12). A significant increment of proteins granules inside a spine was reported after cLTP induction (ctrl vs cLTP 60' p= 0.0085, F). All together these results suggest that the CDS of BDNF after cLTP seemed to be more present inside spines.

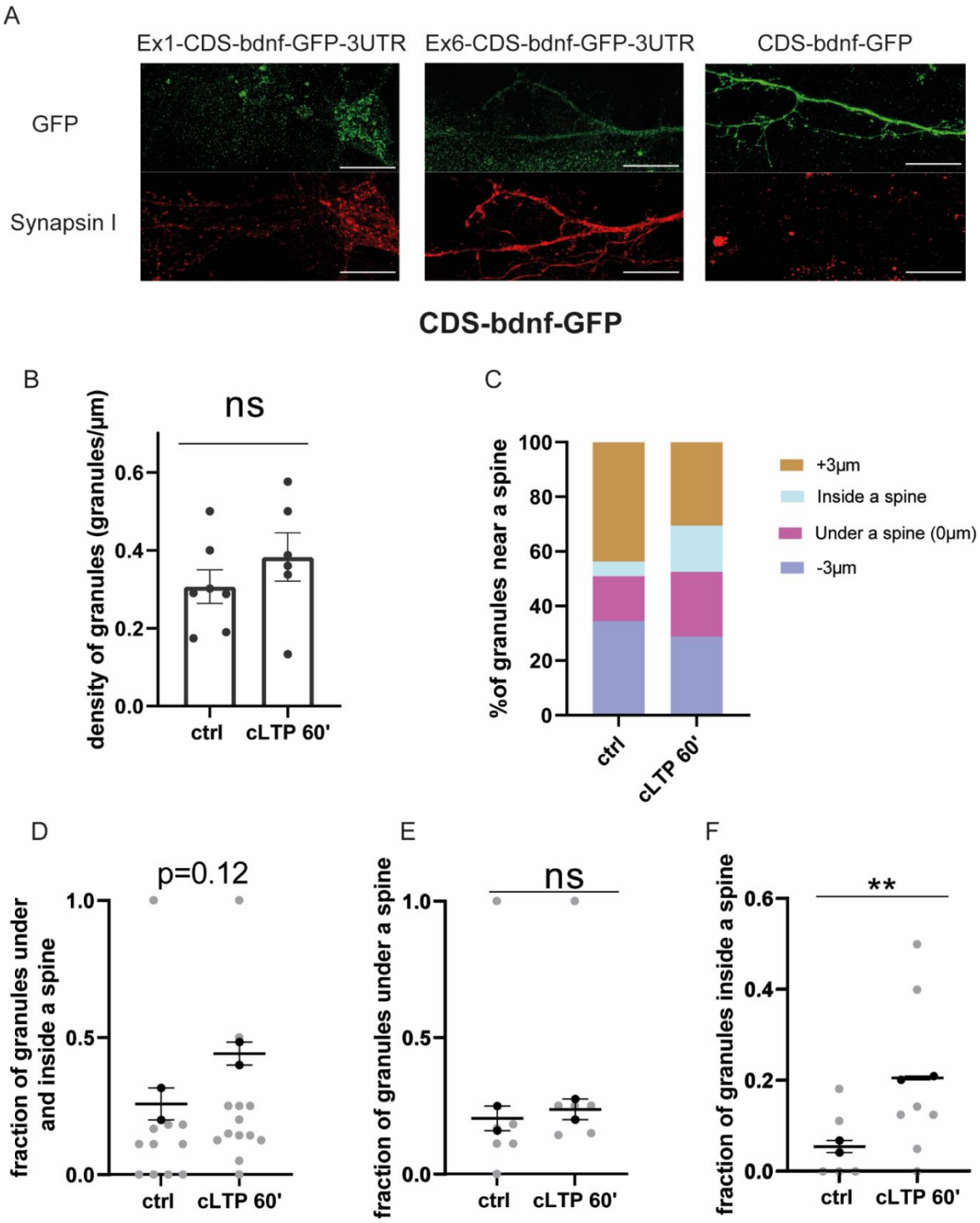

Figure 26: BDNF protein near a spine: A) Representative images of Ex6-BDNF-GFP-3UTR and Ex1-BDNF-GFP-3UTR and CDS-GFP transfected neurons. Neurons were fixed and labelled with Synapsin I. Scale bar 10 µm. **B) CDS-bdnf-GFP granules** on the left, protein spots counted in each dendrite stretches of 30-50 µm. Unpaired T-test revealed no significant difference in the density of CDS-BDNF spots after cLTP stimulation C) protein spots distribution near a spine after cLTP induction. Spots under a spine and inside a spine were considered D) protein spots under and inside a spine were considered at different cLTP induction. After 60' from cLTP induction there is an tendency p=0.12 E) CDS-BDNF granules under a spine were not significantly higher after cLTP induction F) CDS-BDNF spots inside a spine were significantly higher after 60' from cLTP ctrl vs 60' p=0.0085

5.DISCUSSION

The main biological questions behind this doctoral project concerned the dynamics of BDNF mRNA trafficking and its local translation in living neurons at potentiated synapses. As mentioned in previous Sections, the tool chosen for the visualization of BDNF mRNA was the MS2 stem loops, consisting of 12 bacteriophage loops cloned to our cDNA of interest (ex1-cdsBDNF-3 UTR and ex6-cdsBDNF-3UTR). For the protein visualization plasmids of ex1-cdsBDNF-GFP-3UTR, ex6-cds-GFP-3UTR and cds-BDNF-GFP have been used. The two BDNF isoforms exon1 and exon6 considered include the 3'UTR Long isoform for of the BDNF gene. For the visualization of potentiated synapses, the Synactive tool has been tested. To induce potentiation in neuronal hippocampal cultures, different protocols of cLTP have been tested. Live imaging of transfected neurons has been settled on an epifluorescence microscope.

The main original findings of this thesis are summarized as follows.

a) The glycinergic protocol, as well as the glutamate protocol, are not able to induce potentiation in neuronal cultures.
b) Glutamax in cultures is more appropriate for protocols of cLTP induction.
c) Forskolin 10 µM is able to induce cLTP in our system.
d) The vast majority of BDNF mRNA granules show confined behaviour.
e) After cLTP induction the BDNF mRNA granules show even more confined behaviour with a reduction of anterograde and retrograde movement.
f) After cLTP induction the % of BDNF mRNA granules present inside and under a spine increases.
g) The CDS of BDNF protein is mainly confined before and after the cLTP stimulation.
h) After 60' from cLTP induction, the CDS of BDNF is mainly located inside spines.

MS2 system optimization

In the scenario of tagging molecules, the MS2 system is a quite old technique, with possibly many drawbacks and limitations. Some of these limitations have been showed also in this thesis work. First of all, the MS2 loops are difficult to clone because of recombination issues (also faced during the molecular cloning settings). In addition, the tool allows only the tracking of exogenous constructs. Thus, along the second year of my PhD I considered two possible alternative strategies: the first was to use CRISPR-Cas9, the second was the molecular beacons. Both strategies consist in tagging and tracking endogenous BDNF mRNA, but both were excluded for further experimental optimization procedures because of time constrains, available techniques and resources present in the laboratory. One possible advantage in the use of MS2 system is to “force” the system to express the isoform of BDNF in which we are more interested: exon1 and exon6. The cloning of the loops has been considerably time consuming. The fact that two specialized companies (Gentech and Genescript) failed in the cloning of the 24 loops, suggests that the cloning strategy was indeed tremendously ambitious. The difficulties in the cloning procedure have been probably caused by the tendency of the stem loops to recombine, as also reported in other experimental thesis works (Bauer, 2019). Genescript succeeded in cloning the BDNF constructs with 12 MS2 loops: Ex1-cdsBDNF-12L-3UTR L and Ex6-cdsdBDNF-12L-3UTR. At this point, an optimization for the transfection and the imaging of the neurons with these two constructs was performed revealing that the best timing for imaging neurons was at 17-18 hours post transfection. Indeed, this timing turned out to reduce the drawbacks related to the exogenous overexpression of the construct, that has also been reported to clock the neurons (Dahm et al., 2008).

Synactive optimization

The original aim of the project was to evaluate the BDNF mRNA and the BDNF protein subcellular localization in neurons upon a synaptic stimulation. The Synactive construct was the tool necessary for the visualization of potentiated spines since it allows the expression of proteins at synapses in an input-specific, activity-dependent manner by combining RNA targeting elements and a short protein tag. In the original scheme of the project, the constructs

to be transfected were the BDNF mRNA with the loops, the fluorescent loops binding protein and the two constructs of Synactive. The viral trasduction of Synactive was considered as a beneficial help to overcome the difficulties of the transfection of 4 different constructs with high molecular weight (9.5 kb for BDNF mRNA, 6.5 kb for the RNA fluorescent binding protein, 7.5 kb for the mVenus construct and 7.5 kb for the filler construct). This choice was also motivated by the fact that the mRNA should not be overexpressed for too long, because of artifacts, and that Synactive is usually transfected at DIV 3 (personal communication from Ajesh Jacob, Cattaneo's group). Therefore, a unique transfection of the four constructs was not considered as the best solution. The serotype chosen is the AVVDJ. This is reported to be extremely good for in vivo experiments (Haggerty et al., 2020; Mao et al., 2016). Few data has been published regarding the AAVDJ in vitro, but the high efficacy reported in (Domenger and Grimm, 2019; Grimm et al., 2008; Haery et al., 2019; Haggerty et al., 2020) was evaluated to be enough for our purpose. In order to improve the transfection/transduction of the constructs, a possible further advantage could be having a second virus for the filler pAAV::syn-rTA-tdTomato, allowing a single transduction with two viruses. Another improvement for Synactive tool could be the replacement of the two fluorophores: considering mplum and banana instead of mVENUS and TdTomato, whose spectra are quite overlapped. As reported in Materials and Methods, the epifluorescence microscope was equipped with a filter specific for the detection of the YFP bands (Ex 500/24_DM 520_BA 542/27), however this filter was not available at the confocal or Elyra microscope. As soon as, in the future, the Synactive tool will be applied with BDNF-GFP protein, or with BDNF mRNA with the MCP in mcherry, modifications of fluorophores will be needed. So far, in the experiments where Synactive was used, the glycinergic protocol was applied. As showed in the Results, using the glycinergic protocol and 50mM KCl, Synactive was not enriched at spines. Considering this last point, the next further optimization should be trying Synactive with another cLTP protocol, for instance Forskolin 10 µM for 90 minutes.

Induction of cLTP

The development and optimization of a cLTP induction protocol took quite long time. Indeed, the first protocol tested, the glycinergic cLTP, did not give the expected potentiation. The read outs used were many and different: endogenous BDNF increment, Glua1-VGLUT1 and

VGLUT1-PSD95 quantification, Synactive enrichment at spine and C-fos intensity measurement. All these read-outs together demonstrated that the glycinergic protocol in my cultures did not work. Also changing the AraC concentration in the cultures, allowing a higher proliferation of glial cells, was not enough to induce cLTP. A possible interpretation is that the density of the used cultures was not sufficient for the cLTP activation. Indeed, to have cLTP activation and potentiation through glycin treatment, cultures should be very dense and the network between neurons should be mature enough. Using the second protocol, with Glutamate, not all the read-outs used for glycinergic cLTP were performed. However, the C-fos intensity and the VGLUT1 and PSD95 quantification did not show an induction of cLTP in cultures. In conclusion, the Forskolin protocol turned out to be the only to produce a clear activation of C-fos. However, even with the Forskolin, the C-fos intensity increased only when the glutamine in the Neurobasal medium was replaced by the glutamax, a more stable form of glutamine. It is possible that glutamine acted by limiting the potentiation of cultures. Different time points (90, 60, 30 minutes) were tested to see if Forskolin was able to induce cLTP potentiation also before the 90 minutes. Through the analysis of C-fos intensity, the time points 90 minutes and the 30 minutes showed a significant increase. However, at the same time points (90' and 30' from the cLTP induction) the VGLUT1 number and size puncta did not show any significant difference in control and after cLTP activation. A possible explanation for the difficulties I faced in the cLTP induction could be the presence of highly active neurons in the cultures, a phenomenon already reported in the literature (Okada et al., 2021). In addition, it is worth to mention that all the protocols reported dealt with the application of components in the bath, resulting in a general activation of the culture, whereas the original idea was to assess the local translation at individual synapses, possibly activating only a single spine or a small subset of them.

BDNF mRNA dynamics in living neurons

The first task of the project was to evaluate if BDNF mRNA granules display directional trafficking following LTP and if they stop in proximity to activated synapses. Through the live imaging approach, the spines were not visible because of resolution limits, however it was possible to assess the nature of the granule movements in the dendrites. The performed analysis suggested that the great majority of granules were confined for all the four constructs

(EX1-cds BDNF-12L-3'UTR, EX6-cds BDNF-12L-3'UTR, CamkIIa-8L-3'UTR and 12L). This result is in agreement with a recent paper (Donlin-asp et al., 2021) that used molecular beacons to track endogenous CamKII and PSD95 mRNA. The same work also reported that the vast majority of granules having an anterograde or retrograde movement, stopped and froze after the cLTP induction. As showed in the Results section, I observed the same behavior. The soundness of our approach using an exogenous system, as the MS2 stem loop technique, was thus confirmed by the comparison with similar findings (Donlin-asp et al., 2021) where the endogenous mRNA was detected by a more physiological method by means of molecular beacons. As reported in the Results section, the EX1-cds BDNF-12L-3'UTR, EX6-cds BDNF-12L-3'UTR, CamkIIa-8L-3'UTR showed a slight bias, even though not significant, for the anterograde movements. This bias could be caused by the 3'UTR sequence, that, as already reported, is important for the dendritic localization of BDNF mRNA (An et al., 2008b; Tang et al., 2008; Vicario et al., 2015) and other mRNAs (Bauer et al., 2019). This explanation is strengthened by the observation that the 12 L construct, without the 3' UTR sequence, did not show any bias for the anterograde movements, showing an equal distribution of anterograde and retrograde movements. The anterograde velocity for the EX6-cds-BDNF-12L-3'UTR showed a significant increment when compared with the anterograde velocity for the EX1-cds BDNF-12L-3'UTR (Ex6 vs Ex1 $p=0.0355$). This statement could be linked to the already reported result that the Ex6-BDNF is located at more distal part of dendrites in comparison with the Ex1-BDNF (Baj et al., 2011). After the cLTP induction, granules froze becoming more confined: the increment of confined movements was visible for all the four constructs, even for the 12 L. Even though the presence and the movements of granules with the loops alone was reported in literature (Bauer et al., 2019), however it was reasonable to not expect any response to cLTP for the 12 L construct. Indeed, unlike BDNF and CamkII, 12 L construct should not give rise to any biological mechanism in response to cLTP. Considering 20 neurons imaged for each construct, the total number of granules detected for the 12 L was significantly lower than for the other constructs. After the cLTP induction the number of anterograde movements decreased for the EX6-cds BDNF-12L-3'UTR and EX1-cds BDNF-12L-3'UTR, but not for the CamkIIa-8L-3'UTR and 12 L. On the contrary, the number of retrograde movements decreased after cLTP for CamkIIa-8L-3'UTR and 12 L (CamkII $p=0.0020$, 12L $p=0.0313$) but not for the BDNF mRNA (even if for the Ex1 there was a tendency, $p=0.0625$). The significance of this difference is not entirely clear, although probably it could depend on the different localization of the granules.

Speculating on these results, I could mention that the movements of BDNF and CamkII upon cLTP induction could be dictated by the localization of these granules near a potentiated spine. Upon cLTP induction, some BDNF mRNA granules continue to move through the soma, probably targeting the nearest Golgi outposts, whereas CamkII mRNA granules seemed to continue going to the periphery. However, more detailed and accurate studies are needed to clarify if the observed differences can have a biological significance. Furthermore, I evaluated the number of neurons in which I detected a decrease of the number of mRNA granules in response to the cLTP induction. This is possibly due to the mRNA translation into protein. Although I observed a significant decrease in the number of CamkII mRNA granules compared to the 12 L, it is difficult to univocally determine the cLTP as the reason of this phenomenon. Indeed, the disappearance of the granules could be caused by any technically artifact. A better understanding of the disappearance phenomenon could be given by the PLA-assay technique that allows the observation of newly synthetized proteins (Donlin-asp et al., 2021).

Tracking the BDNF protein in living neurons

Once that the mRNA of BDNF was tracked in live neurons in control and in response to cLTP stimulation, my goal was to evaluate what happens to the BDNF protein after the cLTP induction. cLTP stimulation and protein synthesis are closely related. Indeed, the group of Erin Shuman recently demonstrated that there is new protein synthesis in the proximity to an activated spine (Sun et al., 2021). Having in the laboratory the constructs EX1-cds BDNF-GFP-3'UTR long and the EX6-cds BDNF-GFP-3'UTR long, used as a backbone for the 12 MS2 loops for the tracking of mRNA, I decided to use the same constructs to see the BDNF mRNA protein. However, after many trials for the optimization of the transfection of these constructs, the neurons seemed always to be not transfected, or at least the pattern appeared so weak that in live imaging it was not possible to analyse the neurons for further experiments. A possible explanation is that the two constructs are quite big. In addition, they have the 3' UTR long sequence, which has been reported to confers a very poor translatability to the GFP reporter (Lau et al., 2010). Therefore, I performed the live imaging experiments by using the CDS-BDNF construct alone. Unfortunately, an exhaustive comparison between protein and mRNA dynamics for the same construct was not possible. However, I evaluated the localization of CDS- BDNF-GFP protein spots, reporting that most spots were localized at proximal dendrites,

but they were also at distal dendrites. Indeed, it has been reported that the CDS contains a constitutively active dendritic targeting element which confers dendritic localization even under basal conditions in hippocampal neurons (Chiaruttini et al., 2009b). Besides the characterization of the CDS-BDNF-GFP protein spots, the aim was to see newly protein synthesis. Two approaches were conducted to see the protein synthesis through the CDS-BDFN-GFP construct: the first one was to evaluate the fluorescence of every CDS spot before and after cLTP, the second one was to evaluate the frequency of spots observed after the cLTP and not detected previously during the control recording. Regarding the first analysis, I could not report an increase in the fluorescence of the GFP fused to the CDS-BDNF. The decreased fluorescence reported for the activated condition could be caused by a technical issue, as for instance the photobleaching of the fluorescence of CDS-GFP. About this possibility, I could be confident that the time for taking the image was in the range of ms and this time is too short to have photobleaching. However, the supposed increment of fluorescence intensity was not detected, suggesting that, probably, the increase was small, and the sensitivity of the analysis conducted was not enough to observe the increment. On the other hand, considering the second analysis, I observed that the 8.69% of the detected population of protein spots consisted of “new-born” spots. However, to demonstrate that this phenomenon of new-born spots is related to the cLTP induction, I should have performed some additional experiments, as for instance a 60-minute recording without any cLTP induction. Anyway, in the 10 minutes of my control recording I did not detect the appearance of any “new-born” spot. Instead, I detected some events of “spot disappearance”, with a frequency corresponding to the 4% of the total population. This phenomenon of disappearance could be caused by stochastic events, or rather could have a biological significance, such for example capturing events occurring at spines.

BDNF mRNA and protein near a spine

After the analysis of BDNF mRNA and protein in living neurons, I tried to identify the subcellular localization of mRNA granules and spots proteins near a spine in fixed neurons. The task of the project was to understand if BDNF mRNA and BDNF protein are in proximity of an activated spine, after cLTP induction. Although the analysis on potentiated spines could not be addressed, I evaluated the distance between a granule and the nearest spine, considering a range of +3 µm, -3 µm centered on the spine. Evaluating the mRNA granules, it was possible

to delineate a similar pattern: CamkIIa as well as the BDNF granules after 15’ from cLTP were increased under the spines, while after 30’ or 60’ from cLTP granules were higher inside the spine in comparison with the dendritic shaft for Ex1-bdnfCDS-12L-3UTR and for CamkIIa-8L-3’UTR. For EX6-cds BDNF-12l -3’UTR long there was a tendency at 30 minutes for an increment of granules inside the spines. A possible interpretation is that after short periods (15-30 minutes) from cLTP induction, granules were more localized under a spine, whereas, after longer periods (60 minutes) granules were more localized inside a spine. The construct with only the 12 stem loops (12 L) did not show any significant increase in the number of granules under or inside the spine, suggesting that the distribution of granules was cLTP independent. This result seems to be more coherent with what I expected in comparison to the results already discussed for the live imaging. Moreover, considering that the resolution of the fixed neurons experiments is higher, this result appears more reliable. On the other hand, taking in consideration the BDNF protein, the results suggested that after 60 minutes of cLTP induction, there was an increment of protein spots inside a spine. However, as I just mentioned before, I could not assess if the spines taken in consideration were potentiated or not among the cLTP induction. In addition, the second task for the project was to assess if local translation of BDNF occurred at single synapses after cLTP activation. This last part, considering the tools used was impossible to be assessed because inducing the cLTP with a bath application, I lost the specificity of single activated spines. Anyway, it has been reported that, after the induction of cLTP through the glutamate uncaging (Sun et al., 2021) there was a massive protein synthesis, probably, also BNDF is one of these proteins.

6.CONCLUSION AND FUTURE PERSPECTIVES

From a technical point of view the setting up of all the applied tools, such as the cloning of BDNF constructs, the optimization of Synactive, the protocols for the induction of cLTP, as well as the optimization of the neuronal cultures protocol and the adjustment of the imaging analysis and the live imaging of neurons were extremely time demanding. I moved through many trials and errors, testing different approaches and read-outs. However, together with all the discussed methodological results, I achieved several preliminary results concerning the dynamics of BDNF mRNA and BDNF proteins, as discussed in the thesis. Considering the current scenario of the field, my results can be considered as incremental to what recently published by other groups (Donlin-asp et al., 2021; Glock et al., 2017). My data, together with the ones recently published by (Donlin-asp et al., 2021) suggest that further research work is needed to reconcile the sushi belt model with the observation that most mRNA granules is confined.

As future perspectives, it could be interesting to use the GRASP technique to identify potentiated spines. The advantages of molecular beacons or CRISPR-related techniques could allow a better understanding of what happens at endogenous level in spines after a potentiation paradigm. A multidisciplinary approach taking advantage of data from proteomics and from RNA-seq of potentiated spines is needed to improve our knowledge of activated spines and of how the production of proteins locally aids in the formation of new memories. As an extension of the project on BDNF, it could be interesting to develop molecular beacons and/or CRISPR related techniques that could address the endogenous levels of the mRNA and the protein, thus allowing a comprehensive understanding of the BDNF in the engram formation and recall of memories.

BIBLIOGRAPHY

An, J.J., Gharami, K., Liao, G., Woo, N.H., Lau, A.G., Vanevski, F., Torre, E.R., Jones, K.R., Feng, Y., Lu, B., et al. (2008a). Distinct Role of Long 3 0 UTR BDNF mRNA in Spine Morphology and Synaptic Plasticity in Hippocampal Neurons. 175–187.

An, J.J., Gharami, K., Liao, G.-Y., Woo, N.H., Lau, A.G., Vanevski, F., Torre, E.R., Jones, K.R., Feng, Y., Lu, B., et al. (2008b). Distinct role of long 3' UTR BDNF mRNA in spine morphology and synaptic plasticity in hippocampal neurons. Cell *134*, 175–187.

Bae, B., and Miura, P. (2020). Emerging roles for 3' UTRs in neurons. Int. J. Mol. Sci. *21*, 1–24.

Bailey, C.H., and Chen, M. (1983). Morphological basis of long-term habituation and sensitization in Aplysia. Science *220*, 91–93.

Bailey, C.H., Kandel, E.R., and Harris, K.M. (2015). Structural Components of Synaptic Plasticity and Memory Consolidation. Cold Spring Harb. Perspect. Biol. *7*, a021758.

Baj, G., Leone, E., Chao, M. V., and Tongiorgi, E. (2011). Spatial segregation of BDNF transcripts enables BDNF to differentially shape distinct dendritic compartments. Proc. Natl. Acad. Sci. U. S. A. *108*, 16813–16818.

Baj, G., Del Turco, D., Schlaudraff, J., Torelli, L., Deller, T., and Tongiorgi, E. (2013). Regulation of the spatial code for BDNF mRNA isoforms in the rat hippocampus following pilocarpine-treatment: A systematic analysis using laser microdissection and quantitative real-time PCR. Hippocampus *23*, 413–423.

Baj, G., Pinhero, V., Vaghi, V., and Tongiorgi, E. (2016). Signaling pathways controlling activity-dependent local translation of BDNF and their localization in dendritic arbors. J. Cell Sci. *129*, 2852–2864.

Barco, A., Patterson, S.L., Alarcon, J.M., Gromova, P., Mata-Roig, M., Morozov, A., and Kandel, E.R. (2005). Gene expression profiling of facilitated L-LTP in VP16-CREB mice reveals that BDNF is critical for the maintenance of LTP and its synaptic capture. Neuron *48*, 123–137.

Bassell, G.J., and Warren, S.T. (2008). Fragile X Syndrome: Loss of Local mRNA Regulation Alters Synaptic Development and Function. Neuron *60*, 201–214.

Basu, J., and Siegelbaum, S.A. (2020). Plasticity , and Memory.

Bauer, K.E. (2019). LIVE MICROSCOPY OF RNA GRANULE SORTING IN HIPPOCAMPAL NEURONS IN SPACE AND TIME.

Bauer, K.E., Kiebler, M.A., and Segura, I. (2017). Visualizing RNA granule transport and translation in living neurons. Methods *126*, 177–185.

Bauer, K.E., Segura, I., Gaspar, I., Scheuss, V., Illig, C., Ammer, G., Hutten, S., Basyuk, E., Fernández-Moya, S.M., Ehses, J., et al. (2019). Live cell imaging reveals 3′-UTR dependent mRNA sorting to synapses. Nat. Commun. *10*.

Bekkers, J.M., and Stevens, C.F. (1990). Presynaptic mechanism for long-term potentiation in the hippocampus. Nature *346*, 724–729.

Berkemeier, L.R., Winslow, J.W., Kaplan, D.R., Nikolics, K., Goeddel, D. V, and Rosenthal, A. (1991). Neurotrophin-5: a novel neurotrophic factor that activates trk and trkB. Neuron *7*, 857–866.

Bertrand, E., Chartrand, P., Schaefer, M., Shenoy, S.M., Singer, R.H., and Long, R.M. (1998). Localization of ASH1 mRNA particles in living yeast. Mol. Cell *2*, 437–445.

Biever, A., Glock, C., Tushev, G., Ciirdaeva, E., Dalmay, T., Langer, J.D., and Schuman, E.M. (2020). Monosomes actively translate synaptic mRNAs in neuronal processes. *4991*.

Binder, S., Berg, K., Gasca, F., Lafon, B., Parra, L.C., Born, J., and Marshall, L. (2014). Transcranial slow oscillation stimulation during sleep enhances memory consolidation in rats. Brain Stimul. *7*, 508–515.

Bozzi, Y., Pizzorusso, T., Cremisi, F., Rossi, F.M., Barsacchi, G., and Maffei, L. (1995). Monocular deprivation decreases the expression of messenger RNA for brain-derived neurotrophic factor in the rat visual cortex. Neuroscience *69*, 1133–1144.

Braselmann, E., Rathbun, C., Richards, E.M., and Palmer, A.E. (2020). Illuminating RNA Biology: Tools for Imaging RNA in Live Mammalian Cells. Cell Chem. Biol. *27*, 891–903.

Bullitt, E. (1990). Expression of C-fos-like protein as a marker for neuronal activity following

noxious stimulation in the rat. J. Comp. Neurol. *296*, 517–530.

Cajigas, J., Tushev, G., Will, T.J., Dieck, S., Fuerst, N., and Schuman, E.M. (2012). NeuroResource The Local Transcriptome in the Synaptic Neuropil Revealed by Deep Sequencing and High-Resolution Imaging. 453–466.

Capsoni, S., Tongiorgi, E., Cattaneo, A., and Domenici, L. (1999a). Differential regulation of brain-derived neurotrophic factor messenger RNA cellular expression in the adult rat visual cortex. Neuroscience *93*, 1033–1040.

Capsoni, S., Tongiorgi, E., Cattaneo, A., and Domenici, L. (1999b). Dark rearing blocks the developmental down-regulation of brain-derived neurotrophic factor messenger RNA expression in layers IV and V of the rat visual cortex. Neuroscience *88*, 393–403.

Casaccia-Bonnefil, P., Gu, C., and Chao, M. V (1999). Neurotrophins in cell survival/death decisions. Adv. Exp. Med. Biol. *468*, 275–282.

Castrén, E., and Rantamäki, T. (2010). The role of BDNF and its receptors in depression and antidepressant drug action: Reactivation of developmental plasticity. Dev. Neurobiol. *70*, 289–297.

Castrén, E., Zafra, F., Thoenen, H., and Lindholm, D. (1992). Light regulates expression of brain-derived neurotrophic factor mRNA in rat visual cortex. Proc. Natl. Acad. Sci. U. S. A. *89*, 9444–9448.

Castrén, E., Pitkänen, M., Sirviö, J., Parsadanian, A., Lindholm, D., Thoenen, H., and Riekkinen, P.J. (1993). The induction of ltp increases bdnf and ngf mrna but decreases nt-3 mrna in the dentate gyrus. Neuroreport *4*, 895–898.

Chao, M. V (2003). Neurotrophins and their receptors: A convergence point for many signalling pathways. Nat. Rev. Neurosci. *4*, 299–309.

Chen, G., Kolbeck, R., Barde, Y.A., Bonhoeffer, T., and Kossel, A. (1999). Relative contribution of endogenous neurotrophins in hippocampal long-term potentiation. J. Neurosci. Off. J. Soc. Neurosci. *19*, 7983–7990.

Cheng, Q., and Yeh, H.H. (2003). Brain-derived neurotrophic factor attenuates mouse cerebellar granule cell GABA(A) receptor-mediated responses via postsynaptic mechanisms. J. Physiol. *548*, 711–721.

Chiaruttini, C., Vicario, A., Li, Z., Baj, G., Braiuca, P., Wu, Y., Lee, F.S., Gardossi, L., Baraban, J.M., and Tongiorgi, E. (2009a). Dendritic trafficking of BDNF mRNA is mediated by translin and blocked by the G196A (Val66Met) mutation. Proc. Natl. Acad. Sci. U. S. A. *106*, 16481–16486.

Chiaruttini, C., Vicario, A., Li, Z., Baj, G., Braiuca, P., Wu, Y., Lee, F.S., Gardossi, L., Baraban, J.M., and Tongiorgi, E. (2009b). Dendritic trafficking of BDNF mRNA is mediated by translin and blocked by the G196A (Val66Met) mutation. Proc. Natl. Acad. Sci. U. S. A. *106*, 16481–16486.

Choi, J., Sim, S., Kim, J., Choi, D. Il, Oh, J., Ye, S., Lee, J., Kim, T., Ko, H., and Lim, C. (2018). Interregional synaptic maps among engram cells underlie memory formation. *435*, 430–435.

Colliva, A., and Tongiorgi, E. (2021). Distinct role of 5 ′ UTR sequences in dendritic trafficking of BDNF mRNA : additional mechanisms for the BDNF splice variants spatial code. Mol. Brain 1–13.

Conner, J.M., Lauterborn, J.C., Yan, Q., Gall, C.M., and Varon, S. (1997). Distribution of Brain-Derived Neurotrophic Factor (BDNF) Protein and mRNA in the Normal Adult Rat CNS : Evidence for Anterograde Axonal Transport. *17*, 2295–2313.

Cui-Wang, T., Hanus, C., Cui, T., Helton, T., Bourne, J., Watson, D., Harris, K.M., and Ehlers, M.D. (2012). Local zones of endoplasmic reticulum complexity confine cargo in neuronal dendrites. Cell *148*, 309–321.

Dahm, R., Zeitelhofer, M., Götze, B., Kiebler, M.A., and Macchi, P. (2008). Visualizing mRNA Localization and Local Protein Translation in Neurons. In Methods in Cell Biology, pp. 293–327.

David P. Clark, Nanette J. Pazdernik, in Molecular Biology (Second Edition), 2013 (2013). Polymerase Chain Reaction. 163–193.

Dictenberg, J.B., Swanger, S.A., Antar, L.N., Singer, R.H., and Bassell, G.J. (2008). A direct role for FMRP in activity-dependent dendritic mRNA transport links filopodial-spine morphogenesis to fragile X syndrome. Dev. Cell *14*, 926–939.

Dieck, S., Kochen, L., Hanus, C., Heumüller, M., Bartnik, I., Nassim-assir, B., Merk, K.,

Mosler, T., Garg, S., Bunse, S., et al. (2015). Direct visualization of newly synthesized target proteins in situ. *12*, 1–7.

Dieni, S., Matsumoto, T., Dekkers, M., Rauskolb, S., Ionescu, M.S., Deogracias, R., Gundelfinger, E.D., Kojima, M., Nestel, S., Frotscher, M., et al. (2012). BDNF and its pro-peptide are stored in presynaptic dense core vesicles in brain neurons. J. Cell Biol. *196*, 775–788.

Domenger, C., and Grimm, D. (2019). Next-generation AAV vectors-do not judge a virus (only) by its cover. Hum. Mol. Genet. *28*, R3–R14.

Donlin-asp, P.G., Polisseni, C., Klimek, R., Heckel, A., and Schuman, E.M. (2021). Differential regulation of local mRNA dynamics and translation following long-term potentiation and depression. *118*.

Doyle, M., and Kiebler, M.A. (2011). Mechanisms of dendritic mRNA transport and its role in synaptic tagging. EMBO J. *30*, 3540–3552.

Dragunow, M., Beilharz, E., Mason, B., Lawlor, P., Abraham, W., and Gluckman, P. (1993). Brain-derived neurotrophic factor expression after long-term potentiation. Neurosci. Lett. *160*, 232–236.

Egan, M.F., Kojima, M., Callicott, J.H., Goldberg, T.E., Kolachana, B.S., Bertolino, A., Zaitsev, E., Gold, B., Goldman, D., Dean, M., et al. (2003). The BDNF val66met polymorphism affects activity-dependent secretion of BDNF and human memory and hippocampal function. Cell *112*, 257–269.

Ernfors, P., Bengzon, J., Kokaia, Z., Persson, H., and Lindvall, O. (1991). Increased levels of messenger RNAs for neurotrophic factors in the brain during kindling epileptogenesis. Neuron *7*, 165–176.

Ferhat, L., Khrestchatisky, M., Roisin, M. -P, and Barbin, G. (1993). Basic Fibroblast Growth Factor-Induced Increase in zif/268 and c-fos mRNA Levels Is Ca2+ Dependent in Primary Cultures of Hippocampal Neurons. J. Neurochem. *61*, 1105–1112.

Fernandez-Moya, S.M., Bauer, K.E., and Kiebler, M.A. (2014). Meet the players: local translation at the synapse. Front. Mol. Neurosci. *7*, 84.

Franceschi Biagioni, A., Cellot, G., Pati, E., Lozano, N., Ballesteros, B., Casani, R., Coimbra,

N.C., Kostarelos, K., and Ballerini, L. (2021). Graphene oxide prevents lateral amygdala dysfunctional synaptic plasticity and reverts long lasting anxiety behavior in rats. Biomaterials *271*.

Frey, U., and Morris, R.G. (1997). Synaptic tagging and long-term potentiation. Nature *385*, 533–536.

Frey, U., Krug, M., Reymann, K.G., and Matthies, H. (1988). Anisomycin, an inhibitor of protein synthesis, blocks late phases of LTP phenomena in the hippocampal CA1 region in vitro. Brain Res. *452*, 57–65.

Gall, J.G., and Pardue, M.L. (1969). Formation and detection of RNA-DNA hybrid molecules in cytological preparations. Proc. Natl. Acad. Sci. U. S. A. *63*, 378–383.

Garner, C.C., Brugg, B., and Matus, A. (1988). A 70-kilodalton microtubule-associated protein (MAP2c), related to MAP2. J. Neurochem. *50*, 609–615.

George, L., Indig, F.E., Abdelmohsen, K., and Gorospe, M. (2018). Intracellular RNA-tracking methods.

Ghosh, A., Carnahan, J., and Greenberg, M.E. (1994). Requirement for BDNF in activity-dependent survival of cortical neurons. Science *263*, 1618–1623.

Glock, C., Heumüller, M., and Schuman, E.M. (2017). mRNA transport & local translation in neurons. Curr. Opin. Neurobiol. *45*, 169–177.

Gobbo, F., Marchetti, L., Jacob, A., Pinto, B., Binini, N., Pecoraro Bisogni, F., Alia, C., Luin, S., Caleo, M., Fellin, T., et al. (2017). Activity-dependent expression of Channelrhodopsin at neuronal synapses. Nat. Commun. *8*.

Golmohammadi, R., Valegård, K., Fridborg, K., and Liljas, L. (1993). The Refined Structure of Bacteriophage MS2 at 2·8 Å Resolution. J. Mol. Biol. *234*, 620–639.

Goodman, L.J., Valverde, J., Lim, F., Geschwind, M.D., Federoff, H.J., Geller, A.I., and Hefti, F. (1996). Regulated release and polarized localization of brain-derived neurotrophic factor in hippocampal neurons. Mol. Cell. Neurosci. *7*, 222–238.

Gorski, J.A., Zeiler, S.R., Tamowski, S., and Jones, K.R. (2003). Brain-derived neurotrophic factor is required for the maintenance of cortical dendrites. J. Neurosci. Off. J. Soc.

Neurosci. *23*, 6856–6865.

Govindarajan, A., Kelleher, R.J., and Tonegawa, S. (2006). A clustered plasticity model of long-term memory engrams. Nat. Rev. Neurosci. *7*, 575–583.

Govindarajan, A., Israely, I., Huang, S.Y., and Tonegawa, S. (2011a). The Dendritic Branch Is the Preferred Integrative Unit for Protein Synthesis-Dependent LTP. Neuron *69*, 132–146.

Govindarajan, A., Israely, I., Huang, S.-Y., and Tonegawa, S. (2011b). The dendritic branch is the preferred integrative unit for protein synthesis-dependent LTP. Neuron *69*, 132–146.

Gray, N.W., Weimer, R.M., Bureau, I., and Svoboda, K. (2006). Rapid redistribution of synaptic PSD-95 in the neocortex in vivo. PLoS Biol. *4*, e370.

Grimm, D., Lee, J.S., Wang, L., Desai, T., Akache, B., Storm, T.A., and Kay, M.A. (2008). In Vitro and In Vivo Gene Therapy Vector Evolution via Multispecies Interbreeding and Retargeting of Adeno-Associated Viruses. J. Virol. *82*, 5887–5911.

Guzowski, J.F., Lyford, G.L., Stevenson, G.D., Houston, F.P., McGaugh, J.L., Worley, P.F., and Barnes, C.A. (2000). Inhibition of activity-dependent arc protein expression in the rat hippocampus impairs the maintenance of long-term potentiation and the consolidation of long-term memory. J. Neurosci. *20*, 3993–4001.

Haery, L., Deverman, B.E., Matho, K.S., Cetin, A., Woodard, K., Cepko, C., Guerin, K.I., Rego, M.A., Ersing, I., Bachle, S.M., et al. (2019). Adeno-Associated Virus Technologies and Methods for Targeted Neuronal Manipulation. Front. Neuroanat. *13*.

Haggerty, D.L., Grecco, G.G., Reeves, K.C., and Atwood, B. (2020). Adeno-Associated Viral Vectors in Neuroscience Research. Mol. Ther. Methods Clin. Dev. *17*, 69–82.

Herdegen, T., and Leah, J.D. (1998). Inducible and constitutive transcription factors in the mammalian nervous system: Control of gene expression by Jun, Fos and Krox, and CREB/ATF proteins. Brain Res. Rev. *28*, 370–490.

Herzog, K.H., Bailey, K., and Barde, Y.A. (1994). Expression of the BDNF gene in the developing visual system of the chick. Development *120*, 1643–1649.

Hofer, M., Pagliusi, S.R., Hohn, A., Leibrock, J., and Barde, Y.A. (1990). Regional distribution of brain-derived neurotrophic factor mRNA in the adult mouse brain. EMBO J. *9*, 2459–2464.

Holt, C.E., and Bullock, S.L. (2009). Subcellular mRNA localization in animal cells and why it matters. Science *326*, 1212–1216.

Horn, W.T., Convery, M.A., Stonehouse, N.J., Adams, C.J., Liljas, L., Phillips, S.E. V, and Stockley, P.G. (2004). The crystal structure of a high affinity RNA stem-loop complexed with the bacteriophage MS2 capsid: further challenges in the modeling of ligand-RNA interactions. RNA *10*, 1776–1782.

Horton, A.C., and Ehlers, M.D. (2003). Dual modes of endoplasmic reticulum-to-Golgi transport in dendrites revealed by live-cell imaging. J. Neurosci. *23*, 6188–6199.

Howard, D.B., and Harvey, B.K. (2017). Assaying the Stability and Inactivation of AAV Serotype 1 Vectors. Hum. Gene Ther. Methods *28*, 39–48.

Huang, Y.-S., Carson, J.H., Barbarese, E., and Richter, J.D. (2003). Facilitation of dendritic mRNA transport by CPEB. Genes Dev. *17*, 638–653.

Huganir, R.L., and Nicoll, R.A. (2013). AMPARs and synaptic plasticity: The last 25 years. Neuron *80*, 704–717.

Johansson, H.E., Liljas, L., and Uhlenbeck, O.C. (1997). RNA Recognition by the MS2 Phage Coat Protein. Semin. Virol. *8*, 176–185.

Josselyn, S.A., Köhler, S., and Frankland, P.W. (2017). Heroes of the engram. J. Neurosci. *37*, 4647–4657.

Kanai, Y., Dohmae, N., and Hirokawa, N. (2004). Kinesin transports RNA: isolation and characterization of an RNA-transporting granule. Neuron *43*, 513–525.

Kang, H., and Schuman, E.M. (1995). Long-lasting neurotrophin-induced enhancement of synaptic transmission in the adult hippocampus. Science *267*, 1658–1662.

Kang, H., and Schuman, E.M. (1996). A requirement for local protein synthesis in neurotrophin-induced hippocampal synaptic plasticity. Science *273*, 1402–1406.

Kang, H., Welcher, A.A., Shelton, D., and Schuman, E.M. (1997). Neurotrophins and time: different roles for TrkB signaling in hippocampal long-term potentiation. Neuron *19*, 653–664.

Keene, J.D., and Tenenbaum, S.A. (2002). Eukaryotic mRNPs may represent posttranscriptional operons. Mol. Cell *9*, 1161–1167.

Kelleher, R.J. 3rd, Govindarajan, A., and Tonegawa, S. (2004). Translational regulatory mechanisms in persistent forms of synaptic plasticity. Neuron *44*, 59–73.

Kiebler, M.A., and Bassell, G.J. (2006). Neuronal RNA granules: movers and makers. Neuron *51*, 685–690.

Köhrmann, M., Luo, M., Kaether, C., DesGroseillers, L., Dotti, C.G., and Kiebler, M.A. (1999). Microtubule-dependent recruitment of Staufen-green fluorescent protein into large RNA-containing granules and subsequent dendritic transport in living hippocampal neurons. Mol. Biol. Cell *10*, 2945–2953.

Korte, M., Carroll, P., Wolf, E., Brem, G., Thoenen, H., and Bonhoeffer, T. (1995). Hippocampal long-term potentiation is impaired in mice lacking brain-derived neurotrophic factor. Proc. Natl. Acad. Sci. U. S. A. *92*, 8856–8860.

Korte, M., Griesbeck, O., Gravel, C., Carroll, P., Staiger, V., Thoenen, H., and Bonhoeffer, T. (1996). Virus-mediated gene transfer into hippocampal CA1 region restores long-term potentiation in brain-derived neurotrophic factor mutant mice. Proc. Natl. Acad. Sci. U. S. A. *93*, 12547–12552.

Kuklin, E.A., Alkins, S., Bakthavachalu, B., Genco, M.C., Sudhakaran, I., Raghavan, K.V., Ramaswami, M., and Griffith, L.C. (2017). The Long 3'UTR mRNA of CaMKII Is Essential for Translation-Dependent Plasticity of Spontaneous Release in Drosophila melanogaster. J. Neurosci. Off. J. Soc. Neurosci. *37*, 10554–10566.

Lam, B.Y.H., Zhang, W., Enticknap, N., Haggis, E., Cader, M.Z., and Chawla, S. (2009). Inverse regulation of plasticity-related immediate early genes by calcineurin in hippocampal neurons. J. Biol. Chem. *284*, 12562–12571.

Lau, A.G., Irier, H.A., Gu, J., Tian, D., Ku, L., Liu, G., Xia, M., and Fritsch, B. (2010). Distinct 3 ′ UTRs differentially regulate activity- dependent translation of brain-derived neurotrophic factor (BDNF). *107*, 3–8.

Lazear, K., and Boterf, E. (2007). Quick Guide Quick Guide. Curr. Biol. *47*, 2–3.

Leal, G., Bramham, C.R., and Duarte, C.B. (2017). BDNF and Hippocampal Synaptic Plasticity. Vitam. Horm. *104*, 153–195.

Lee, P.R., Cohen, J.E., Becker, K.G., and Fields, R.D. (2005). Gene expression in the

conversion of early-phase to late-phase long-term potentiation. Ann. N. Y. Acad. Sci. *1048*, 259–271.

Lein, E.S., Hawrylycz, M.J., Ao, N., Ayres, M., Bensinger, A., Bernard, A., Boe, A.F., Boguski, M.S., Brockway, K.S., Byrnes, E.J., et al. (2007). Genome-wide atlas of gene expression in the adult mouse brain. Nature *445*, 168–176.

Lu, B., and Chow, A. (1999). Neurotrophins and hippocampal synaptic transmission and plasticity. J. Neurosci. Res. *58*, 76–87.

Lu, B., and Figurov, A. (1997). Role of neurotrophins in synapse development and plasticity. Rev. Neurosci. *8*, 1–12.

Lu, B., Pang, P.T., and Woo, N.H. (2005). The yin and yang of neurotrophin action. Nat. Rev. Neurosci. *6*, 603–614.

Lu, W.Y., Man, H.Y., Ju, W., Trimble, W.S., MacDonald, J.F., and Wang, Y.T. (2001). Activation of synaptic NMDA receptors induces membrane insertion of new AMPA receptors and LTP in cultured hippocampal neurons. Neuron *29*, 243–254.

Lu, Y., Christian, K., and Lu, B. (2008). BDNF: A key regulator for protein synthesis-dependent LTP and long-term memory? Neurobiol. Learn. Mem. *89*, 312–323.

Malenka, R.C., and Bear, M.F. (2004). LTP and LTD: an embarrassment of riches. Neuron *44*, 5–21.

Malenka, R.C., and Nicoll, R.A. (1999). Long-term potentiation--a decade of progress? Science *285*, 1870–1874.

Malgaroli, A., and Tsien, R.W. (1992). Glutamate-induced long-term potentiation of the frequency of miniature synaptic currents in cultured hippocampal neurons. Nature *357*, 134–139.

Mao, S., Ying, Y., Wu, R., and Chen, A.K. (2020). Recent Advances in the Molecular Beacon Technology for Live-Cell Single-Molecule Imaging. IScience *23*, 101801.

Mao, Y., Wang, X., Yan, R., Hu, W., Li, A., Wang, S., and Li, H. (2016). Single point mutation in adeno-associated viral vectors -DJ capsid leads to improvement for gene delivery in vivo. BMC Biotechnol. *16*, 1–9.

Martin, K.C., and Ephrussi, A. (2009). mRNA localization: gene expression in the spatial dimension. Cell *136*, 719–730.

Matsuda, N., Lu, H., Fukata, Y., Noritake, J., Gao, H., Mukherjee, S., Nemoto, T., Fukata, M., and Poo, M.M. (2009). Differential activity-dependent secretion of brain-derived neurotrophic factor from axon and dendrite. J. Neurosci. *29*, 14185–14198.

Mayr, C. (2017). Regulation by 3'-Untranslated Regions. Annu. Rev. Genet. *51*, 171–194.

McAllister, A.K., Katz, L.C., and Lo, D.C. (1997). Opposing Roles for Endogenous BDNF and NT-3 in Regulating Cortical Dendritic Growth. Neuron *18*, 767–778.

Meignin, C., and Davis, I. (2010). Transmitting the message: intracellular mRNA localization. Curr. Opin. Cell Biol. *22*, 112–119.

Minichiello, L., Korte, M., Wolfer, D., Kühn, R., Unsicker, K., Cestari, V., Rossi-Arnaud, C., Lipp, H.P., Bonhoeffer, T., and Klein, R. (1999). Essential role for TrkB receptors in hippocampus-mediated learning. Neuron *24*, 401–414.

Miura, P., Sanfilippo, P., Shenker, S., and Lai, E.C. (2014). Alternative polyadenylation in the nervous system: to what lengths will 3' UTR extensions take us? Bioessays *36*, 766–777.

Mowla, S.J., Farhadi, H.F., Pareek, S., Atwal, J.K., Morris, S.J., Seidah, N.G., and Murphy, R.A. (2001). Biosynthesis and post-translational processing of the precursor to brain-derived neurotrophic factor. J. Biol. Chem. *276*, 12660–12666.

Murer, M.G., Yan, Q., and Raisman-Vozari, R. (2001). Brain-derived neurotrophic factor in the control human brain, and in Alzheimer's disease and Parkinson's disease. Prog. Neurobiol. *63*, 71–124.

Nicoll, R.A., Kauer, J.A., and Malenka, R.C. (1988). The current excitement in long-term potentiation. Neuron *1*, 97–103.

O'Neill, K.M., Donohue, K.E., Omelchenko, A., and Firestein, B.L. (2018). The 3' UTRs of Brain-Derived Neurotrophic Factor Transcripts Differentially Regulate the Dendritic Arbor. Front. Cell. Neurosci. *12*, 60.

Okada, M., Kono, R., Sato, Y., Kobayashi, C., Koyama, R., and Ikegaya, Y. (2021). Highly active neurons emerging in vitro. J. Neurophysiol. *125*, 1322–1329.

Orefice, L.L., Waterhouse, E.G., Partridge, J.G., Lalchandani, R.R., Vicini, S., and Xu, B. (2013). Distinct roles for somatically and dendritically synthesized brain-derived neurotrophic factor in morphogenesis of dendritic spines. J. Neurosci. Off. J. Soc. Neurosci. *33*, 11618–11632.

Ostroff, L.E., Fiala, J.C., Allwardt, B., Harris, K.M., and Street, C. (2002). Polyribosomes Redistribute from Dendritic Shafts into Spines with Enlarged Synapses during LTP in Developing Rat Hippocampal Slices. *35*, 535–545.

Palacios, I.M., and St Johnston, D. (2001). Getting the message across: the intracellular localization of mRNAs in higher eukaryotes. Annu. Rev. Cell Dev. Biol. *17*, 569–614.

Pang, P.T., and Lu, B. (2004). Regulation of late-phase LTP and long-term memory in normal and aging hippocampus: role of secreted proteins tPA and BDNF. Ageing Res. Rev. *3*, 407–430.

Park, H.Y., Lim, H., Yoon, Y.J., Follenzi, A., Nwokafor, C., Lopez-Jones, M., Meng, X., and Singer, R.H. (2014). Visualization of dynamics of single endogenous mRNA labeled in live mouse. Science *343*, 422–424.

Pattabiraman, P.P., Tropea, D., Chiaruttini, C., Tongiorgi, E., Cattaneo, A., and Domenici, L. (2005). Neuronal activity regulates the developmental expression and subcellular localization of cortical BDNF mRNA isoforms in vivo. Mol. Cell. Neurosci. *28*, 556–570.

Patterson, S.L., Grover, L.M., Schwartzkroin, P.A., and Bothwell, M. (1992). Neurotrophin expression in rat hippocampal slices: a stimulus paradigm inducing LTP in CA1 evokes increases in BDNF and NT-3 mRNAs. Neuron *9*, 1081–1088.

Patterson, S.L., Abel, T., Deuel, T.A., Martin, K.C., Rose, J.C., and Kandel, E.R. (1996). Recombinant BDNF rescues deficits in basal synaptic transmission and hippocampal LTP in BDNF knockout mice. Neuron *16*, 1137–1145.

Patterson, S.L., Pittenger, C., Morozov, A., Martin, K.C., Scanlin, H., Drake, C., and Kandel, E.R. (2001). Some forms of cAMP-mediated long-lasting potentiation are associated with release of BDNF and nuclear translocation of phospho-MAP kinase. Neuron *32*, 123–140.

Peabody, D.S. (1993). The RNA binding size of bacteriophage MS2 coat protein. EMBO J. *12*, 595–600.

Phillips, H.S., Hains, J.M., Laramee, G.R., Rosenthal, A., and Winslow, J.W. (1990). Widespread expression of BDNF but not NT3 by target areas of basal forebrain cholinergic neurons. Science *250*, 290–294.

Pickard, B.S., Knight, H.M., Hamilton, R.S., Soares, D.C., Walker, R., Boyd, J.K.F., Machell, J., Maclean, A., McGhee, K.A., Condie, A., et al. (2008). A common variant in the 3'UTR of the GRIK4 glutamate receptor gene affects transcript abundance and protects against bipolar disorder. Proc. Natl. Acad. Sci. U. S. A. *105*, 14940–14945.

Pierce, J.P., van Leyen, K., and McCarthy, J.B. (2000). Translocation machinery for synthesis of integral membrane and secretory proteins in dendritic spines. Nat. Neurosci. *3*, 311–313.

Poon, M.M., Choi, S., Jamieson, C.A.M., Geschwind, D.H., and Martin, K.C. (2006). Identification of Process-Localized mRNAs from Cultured Rodent Hippocampal Neurons. *26*, 13390–13399.

Pradhan, J., Noakes, P.G., and Bellingham, M.C. (2019). The Role of Altered BDNF/TrkB Signaling in Amyotrophic Lateral Sclerosis. Front. Cell. Neurosci. *13*, 1–16.

Pruunsild, P., Kazantseva, A., Aid, T., Palm, K., and Timmusk, T. (2007). Dissecting the human BDNF locus: bidirectional transcription, complex splicing, and multiple promoters. Genomics *90*, 397–406.

Rangaraju, V., tom Dieck, S., and Schuman, E.M. (2017). Local translation in neuronal compartments: how local is local? EMBO Rep. *18*, 693–711.

Righi, M., Tongiorgi, E., and Cattaneo, A. (2000). Brain-derived neurotrophic factor (BDNF) induces dendritic targeting of BDNF and tyrosine kinase B mRNAs in hippocampal neurons through a phosphatidylinositol-3 kinase-dependent pathway. J. Neurosci. Off. J. Soc. Neurosci. *20*, 3165–3174.

Rook, M.S., Lu, M., and Kosik, K.S. (2000). CaMKIIα 3' untranslated region-directed mRNA translocation in living neurons: Visualization by GFP linkage. J. Neurosci. *20*, 6385–6393.

Rosenfeld, R.D., Zeni, L., Haniu, M., Talvenheimo, J., Radka, S.F., Bennett, L., Miller, J.A., and Welcher, A.A. (1995). Purification and identification of brain-derived neurotrophic factor from human serum. Protein Expr. Purif. *6*, 465–471.

Russo-Neustadt, A.A., and Chen, M.J. (2005). Brain-derived neurotrophic factor and

antidepressant activity. Curr. Pharm. Des. *11*, 1495–1510.

Schinder, A.F., and Poo, M. ming (2000). The neurotrophin hypothesis for synaptic plasticity. Trends Neurosci. *23*, 639–645.

Schneider, D., Tuerk, C., and Gold, L. (1992). Selection of high affinity RNA ligands to the bacteriophage R17 coat protein. J. Mol. Biol. *228*, 862–869.

Schultz, B.R., and Chamberlain, J.S. (2008). Recombinant adeno-associated virus transduction and integration. Mol. Ther. *16*, 1189–1199.

Schuman, E.M., Dynes, J.L., and Steward, O. (2006). Synaptic regulation of translation of dendritic mRNAs. J. Neurosci. *26*, 7143–7146.

Schwanhäusser, B., Busse, D., Li, N., Dittmar, G., Schuchhardt, J., Wolf, J., Chen, W., and Selbach, M. (2011). Global quantification of mammalian gene expression control. Nature *473*, 337–342.

Shahi, K., and Baudry, M. (1993). Glycine-induced changes in synaptic efficacy in hippocampal slices involve changes in AMPA receptors. Brain Res. *627*, 261–266.

Simonato, M., Bregola, G., Armellin, M., Del Piccolo, P., Rodi, D., Zucchini, S., and Tongiorgi, E. (2002). Dendritic targeting of mRNAs for plasticity genes in experimental models of temporal lobe epilepsy. Epilepsia *43 Suppl 5*, 153–158.

St Johnston, D. (2005). Moving messages: the intracellular localization of mRNAs. Nat. Rev. Mol. Cell Biol. *6*, 363–375.

Stanton, P.K., and Sarvey, J.M. (1984). Blockade of long-term potentiation in rat hippocampal CA1 region by inhibitors of protein synthesis. J. Neurosci. Off. J. Soc. Neurosci. *4*, 3080–3088.

Steward, O., Farris, S., Pirbhoy, P.S., Darnell, J., and Van Driesche, S.J. (2015). Localization and local translation of Arc/Arg3.1 mRNA at synapses: Some observations and paradoxes. Front. Mol. Neurosci. *7*, 1–15.

Stockley, P.G., Stonehouse, N.J., Murray, J.B., Goodman, S.T., Talbot, S.J., Adams, C.J., Liljas, L., and Valegård, K. (1995). Probing sequence-specific RNA recognition by the bacteriophage MS2 coat protein. Nucleic Acids Res. *23*, 2512–2518.

Sun, C., Nold, A., Fusco, C.M., Rangaraju, V., Tchumatchenko, T., Heilemann, M., and Schuman, E.M. (2021). The prevalence and specificity of local protein synthesis during neuronal synaptic plasticity. 1–13.

Sutton, M.A., and Schuman, E.M. (2006). Dendritic Protein Synthesis, Synaptic Plasticity, and Memory. Cell *127*, 49–58.

Tamara Aid, Anna Kazantseva, Marko Piirsoo, Kaia Palm, and T.T. (2007). Journal of Neuroscience Research 85:3244–3253 (2007). J. Neurosci. Res. *3253*, 3244–3253.

Tanaka, J.I., Horiike, Y., Matsuzaki, M., Miyazaki, T., Ellis-Davies, G.C.R., and Kasai, H. (2008). Protein synthesis and neurotrophin-dependent structural plasticity of single dendritic spines. Science (80-.). *319*, 1683–1687.

Tang et al., 2005 (2008). 基因的改变NIH Public Access. Bone *23*, 1–7.

Timmusk, T., Palm, K., Metsis, M., Reintam, T., Paalme, V., Saarma, M., and Persson, H. (1993). Multiple promoters direct tissue-specific expression of the rat BDNF gene. Neuron *10*, 475–489.

Tiruchinapalli, D.M., Oleynikov, Y., Kelic, S., Shenoy, S.M., Hartley, A., Stanton, P.K., Singer, R.H., and Bassell, G.J. (2003). Activity-dependent trafficking and dynamic localization of zipcode binding protein 1 and beta-actin mRNA in dendrites and spines of hippocampal neurons. J. Neurosci. Off. J. Soc. Neurosci. *23*, 3251–3261.

Tongiorgi, E., and Baj, G. (2008). Functions and Mechanisms of BDNF mRNA Trafficking. Growth Factors Psychiatr. Disord. *289*, 136–147.

Tongiorgi, E., Righi, M., and Cattaneo, A. (1997). Activity-dependent dendritic targeting of BDNF and TrkB mRNAs in hippocampal neurons. J. Neurosci. *17*, 9492–9505.

Tongiorgi, E., Armellin, M., Giulianini, P.G., Bregola, G., Zucchini, S., Paradiso, B., Steward, O., Cattaneo, A., and Simonato, M. (2004). Brain-derived neurotrophic factor mRNA and protein are targeted to discrete dendritic laminas by events that trigger epileptogenesis. J. Neurosci. *24*, 6842–6852.

Turner-Bridger, B., Jakobs, M., Muresan, L., Wong, H.H.W., Franze, K., Harris, W.A., and Holt, C.E. (2018). Single-molecule analysis of endogenous β-actin mRNA trafficking reveals a

mechanism for compartmentalized mRNA localization in axons. Proc. Natl. Acad. Sci. U. S. A. *115*, E9697–E9706.

Tushev, G., Glock, C., Heumüller, M., Biever, A., Jovanovic, M., and Schuman, E.M. (2018). Alternative 3' UTRs Modify the Localization, Regulatory Potential, Stability, and Plasticity of mRNAs in Neuronal Compartments. Neuron *98*, 495-511.e6.

Tyler, W.J., Alonso, M., Bramham, C.R., and Pozzo-Miller, L.D. (2002). From acquisition to consolidation: on the role of brain-derived neurotrophic factor signaling in hippocampal-dependent learning. Learn. Mem. *9*, 224–237.

Vaghi, V., Polacchini, A., Baj, G., Pinheiro, V.L.M., Vicario, A., and Tongiorgi, E. (2014). Pharmacological profile of brain-derived neurotrophic factor (BDNF) splice variant translation using a novel drug screening assay b. J. Biol. Chem. *289*, 27702–27713.

Verpelli, C., Piccoli, G., Zibetti, C., Zanchi, A., Gardoni, F., Huang, K., Brambilla, D., Di Luca, M., Sala, C., and Sala, C. (2010). Synaptic activity controls dendritic spine morphology by modulating eEF2-dependent BDNF synthesis. J. Neurosci. *30*, 5830–5842.

Vicario, A., Colliva, A., Ratti, A., Davidovic, L., Baj, G., Gricman, Ł., Colombrita, C., Pallavicini, A., Jones, K.R., Bardoni, B., et al. (2015). Dendritic targeting of short and long 3′ UTR BDNF mRNA is regulated by BDNF or NT-3 and distinct sets of RNA-binding proteins. Front. Mol. Neurosci. *8*, 1–14.

Webster, M.J., Herman, M.M., Kleinman, J.E., and Shannon Weickert, C. (2006). BDNF and trkB mRNA expression in the hippocampus and temporal cortex during the human lifespan. Gene Expr. Patterns *6*, 941–951.

Wetmore, C., Cao, Y.H., Pettersson, R.F., and Olson, L. (1991). Brain-derived neurotrophic factor: subcellular compartmentalization and interneuronal transfer as visualized with anti-peptide antibodies. Proc. Natl. Acad. Sci. U. S. A. *88*, 9843–9847.

Will, T.J., Tushev, G., Kochen, L., Nassim-Assir, B., Cajigas, I.J., Dieck, S.T., and Schuman, E.M. (2013). Deep sequencing and high-resolution imaging reveal compartment-specific localization of Bdnf mRNA in hippocampal neurons. Sci. Signal. *6*.

Wong, Y.H., Lee, C.M., Xie, W., Cui, B., and Poo, M.M. (2015). Activity-dependent BDNF release via endocytic pathways is regulated by synaptotagmin-6 and complexin. Proc. Natl.

Acad. Sci. U. S. A. *112*, E4475–E4484.

Wu, B., Chao, J.A., and Singer, R.H. (2012). Fluorescence fluctuation spectroscopy enables quantitative imaging of single mRNAs in living cells. Biophys. J. *102*, 2936–2944.

Wu, B., Eliscovich, C., Yoon, Y.J., and Singer, R.H. (2016). Translation dynamics of single mRNAs in live cells and neurons. Science (80-.). *352*, 1430–1435.

Yamada, K., Mizuno, M., and Nabeshima, T. (2002). Role for brain-derived neurotrophic factor in learning and memory. Life Sci. *70*, 735–744.

Yang, E., van Nimwegen, E., Zavolan, M., Rajewsky, N., Schroeder, M., Magnasco, M., and Darnell, J.E.J. (2003). Decay rates of human mRNAs: correlation with functional characteristics and sequence attributes. Genome Res. *13*, 1863–1872.

Yoon, Y.J., Wu, B., Buxbaum, A.R., Das, S., Tsai, A., English, B.P., Grimm, J.B., Lavis, L.D., and Singer, R.H. (2016). Glutamate-induced RNA localization and translation in neurons. Proc. Natl. Acad. Sci. U. S. A. *113*, E6877–E6886.

Zafra, F., Hengerer, B., Leibrock, J., Thoenen, H., and Lindholm, D. (1990). Activity dependent regulation of BDNF and NGF mRNAs in the rat hippocampus is mediated by non-NMDA glutamate receptors. EMBO J. *9*, 3545–3550.

Zhong, J., Zhang, T., and Bloch, L.M. (2006). Dendritic mRNAs encode diversified functionalities in hippocampal pyramidal neurons. BMC Neurosci. *7*, 17.

Zuccato, C., Liber, D., Ramos, C., Tarditi, A., Rigamonti, D., Tartari, M., Valenza, M., and Cattaneo, E. (2005). Progressive loss of BDNF in a mouse model of Huntington's disease and rescue by BDNF delivery. Pharmacol. Res. *52*, 133–139.